© 2012 Society of Economic Geologists, Inc.
Special Publication 16, pp. 573–618

Chapter 22

Hydrothermal Controls on Metal Distribution in Porphyry Cu (-Mo-Au) Systems

KALIN KOUZMANOV[1,†] AND GLEB S. POKROVSKI[2]

[1] *Earth and Environmental Sciences, Department of Mineralogy, University of Geneva,*
rue des Maraîchers 13, CH-1205 Geneva, Switzerland

[2] *Géosciences Environnement Toulouse, GET (ex-LMTG), Université de Toulouse,*
CNRS-IRD-OMP, 14 Av. E. Belin, F-31400 Toulouse, France

Abstract

Extensive research during the 20th century on porphyry Cu (-Mo-Au) deposits has revealed the following major geodynamic, petrological, mineralogical, and geochemical features that characterize these deposits: (1) these systems commonly occur in continental and oceanic magmatic arcs or in collisional orogenic belts; (2) they have spatial and genetic relationships to basaltic-to-felsic magmas emplaced in the upper 10 km of the crust; (3) lateral and vertical alteration-mineralization zoning consists of a Cu (± Mo ± Au) ore shell in the shallow portion of a potassic alteration zone, produced by magmatic fluids; this can be overprinted by phyllic alteration, also largely magmatic in signature, that in turn may be overprinted by argillic alteration, with a dominantly meteoric signature; (4) associated deposits such as skarns, Cordilleran vein, and high and intermediate sulfidation epithermal deposits may occur above or adjacent to porphyry orebodies; (5) porphyry systems form from S- and metal-rich, single-phase aqueous fluid of moderate salinity (2–10 wt % NaCl equiv) exsolved from magmas; during its ascent toward the surface this fluid undergoes a variety of processes that can cause metal precipitation, including decompression, phase separation, cooling, interaction with host rocks, and mixing.

In the last 20 years, novel microanalytical techniques for in situ characterization of individual fluid inclusions have provided direct evidence for the chemical and phase composition plus metal content of ore-forming fluids in porphyry systems. In this contribution, we compile a large dataset of published fluid inclusion compositions from more than 30 deposits of the porphyry-skarn-epithermal suite. Four main types of fluid inclusions are identified, based on their origin and phase composition at the time of entrapment: (1) single-phase, intermediate-density inclusions, regarded as equivalent to the primary single-phase fluid exsolved from the magma, (2) vapor-rich and (3) hypersaline liquid inclusions, both resulting from phase separation of the single-phase fluid, and (4) low to intermediate salinity aqueous liquid inclusions. The first three fluid types are characteristic of porphyry and skarn environments at elevated temperatures and depths, whereas the last is present during the retrograde stage, both in skarn and porphyry deposits as well as in the shallow epithermal environment.

Absolute concentrations of ore-related metals in the pristine single-phase magmatic fluids are typically one to three orders of magnitude higher than their average crustal abundances, demonstrating the ability of magmatic-hydrothermal fluid to concentrate and transport metals. Decompression-induced phase separation of this magmatic fluid upon ascent and intersection of the two-phase vapor-liquid boundary of the water-salt system results in metal fractionation, as evidenced by coexisting vapor and hypersaline liquid inclusions. The hypersaline liquid is largely enriched in metals such as Zn, Pb, Fe, Mn, and Ag, whereas Au, As, S and, to a lesser and uncertain extent, Mo may partition into the vapor phase. Copper is likely to have a partitioning behavior intermediate between these groups of elements; however, its true vapor-liquid distribution may be obscured by post-entrapment diffusion processes which lead to an apparent enrichment in Cu in natural S-rich vapor and single-phase fluid inclusions. These metal fractionation trends are quantitatively explained by recent experimental data on vapor-liquid partitioning that show a preferential affinity of Au (and partly Cu) for reduced sulfur and that of other metals for chloride, and by physical-chemical models involving the fluid density. Single-phase, vapor-rich, and hypersaline liquid inclusions from giant porphyry deposits at Bingham, El Teniente, Bajo de la Alumbrera, Questa, and Butte present a characteristic Zn/Pb ratio, ranging from 1 to 6 in the order of the listed deposits, which is constant for a given deposit and is not affected by phase separation of the input magmatic fluid or Cu-Au-Mo precipitation in the porphyry environment, thus implying differences in the Zn/Pb ratio of the parental magmas.

Recent experimental studies on metal speciation and ore mineral solubilities under hydrothermal conditions coupled with thermodynamic modeling allow the reported metal contents in natural inclusion fluids to be interpreted. Modeling shows that cooling of a magmatic fluid, accompanied by water-rock interaction, is likely to be the major cause of most metal deposition, as well as the cause of spatial separation between Cu-Mo and Zn-Pb-Ag mineralization in porphyry systems. Changes in sulfur speciation on cooling lead to SO_2 disproportionation; this is likely to control the observed fractionation of Au from Cu and other base metals during fluid evolution in the transition from the porphyry to epithermal environment. Fluid neutralization by wall-rock reaction appears to be the main driving force for Zn, Pb, Ag, and partially Au deposition in more distal portions of the porphyry system. Fluid immiscibility in the porphyry regime mostly affects Au and to a lesser extent Cu

---

[†] Corresponding author: e-mail, kalin.kouzmanov@unige.ch

and Mo behavior by enabling a significant fraction of these metals to be transported by the vapor phase. Mixing with external waters is uncommon and not directly involved in ore formation in the porphyry environment. These predicted tendencies agree with the commonly observed metal zoning pattern in porphyry systems, and may provide useful clues for specific metal prospecting if the major fluid evolution events can be identified from fluid inclusion, mineralogical, or stable isotope analyses.

Comparison between mineral solubility calculations and metal contents in natural fluids shows that for some metals, such as Cu, Ag, Fe, Zn, and Pb, there is a good consistency. In contrast, thermodynamic predictions for Au and, particularly, Mo commonly underestimate their contents compared to natural fluid compositions. This requires reassessment of existing speciation models for these metals and consideration of recently discovered sulfur species that could potentially be important as metal transporting agents. Further development of microanalytical and in situ experimental approaches in hydrothermal geochemistry may provide new predictive tools in mineral exploration; coupled with physical hydrology models, this will allow the generation of integrated reactive transport models of fluid evolution and three-dimensional ore distribution in magmatic-hydrothermal systems, thus contributing to better exploration strategies.

Introduction

RESEARCH on porphyry Cu (-Mo-Au) systems and associated base and precious metal deposits has been conducted for over a century, and our present understanding of their genesis is based primarily on geologic observations, complemented by petrological, geochemical, mineralogical, structural, geochronological, and geophysical data. This ensemble of data has allowed the genetic link between porphyry Cu deposits and magmatic-hydrothermal processes to be established and has contributed to field observations on the geology to build genetic models successfully used in mineral exploration. However, knowledge of the hydrothermal fluid itself has remained limited. Ore-forming fluids in these deposits have been mainly characterized by conventional fluid inclusion microthermometry, providing a constraint on their PVTX (pressure-volume-temperature-composition) parameters. Their origin and isotopic composition have been inferred by using indirect data from mineral assemblages and isotopic signatures of minerals. Prior to the turn of the century, the metal content of inclusion fluids was studied by bulk crush-leach methods, analyzing a large number of inclusions that were commonly related to different inclusion populations, each associated with a different hydrothermal event.

In the last 15 years, major advances in microanalytical techniques, particularly for individual fluid inclusion characterization, such as laser ablation-inductively coupled plasma- mass spectrometry (LA-ICP-MS), proton-induced X-ray emission spectroscopy (PIXE), synchrotron radiation X-ray fluorescence (SR-XRF), infrared, Raman, and fluorescence spectroscopy, have provided direct data for the chemical and phase composition and metal content of ore-forming fluids. These data have better constrained metal sources and budgets in porphyry systems. In addition, recent progress in experimental approaches and physical-chemical modeling of hydrothermal fluids has provided far more accurate information on the identity and stability of dissolved metal-bearing species, and improved predictions of ore-mineral solubilities, metal vapor-liquid partitioning, and depositional mechanisms.

The principal aim of this contribution is to provide an overview of the current knowledge of hydrothermal fluid compositions and the chemical speciation of ore metals (Cu, Au, Ag, Mo) and accompanying elements (S, Fe, Zn, Pb) in various types of fluids under the conditions relevant to porphyry Cu (-Mo-Au) formation. We have compiled recently published metal concentrations from direct analyses of fluid inclusions, with corresponding temperature and salinity measurements, from more than 30 deposits of porphyry Cu, Cu-Au, Mo, and Cu-Mo systems, Sn-W–mineralized granites, and various porphyry-related skarn, vein, and epithermal deposits. This data set is compared to thermodynamically predicted metal contents of hydrothermal fluids, based on the calculated solubility of the major metal-bearing ore minerals as a function of key intensive parameters (temperature, pressure, Cl content, acidity, redox potential, and sulfur fugacity). The major hydrothermal processes leading to the redistribution and deposition of metals in porphyry systems are discussed in an attempt to illustrate the complexity of factors controlling ore formation in the deep (porphyry and skarn) and shallow (epithermal) parts of these systems. The paper concludes with a summary of near-future analytical, experimental, and theoretical challenges for research on fluid processes in porphyry systems.

Porphyry Systems

Definition and significance

The economic importance of porphyry deposits grew constantly over the last 50 years and now they supply a majority of the world's Cu, Mo, and Re and a substantial amount of Au, together with some Ag, Pd, Te, Se, Bi, Zn, and Pb (Sillitoe, 2010). They are probably the best studied of all hydrothermal ore deposits and their salient features have been discussed in a number of special volumes and review articles published over the past half century (summarized by Hedenquist and Richards, 1998). Several recent papers offer exhaustive overviews of the geologic and geotectonic setting, architecture, associated magmatism, metal and mineral alteration zoning, and space-time relationships of porphyry systems (e.g., Tosdal and Richards, 2001; Richards, 2003, 2011; Cooke et al., 2005; Seedorff et al., 2005; Sillitoe, 2010).

Porphyry deposits are composite magmatic-hydrothermal systems that involve large volumes (~10–100 km^3) of altered rocks resulting from extensive circulation of hydrothermal fluids at shallow crustal levels (Kirkham, 1971; Beane and Titley, 1981; Titley, 1982, 1993; Beane and Bodnar, 1995; Seedorff et al., 2005; Sillitoe, 2010). Porphyry systems typically occur in continental and oceanic arcs, 100s to 1,000s of kilometers long and mainly of Tertiary age, or in collisional orogenic belts (Cooke et al., 2005; Richards, 2011). A diagnostic feature of these deposits is the development of low-grade stockwork Cu, Au, and/or Mo mineralization within and around porphyritic intrusive stocks and associated dike swarms, some of which intrude the base of intermediate to felsic volcanoes; others are emplaced in sedimentary and crystalline rocks (Gustafson and Hunt, 1975; Seedorff et al., 2005). It is generally accepted that porphyry systems are initiated by injection of oxidized magma, saturated with S- and metal-rich aqueous fluids, from cupolas of large underlying parental dioritic-to-granitic composite plutons emplaced in the upper 10 km of the crust (Emmons, 1927; Burnham, 1979; Cline and Bodnar, 1991, 1994; Dilles and Einaudi, 1992; Hedenquist and Lowenstern, 1994; Bodnar, 1995; Richards, 2003, 2011; Halter et al., 2005). Multiple overprinting stages of alteration and mineralization result from aqueous hydrothermal fluid cooling from >700° to <200°C, in parallel with the solidification of the underlying volatile-saturated magma reservoir; subsequent cooling results in the downward propagation of the lithostatic-hydrostatic pressure transition zone (Burnham, 1979; Fournier, 1999; Proffett, 2009; Sillitoe, 2010).

The following section summarizes the typical features of porphyry systems—their characteristic hydrothermal alteration, mineralization, and metal zonation, resulting from depressurization and cooling of the magmatic-hydrothermal fluids, and their reaction with wall rocks.

Architecture of porphyry systems

Porphyry systems, sensu largo (Fig. 1; Sillitoe, 2010), host various ore deposit types that formed at distinct but partly overlapping depths and temperature and pressure ranges. These include porphyry deposits, sensu stricto, associated proximal and distal skarns, subepithermal, carbonate-replacement, high and intermediate sulfidation polymetallic ± Au ± Ag vein deposits, disseminated high-sulfidation Au-Cu-Ag deposits in the shallow epithermal environment, and sediment-hosted disseminated Au ± As ± Sb ± Hg deposits in more distal positions. Mineralization associated with all these deposit types has diagnostic wall-rock alteration assemblages that can be used as a defining feature of the environment of ore formation.

Alteration and mineralization zoning: No matter their age, tectonic setting, and size, porphyry systems around the world share common alteration and mineralization styles with broadly similar spatial distribution patterns (Meyer and Hemley, 1967; Lowell and Guilbert, 1970; Rose, 1970; Beane, 1982). Broad-scale alteration zoning comprises sodic-calcic, potassic, chlorite-sericite, sericitic, and advanced argillic assemblages, from the base upward and outward to propylitic alteration (Fig. 2; see details about definition, characteristics, mineral composition, occurrences, and processes of formation for different alteration types in Seedorff et al., 2005, and Sillitoe, 2010). The temporal evolution observed in porphyry systems starts with early biotite ± K-feldspar ± magnetite assemblages (potassic alteration, also called K-silicate by some, e.g., Meyer and Hemley, 1967) formed at high temperature, continues with lower temperature muscovite ± chlorite assemblages (chlorite-sericite and sericitic alteration), and ends with low-temperature, clay-bearing assemblages (intermediate argillic); shallow advanced argillic alteration begins to form during the deep potassic stage, but can continue to form later in the life of a system. Later assemblages commonly overprint earlier formed alteration, as summarized by Seedorff et al. (2005) and Sillitoe (2010). Such evolution of alteration assemblages is consistent with the progressive cooling and acidification of magmatic fluids during their ascent toward the surface, with an increase in the fluid/rock ratio with time, and prior to their neutralization by wall-rock reactions, as discussed below.

Geologic observations, stable isotopic compositions of minerals and fluids, and fluid inclusion analyses provide evidence that magmatic fluids generally dominate the high-temperature potassic alteration and are still dominant in sericitic alteration; nonmagmatic fluids dominate much deep sodic-calcic and propylitic alteration, whereas advanced argillic—related to condensates of magmatic vapor—and intermediate argillic alteration are influenced by meteoric waters (Seedorff et al., 2005; Sillitoe, 2010, and references therein).

Precipitation of Cu-Fe-sulfide ore minerals (mainly chalcopyrite and bornite), locally associated with molybdenite and/or gold in quartz stockwork veins and disseminations, is governed by the same factors that control wall-rock alteration. In porphyry deposits, detailed field and microscale observation of crosscutting relationships between veins with different mineralogy and alteration provides the most reliable criteria for establishing relative timing of hydrothermal events. Cathodoluminescence imaging of hydrothermal quartz improves the textural interpretation of crosscutting relationships in porphyry stockwork veining and the timing of sulfide precipitation (e.g., Rusk and Reed, 2002; Redmond et al., 2004; Landtwing et al., 2005, 2010; Vry et al., 2010). These studies revealed complex growth histories of sulfide-quartz veins in porphyry Cu (-Mo-Au) deposits; early Cu-bearing quartz veins are usually associated with the high-temperature potassic alteration and cut by molybdenite-quartz veins, which in turn are cut by pyrite-dominated veins with sericitic alteration envelopes (e.g., Meyer and Hemley, 1967; Gustafson and Hunt, 1975; Beane and Titley, 1981; Titley, 1982; Redmond and Einaudi, 2010). This paragenetic scheme is widely generalized; in each individual deposit varied relationships between different vein types occur due to the cyclic behavior of porphyry systems—repetitive emplacement of multiple porphyry stocks and associated hydraulic fracturing that led to complex textural relationships between veins, alteration assemblages, and intrusions (Seedorff et al., 2005, 2008; Sillitoe, 2010). In some deposits, late veins, which contain Cu ± Zn, Pb, Ag, and Au within sericitic, intermediate argillic, and advanced argillic alteration envelopes, cut the early Cu- and Mo-bearing veins (e.g., Meyer et al., 1968; Gustafson and Hunt, 1975; Ossandón et al., 2001; Proffett, 2003; Masterman et al., 2005; Rusk et al., 2008a; Catchpole et al., in review). Such late veins may overprint the deep potassic alteration where telescoping occurs (Sillitoe, 1994).

Epithermal deposits commonly form above or adjacent to porphyry orebodies (Fig. 1). Ore and gangue minerals typically occupy open space in veins, breccia zones, or volumes of secondary porosity (Hayba et al., 1985; Sillitoe and Hedenquist, 2003; Simmons et al., 2005); replacement textures are common in carbonate-replacement analogues of epithermal deposits. Mineralization can be associated with sericitic, chloritic, intermediate argillic, and advanced argillic alteration. Where carbonate-rich sedimentary rocks host porphyry systems, calcic or magnesian endo- and exoskarns develop (Einaudi, 1982). Prograde garnet-pyroxene assemblages in calcic skarns form contemporaneously with early potassic

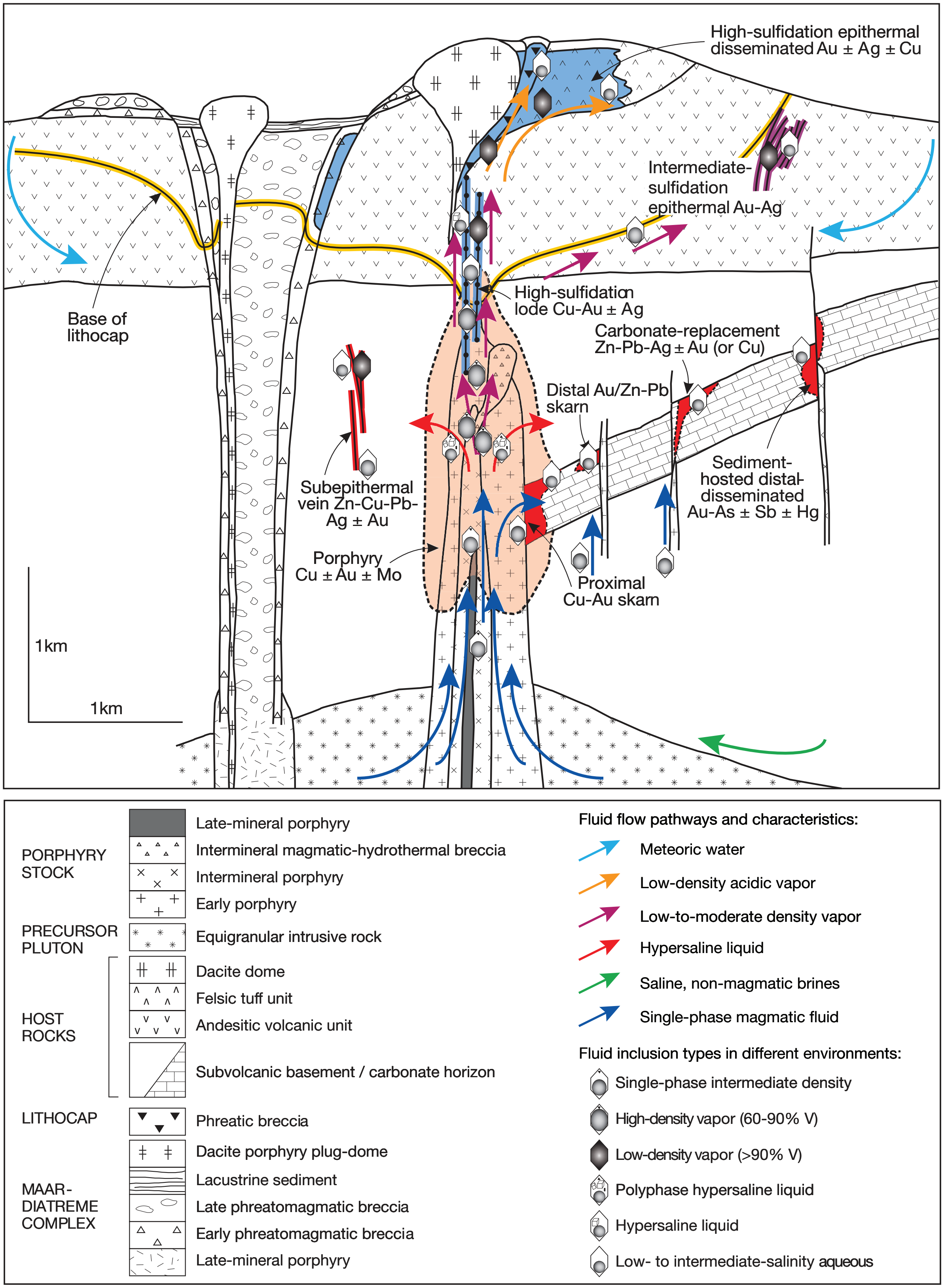

FIG. 1. Schematic cross section through a typical porphyry Cu system showing spatial relationships of the porphyry Cu-Au deposit, centered on a porphyry stock, with peripheral proximal and distal skarns, carbonate-replacement and distal sediment-hosted disseminated deposits, subepithermal veins in noncarbonate rocks, and overlying lithocaps plus high and intermediate sulfidation epithermal deposits (from Sillitoe, 2010; with fluid flow pathways and spatial distribution of the main fluid inclusion types commonly found in different environments added). Figure used with permission of R.H. Sillitoe.

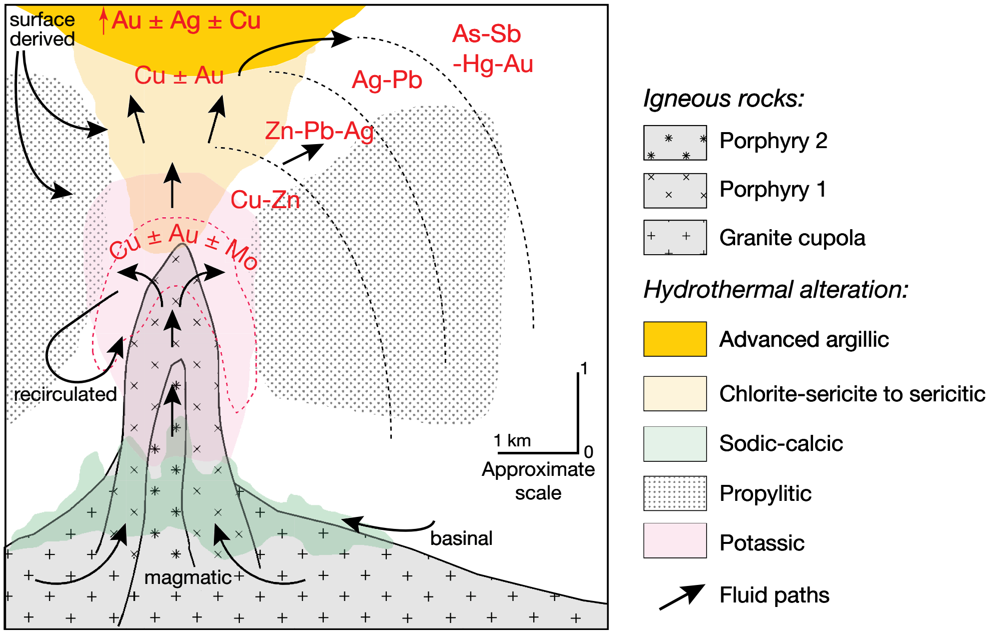

FIG. 2. Generalized scheme of metal zoning, alteration patterns, and fluid paths in a porphyry-centered system. Ore shell of Cu ± Au ± Mo is centered on the porphyry stock and extends to the wall rocks. Outward base-metal zoning, commonly observed in porphyry-centered districts, includes in order of increasing distance from the porphyry: Cu-Zn, Zn-Pb-Ag, Pb-Ag, and As-Sb-Hg-Au zones (see Fig. 1 for the different associated deposit styles). Note that this zonation of metals reflects changes in fluid compositions, as well as metal transport and precipitation mechanisms. High sulfidation Cu ± Au mineralization may develop in the upflow zone over the center of the system; however, due to erosion this part of the system is commonly missing in well-zoned porphyry-centered base-metal districts (e.g., Butte, Morococha). Juvenile magmatic fluids, having potential sources in composite porphyry stocks and/or deeper granitic cupolas, may mix at depth with saline fluids of nonmagmatic origin (e.g., formation waters) or recycled magmatic fluids (e.g., earlier stage residual hypersaline porphyry liquids), as well as surface-derived meteoric waters at later stages of hydrothermal evolution. Adapted from Emmons (1927), Meyer et al. (1968), Corbett and Leach (1998), Dilles et al. (2000), Seedorff et al. (2005, 2008), and Sillitoe (2010).

alteration in aluminosilicate rocks at lithostatic pressures, whereas later hydrated, retrograde skarn assemblages (actinolite, epidote, chlorite, smectite, magnetite, carbonate) associated with sulfides form under hydrostatic conditions, analogous to sericitic alteration in porphyry deposits (Meinert et al., 2003, 2005).

Metal zoning of porphyry systems: A characteristic feature of many porphyry systems is the regular pattern of zonal metal distribution—both vertically from deep levels proximal to the composite porphyry stocks, and laterally from centrally located potassic alteration to marginal propylitic zones (Fig. 2). In porphyry-centered districts like Butte, Montana (Meyer et al., 1968; Rusk et al., 2008a, b), Bingham Canyon, Utah (John, 1978; Babcock et al., 1995), or Morococha, Peru (Catchpole et al., 2011, in review), Cu ± Mo ± Au characterize the central, deep parts of the systems, forming an ore shell in the upper parts of the potassic alteration zones. Vertical Cu ± Au ± Ag zones may be present in the upflow conduits above the centers of the systems, as high-sulfidation Cu-Au-Ag lodes and high-sulfidation disseminated epithermal Au-Ag deposits (Fig. 1). However, due to erosion, these zones are commonly absent in porphyry-centered districts; in such cases, a Cu ± Mo ± Au core ringed by successive Cu-Zn, Zn-Pb-Ag, Pb-Ag (± Mn), and As-Sb-Au-Hg zones is observed in plan view (Fig. 2). Metal zoning both upward and outward from the core is a primary function of mineral solubility, transport, and depositional mechanisms of base and precious metals, controlled by intensive parameters of the fluids, as discussed below.

Lifespan and multiphase character of magmatic-hydrothermal processes: Most porphyry deposits are centered on composite stocks formed during prolonged magmatic evolution, commonly consisting of pre-, syn-, and postmineral intrusions. Recent studies on the geochronology of porphyry systems, combining different geochronometers (most frequently U-Pb, Re-Os, and Ar/Ar), indicate a protracted magmatic and hydrothermal lifespan for some giant porphyry deposits, as long as 4 to 5 m.y. (e.g., Ballard et al., 2001; Maksaev et al., 2004; Valencia et al., 2005; Harris et al., 2008; Sillitoe and Mortensen, 2010; Barra, 2011; Deckart et al., 2012). Elsewhere, magmatic-hydrothermal activity was shorter, ≤1 m.y. (e.g., 0.08 m.y. at Batu Hijau, Indonesia: Garwin, 2002; 0.09 m.y. at Bajo de la Alumbrera, Argentina: von Quadt et al., 2011; 0.10 m.y. at Lepanto-Far Southeast, Philippines: Arribas et al., 1995; 0.32 m.y. at Bingham Canyon: von Quadt et al., 2011; 0.80 m.y. at Grasberg, Indonesia: Pollard et al., 2005; and ~1 m.y. at Elatsite, Bulgaria: von Quadt et al., 2002). The multiphase character of magmatism and the resulting prolonged magmatic-hydrothermal activity in porphyry systems cause a superposition of multiple events that reflect the cyclic evolution of these systems. Such superposition can significantly complicate the interpretation of the alteration, mineralization, and metal zonation of the early events, which can be (partially) destroyed by the younger magmatic and/or hydrothermal events (e.g., Proffett, 2003). Redistribution of metals by later fluid circulation can also occur, resulting in more complex deposit- to district-scale metal zonation than in the ideal case of a single mineralizing intrusion (Fig. 2).

Overprinting of multiple magmatic and hydrothermal events can also complicate the interpretation of PVTX properties of hydrothermal fluids from fluid inclusion analysis, due to possible post-entrapment modification and re-equilibration of the fluid inclusions. Thus, extreme care is needed in acquisition and interpretation of fluid inclusion data in porphyry systems. We next summarize the potential fluid sources, as well as the main physical properties, evolution, and spatial distribution of the principal fluid inclusion types in porphyry systems, as these inclusions are our principle source of information on metal concentrations.

Origin and evolution of fluids in porphyry systems

Fluid sources in porphyry systems: When intermediate-to-felsic magmas ascend in the crust and crystallize in response to pressure decrease and cooling, the residual silicate melt becomes saturated with a volatile phase, generating an aqueous magmatic fluid (Burnham, 1979). The exsolved fluid phase is dominantly aqueous, but contains significant quantities of CO_2 and lesser amounts of SO_2 (± H_2S) and other minor gases (H_2, N_2); in addition, HCl, NaCl, KCl, and metal chlorides are present in variable proportions as a function of the depth of exsolution and parental magma composition (Candela, 1989; Giggenbach, 1992, 1997; Hedenquist, 1995; Einaudi et al., 2003). The salinity of the single-phase magmatic fluid at high pressures, above the two-phase surface in the H_2O-NaCl system (Fig. 3), is typically in the range of 2 to 10 wt % NaCl equiv (Shinohara and Hedenquist, 1997; Hedenquist and Richards, 1998; Audétat and Pettke, 2003; Redmond et al., 2004; Rusk et al., 2004, 2008b; Audétat et al., 2008; Table 1). This magmatic fluid initially has a near-neutral pH because most of acid-like volatiles (HCl, SO_2) are fully associated at high temperatures, but it becomes acidic on cooling, if not sufficiently buffered by aluminosilicate rocks, due to dissociation of acidic components and disproportiation of SO_2 to H_2S and sulfuric acid (Giggenbach, 1997; see below).

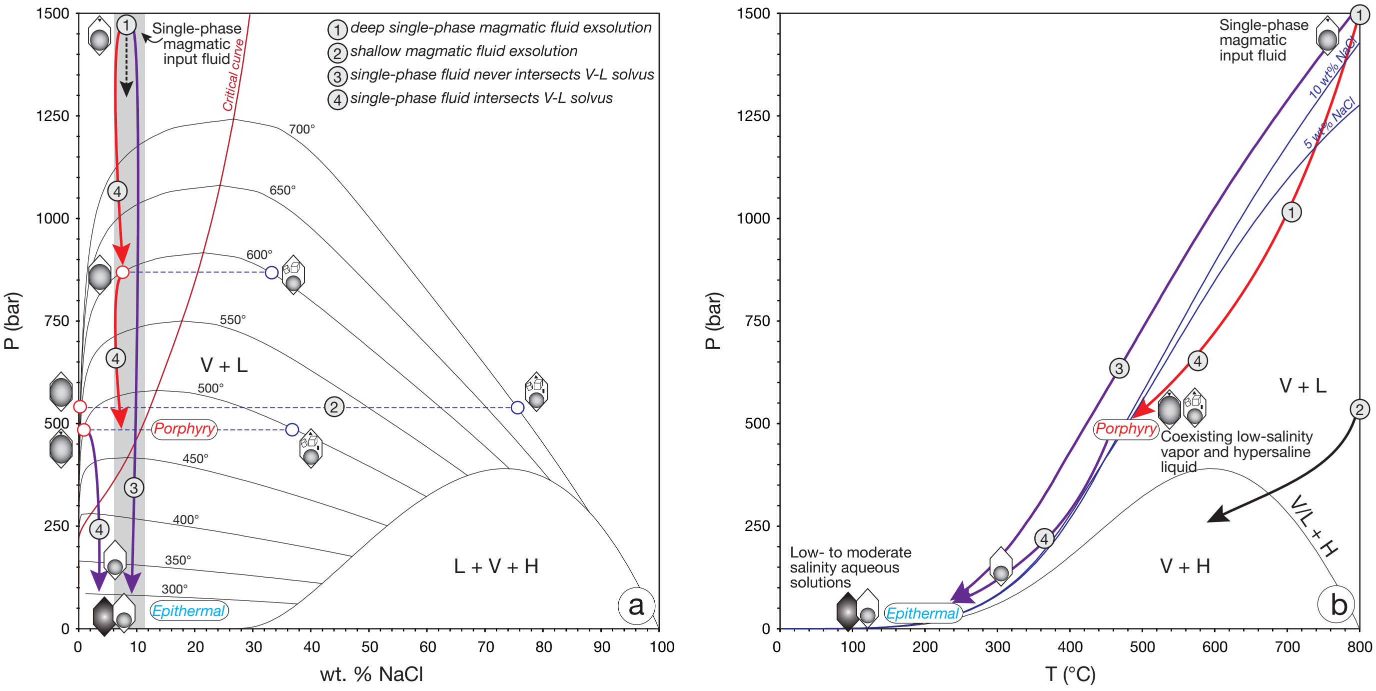

FIG. 3. Pressure-composition (a) and pressure-temperature (b) cross sections of the NaCl-H_2O phase diagram (adapted from Richards, 2011, based on data from Sourirajan and Kennedy, 1962; Driesner, 2007, and Driesner and Heinrich, 2007), illustrating principal evolution pathways of a magmatic-hydrothermal fluid exsolved from a crystallizing magma with an initial bulk salinity of ~10 wt % NaCl (gray area in a). L, V, and H refer respectively to liquid, vapor and halite, which are the three phases in the H_2O-NaCl system. When the single-phase magmatic fluid expands on ascent, its pressure and temperature (P-T) evolution path may or may not intersect the two-phase vapor-liquid domain of the NaCl-H_2O system (V-L solvus). Because of the curvature of the critical curve (i.e., the curve connecting the summits of the V-L solvus at each given temperature in the T-P section) to lower salinities at temperature ~450°C, fluids that intersect the V-L solvus at higher temperatures will be moderate-density vapors and will condensate a small amount of dense hypersaline liquid, while fluids that intersect the solvus at lower temperatures will be liquid and will boil and form a low-density aqueous vapor. Path 1 illustrates deep single-phase magmatic fluid exsolution and path 2 shows fluid exsolution from shallowly emplaced magma. Path 3 refers to the single-phase magmatic fluid contraction to an aqueous low to moderate salinity liquid phase without entering the V-L two phase domain (Hedenquist et al., 1998), and path 4 refers to a fluid evolution with intersection of the V-L solvus, allowing initial condensation of hypersaline liquid and subsequent contraction of the ascending vapor phase to a low-salinity aqueous liquid in the epithermal environment (Heinrich et al., 2004). In both cases, subsequent near-surface boiling of this low salinity liquid may optimize metal deposition in the low P-T epithermal environment, mainly due to loss of H_2S from the liquid. Major fluid inclusion types generated by different P-T fluid evolution paths in porphyry and epithermal environments (Table 1) are shown by the same symbols as in Figure 1 (see text for details). Fluid paths are according to Richards (2011).

Magmas are the main source of fluids that transport metals, salts, and sulfur to the porphyry environment (e.g., Roedder, 1971; Nash, 1976; Eastoe, 1978; Cline and Bodnar, 1991, 1994; Dilles et al., 1992; Hedenquist and Lowenstern, 1994; Hedenquist and Richards, 1998; Halter et al., 2005; Harris et al., 2005; Heinrich et al., 2005). Despite the overall magmatic signature of fluids involved in porphyry systems, in a few cases external fluids (basinal brines, seawater or meteoric water; Fig. 2) may affect alteration zoning patterns, as revealed by stable and radiogenic isotope signatures of hydrothermal minerals (e.g., Sheppard et al., 1971; Chivas et al., 1984; Dilles et al., 1995). In contrast, in the shallow epithermal environment, meteoric water interacts with the ascending magmatic fluids, causing dilution and cooling of the latter; meteoric water also acts as the condenser of magmatic vapor that leads to acidification and creation of epithermal lithocaps above the porphyry centers (e.g., Rye, 1993; Arribas, 1995; Hedenquist et al., 1998; Deyell et al., 2005a, b; Fifarek and Rye, 2005).

Fluid inclusion types: Terminology, physical properties, and spatial distribution: Fluid inclusions trapped in gangue and ore minerals from porphyry systems are direct microsamples of paleomagmatic-hydrothermal fluids responsible for hydrothermal alteration and mineral precipitation (Roedder, 1967). Fluid inclusion data provide direct information on the pressure, temperature, and composition of the fluids at the time of their entrapment; combined with thermodynamic calculations of mineral stabilities, such data can be used to constrain intensive parameters of ore formation.

There are few general review papers on fluid inclusions related to ore formation in porphyry systems sensu largo (Bodnar, 1995; Hedenquist and Richards, 1998, on porphyry deposits; Bodnar et al., 1985, on epithermal deposits; Kwak, 1986, on skarns), compared to the large number of papers that discuss the characteristics of mineralizing fluids based on physical chemistry or indirect mineral alteration patterns of these deposits. Various aspects of fluid inclusion research on porphyry systems can also be found in several reviews on fluid inclusions in ore deposits and shallow intrusions (e.g., Spooner, 1981; Weisbrod, 1981; Roedder, 1984; Lattanzi, 1991, 1994; Roedder and Bodnar, 1997; Wilkinson, 2001).

There is much variability in the terms used in the fluid inclusion literature on ore deposits (Table 2); this can create confusion, especially when fluid inclusions with similar characteristics have different, contradictory names. A summary of terms used to describe fluid types and processes in magmatic-hydrothermal systems and a discussion of their use, misuse, and interpretation can be found in Liebscher and Heinrich (2007) and references therein.

Although the commonly used classifications account accurately for most fluid inclusion aspects at room temperature, they provide little direct information about the fluid characteristics at the pressure and temperature of entrapment. In the present study, we use a genetic classification of fluid inclusions typically observed in porphyry deposits, based on the properties of the fluid at the time of entrapment. Four major types of fluid inclusions are defined; their main characteristics, including phase proportions at room temperature, temperature of homogenization, salinity, density, and metal content are summarized in Table 1. In the following sections we refer to these four types of fluid inclusions and their properties:

1. Single-phase, intermediate-density, aqueous inclusions, containing liquid phase and vapor in equal proportions ($L \approx V$) at room temperature; commonly a small opaque daughter crystal is also present. These fluid inclusions are trapped at high temperature and pressure in the single-phase domain, above the two-phase vapor-liquid boundary of the H_2O-NaCl system (Fig. 3). This fluid inclusion type is typically CO_2-rich (e.g., Roedder, 1971; Nash, 1976; Klemm et al., 2008, Rusk et al., 2008b), with CO_2 content reaching ~12 mol % (Rusk et al., 2008c; 2011). These fluid inclusions have densities between ~0.50 and 0.75 g/cm^3 and are considered as representative of the original single-phase fluid exsolved from magma during crystallization.
2. Vapor-rich fluid inclusions dominated by a vapor phase (>60–65 vol %) at room temperature. They are inferred to have trapped a volatile fluid phase that was produced by magma degassing and/or vapor-liquid separation over a wide temperature range (800°–~300°C). The density of such fluids is less than the critical density for a given fluid composition, typically <0.3 to 0.5 g/cm^3.
3. Hypersaline liquid inclusions trapped a high-salinity (26–80 wt % NaCl equiv) liquid phase containing a high concentrations of dissolved salts, typically NaCl>KCl>$FeCl_2$. Fluid density is greater than the critical density for a given fluid composition and can reach >1.3 g/cm^3. At room temperature, these inclusions contain a vapor bubble, liquid phase, and one or more daughter crystals in addition to a halite crystal; the presence of opaque daughters and/or red hematite plates is common. In porphyry deposits, such fluids are typically produced by fluid phase separation under magmatic or hydrothermal conditions (Fig. 3).
4. Aqueous, low-to-intermediate salinity inclusions are dominated by liquid water and have a small vapor bubble, typically 20 to 40 vol % at room temperature. Fluid density is generally low – 0.1 to 0.6 g/cm^3; temperature and pressure of entrapment are much lower than those of single-phase fluids. These inclusions are free of daughter phases; however, in some cases, they may contain accidentally trapped crystals.

Each fluid inclusion type has a particular spatial distribution in porphyry systems (Table 1): single-phase fluids are typical of the deep central and peripheral zones; hypersaline liquid and coexisting vapor inclusions mark the level where phase separation takes place in the porphyry environment, and low-density buoyant vapor ascends toward the surface; low-salinity aqueous fluids dominate the shallow parts of the systems (Fig. 1). Although potassic alteration in the core of systems (Fig. 2) can be produced by a single-phase magmatic fluid (Redmond et al., 2004; Rusk et al., 2008b; Redmond and Einaudi, 2010), it may also form in the domain of coexisting vapor + hypersaline liquid cooling together from ~700°C to ~350°C, as evidenced by stable isotope analyses of hydrothermal minerals and fluid inclusion microthermometry (e.g., Hedenquist et al., 1998; Redmond et al., 2004). In proximal and distal skarns, the fluid associated with the early prograde skarn formation is dominantly high temperature (temperatures exceeding 350°–400°C), single-phase and/or hypersaline

Table 1. Various Types of Fluid Inclusions Commonly Found in Porphyry and Epithermal Environments with Their

Fluid inclusion types	Nomenclature based on genetic aspects (see text)	Environment	Temperature of hom. (°C)	Salinity (wt % NaCl equiv)
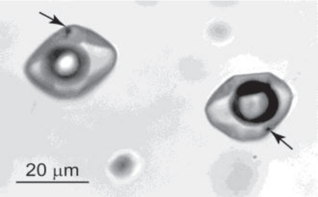	*Single-phase inclusions* are intermediate-density aqueous inclusions containing equal proportions of liquid and vapor; many contain small opaque daughter crystals (arrow) of constant relative size	Deep barren and deep central and peripheral Cu-Au (Mo) ore zones in PCD; porphyry-associated skarns	300–650	2–16
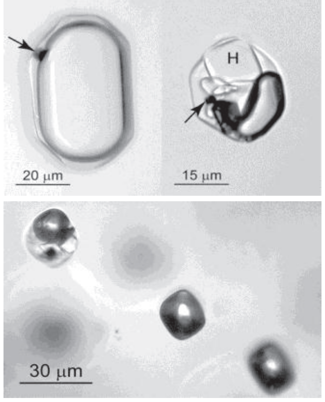	*Vapor-rich inclusions* can be high- (60-90% vapor) or low-density (>90% vapor) and commonly contain small opaque daughter crystals (arrow); *hypersaline liquid inclusions* always contain a vapor bubble, a saline aqueous liquid and halite (H); additionally, polyphase inclusions contain a few other transparent and opaque daughter phases; in many cases vapor-rich and hypersaline liquid inclusions form boiling assemblages	Stockwork mineralization at moderate to shallow depth in central parts of Cu-Au (Mo) ore zones and upper parts of Cu-rich periphery; porphyry-associated skarns	260–650, rarely up to 800	*vapor:* 0.2–20 *hypersaline liquid:* 26–75
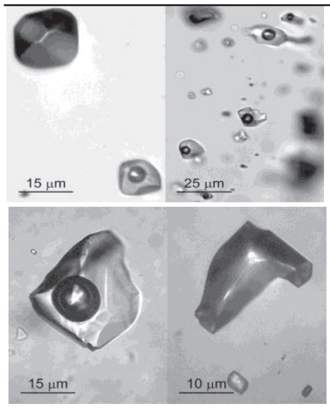	*Aqueous low- to intermediate-salinity inclusions* with predominantly liquid water and smaller vapor bubbles ranging from 20 to 40 vol % may occur together or not with *low-density vapor-rich inclusions* (>90 % vapor); aqueous inclusions are usually free of daughter crystals; however, some may contain accidentally trapped sericite crystals; coexistence of aqueous and low-density vapor inclusions is indicative of fluid boiling at low pressure	Late-stage porphyry veining (quartz-sericite-pyrite); base and precious metal mineralization in skarns, carbonate-replacement and epithermal orebodies	150–450	*vapor:* <0.5 *liquid:* 0–20

liquid, whereas during the retrograde stage low-to-moderate salinity aqueous fluids are dominant (e.g., Meinert et al., 2003, 2005; Baker et al., 2004; Vallance et al., 2009; Williams-Jones et al., 2010). In contrast, in the shallow, low-pressure and temperature, high-sulfidation epithermal environment, ore-precipitating fluids are aqueous solutions of low-to-moderate salinity, 0.2 to 8 wt % NaCl equiv (e.g., Mancano and Campbell, 1995; Ruggieri et al., 1997; Jannas et al., 1999; Wang et al., 1999; Kouzmanov et al., 2002; Molnár et al., 2008; Moritz and Benkhelfa, 2009; Fig. 1). However, these low salinity fluids are still dominantly of magmatic origin, as evidenced by stable isotope analyses of alteration minerals (e.g., Vennemann et al., 1993; Hedenquist et al., 1998; Catchpole et al., in review).

The formation and properties of the four main fluid types are largely controlled by the PVTX properties of a water-salt-volatile system, which may be reasonably approximated by the well-known H_2O-NaCl system (Fig. 3).

PVTX evolution of single-phase magmatic fluid on ascent: Figure 3, based on the H_2O-NaCl model system (Sourirajan and Kennedy, 1962; Driesner, 2007; Driesner and Heinrich, 2007), schematically illustrates possible evolutionary pathways of an intermediate-density aqueous fluid exsolved from a hydrous magma at depth, on its ascent through porphyry and epithermal environments toward the surface, projected onto pressure-composition and pressure-temperature space (according to Heinrich, 2007, and Richards, 2011). The fluid paths are strongly controlled by the initial density, and salt and volatile composition of the exsolved magmatic fluid and the nature of its pressure-temperature evolution, which can vary from deposit to deposit. According to Richards (2011) such paths are summarized as follows (Fig. 3): (1) path 1 illustrates the generation and deep exsolution of a single-phase magmatic fluid with initial salinity of 2 to 10 wt % NaCl equiv, at magmatic temperature and pressure exceeding 1 kbar; (2) path 2 illustrates magmatic fluid exsolution from shallowly

Typical Ranges of Temperature, Salinity, Pressure, Density, Metal, and Sulfur Concentrations (range and average)[1]

Pressure (bar)	Density (g/cm^3)	Cu (ppm)	Mo (ppm)	Au (ppm)	Ag (ppm)	As (ppm)	Sb (ppm)	Zn (ppm)	Pb (ppm)	S (ppm)
300– >2000	0.4–0.7	20–20000	2–300	<1–20	<1–300	20–2000	<1–30	20–6500	10–4500	2600–23000
		2660	70	1.6	30	250	9	600	330	9400
90–1300	*vapor:* 0.01–0.4	<1–33000	1–70	0.05–11	<1–600	2 –1200	1–150	<1–6800	<1–4000	960–26000
		4300	25	1.9	45	175	35	660	340	6300
	hypersaline liquid: 0.8–>1	3–30000	1–2000	0.03–22	2–3400	6–6600	1–1200	90 –40000	5 –60000	220–25000
		4770	180	1.5	95	230	95	4620	3790	7600
<100	*vapor:* <0.02	No data available for metals								
	liquid: 0.1–0.6	<1–5500	2–160	0.08–26	<1–100	<1–3200	<1–950	<1–22000	<1 –4000	810–11280
		325	30	2.9	10	415	85	715	165	2700

---

[1] Data sources: Allan et al. (2011), Anderson et al. (1989), Audétat et al. (2000a, b), Audétat and Pettke (2003), Audétat et al. (2008), Baker et al. (2004), Beuchat et al. (2004), Catchpole et al. (2011, in review), Cline and Vanko (1995), Gysi and Herbort (2006), Harris et al. (2003), Heinrich et al. (1992, 1999), Kamenetsky et al. (2002, 2004), Kehayov et al. (2003), Klemm et al. (2007, 2008), Kostova et al. (2004), Kotzeva et al. (2011), Kouzmanov et al. (2010), Kurosawa et al. (2003, 2010), Landtwing et al. (2005, 2010), LeFort et al. (2011), Müller et al. (2001), Pettke (2008), Pettke et al. (2001, 2012), Pudack et al. (2009), Rusk et al. (2004, 2008b, c), Seo et al. (2009, 2011, 2012), Ulrich et al. (1999, 2001), Vanko et al. (2001), Wallier et al. (2006), Williams-Jones and Heinrich (2005), Williams-Jones et al. (2010), Wolfe and Cooke (2011). Abbreviations: hom = homogenization, PCD = porphyry copper deposits

emplaced magma; and (3) paths 3 and 4 refer to single-phase magmatic fluid evolution through the porphyry to the shallow epithermal environment without and with intersection of the two-phase vapor-liquid domain of the NaCl-H_2O system, respectively.

During decompression, the ascending magmatic fluid of relatively low salinity will intersect the two-phase liquid + vapor surface (V-L solvus) on the vapor-rich side of the critical curve, leading to condensation of small amounts of hypersaline liquid from the intermediate-density juvenile fluid (path 4; Fig. 3a). This results from the physical-chemical properties of the H_2O-NaCl ± CO_2 system that allow for a large domain of coexistence of the vapor and hypersaline liquid, extending over a temperature range from 700° to ~200°C and with pressures below ~1.5 kbar (Sourirajan and Kennedy, 1962; Takenouchi and Kennedy, 1965; Henley and McNabb, 1978; Fig. 3). This fluid unmixing results in the generation of two phases, a vapor and a liquid, with contrasting density, salinity, and volatile and metal content (Table 1); this process has important implications for ore-forming processes both in the porphyry and epithermal environments. Henley and McNabb (1978) suggested that the hypersaline liquid phase, because of its high density and viscosity that restrict its upward migration, would accumulate at depth close to the site of phase separation, and then progressively drain under gravity and divert toward the margins of the system. In contrast, the more voluminous and lower-density vapor phase, rich in volatile components, would dominate the center of the system and form a magmatic vapor plume over the top of the porphyry intrusion due to its low-density, buoyant nature (Henley and McNabb, 1978; Fournier, 1999). Toward the periphery of the system, mixing with groundwater would eventually cause dilution and decrease of the magmatic component of the fluids.

If hydrous magma is emplaced at shallow depth, under low pressure within the two-phase V+L field (path 2; Fig. 3), its

TABLE 2. Comparative Terminology of the Main Fluid Inclusion Types in Porphyry Systems

Fluid inclusion types (this study),	Terminology used in the literature for petrographically similar fluid inclusion types	References
Single-phase	B60	Rusk et al. (2004, 2008b, c, 2011)
	Critical	Baker et al. (2004)
	Deep supercritical magmatic fluid	Richards (2011)
	High-temperature magmatic fluid	Hedenquist and Richards (1998)
	Intermediate-density	Catchpole et al. (in review), Klemm et al. (2007, 2008), Pudack et al. (2009), Seo et al. (2012)
	Liquid-rich low salinity	Cline and Bodnar (1994)
	Liquid-rich with V>50%	Beane and Bodnar (1995), Bodnar and Beane (1980)
	Liquid-vapor aqueous (liquid fraction 0.3-0.7),	Allan et al. (2011)
	Moderate salinity inclusions	Nash (1976)
	Single-phase	Audétat et al. (2000a, 2008)
	Supercritical fluid	Audétat and Pettke (2003)
	Two-phase	Kurosawa et al. (2003)
	Vapor-rich low salinity	Cline and Bodnar (1994)
Vapor-rich	B85	Rusk et al. (2004, 2008c)
	Gas rich	Nash (1976)
	Liquid-vapor aqueous (liquid fraction <0.3),	Allan et al. (2011)
	Steam	Roedder (1971)
	Vapor	Audétat and Pettke (2003), Audétatet al. (1998, 2000a, 2000b, 2008), Baker et al. (2004), Catchploe et al. (2011, 2012), Heinrich et al. (1992, 1999), Klemm et al. (2007, 2008), Landtwing et al. (2005, 2010), Pudack et al. (2009), Richards (2011), Seo et al. (2009, 2011, 2012), Ulrich et al. (1999, 2001)
	Vapor-phase	Cauzid et al. (2007)
	Vapor rich	Beane and Bodnar (1995), Cline and Bodnar (1994), Harris et al. (2003), Hedenquist and Richards (1998), Kamenetsky et al. (2002), Kouzmanov et al. (2010), Wolfe and Cooke (2011)
Hypersaline liquid	Aqueous inclusions with solid daugther phases	Allan et al. (2011)
	B15H	Rusk et al. (2004, 2008c)
	Brine	Audétat and Pettke (2003), Audétatet al. (1998, 2000a, 2000b, 2008), Baker et al. (2004), Catchpole et al. (2012), Guillong et al. (2008), Harris et al. (2003), Heinrich et al. (1992 (1999), Kamenetsky et al. (2002), Klemm et al. (2007, 2008), Landtwing et al. (2005, 2010), Pudack et al. (2009), Richards (2011), Seo et al. (2009, 2011, 2012), Ulrich et al. (1999, 2001), Wolfe and Cooke (2011)
	Halite-bearing	Nash (1976), Eastoe (1978), Beane and Bodnar (1995)
	Hypersaline liquid	Redmond et al. (2004)
	Hypersaline liquid-rich	Hedenquist and Richards (1998)
	Liquid-phase	Cauzid et al. (2007)
	Liquid rich	Cline and Bodnar (1994)
	Liquid-vapor-halite / LVH	Kouzmanov et al. (2010), Williams-Jones et al. (2010)
	Multiphase	Bodnar and Beane (1980), Kamenetsky et al. (2004), Roedder (1971)
	NaCl-saturated liquid rich	Hedenquist et al. (1998)
	Polyphase	Kurosawa et al. (2003)
	Polyphase hypersaline	Harris et al. (2003)
Low-salinity aqueous	Aqueous	Audétat et al. (2000), Klemm et al. (2007, 2008), Landtwing et al. (2005, 2010), Pudack et al. (2009), Seo et al. (2012)
	B20	Rusk et al. (2004, 2008c)
	NaCl-undersaturated liquid rich	Hedenquist et al. (1998)
	Liquid rich	Baker et al. (2004), Catchpole et al. (2011, in review), Wolfe and Cooke (2011)
	Liquid rich low-salinity	Cline and Bodnar (1994)
	Liquid rich with V<50%	Beane and Bodnar (1995), Bodnar and Beane (1980)
	Liquid-vapor / LV	Kouzmanov et al. (2010), Williams-Jones et al. (2010)
	Moderately saline liquid	Richards (2011)
	Liquid-vapor aqueous (liquid fraction >0.7),	Allan et al. (2011)
	Two-phase	LeFort et al. (2011), Roedder (1971)

crystallization leads to expulsion of high-temperature, low-density vapor with minor segregation of hypersaline brine, the salinity of which normally exceeds 60 wt % NaCl equiv. The vapor, enriched in acidic volatiles (SO_2, HCl), condenses into groundwater on ascent toward the surface, producing an acidic solution; this leads to leaching (residual quartz, typically with a vuggy texture) and pervasive advanced argillic alteration, in the upper parts of magmatic-hydrothermal systems (Fig. 1; Hedenquist and Aoki, 1991; Rye, 1993; Hedenquist et al., 1998; Sillitoe, 2010; Chang et al., 2011). High sulfidation epithermal Au deposits can subsequently form in this environment, where the residual quartz provides the permeable host for metal deposition, introduced by later aqueous fluids that are also magmatic in origin (e.g., Deen et al., 1994; Hedenquist et al., 1994b, 1998; Arribas, 1995; Bethke et al., 2005; Deyell et al., 2005a, b; Baumgartner et al., 2008).

Richards (2011) summarized two scenarios to explain how a single-phase intermediate-density magmatic fluid can evolve into an epithermal aqueous ore-forming solution without significant loss of metals due to sulfide precipitation: (1) cooling at sufficient pressure, prohibiting the single-phase fluid from intersecting the two-phase V-L surface before reaching epithermal pressure and temperature conditions (path 3; Fig. 3), as suggested by Hedenquist et al. (1998); (2) brief intersection of the V-L solvus at high pressure and temperature (path 4; Fig. 3a), resulting in partitioning of salts and chloride-complexed metals (e.g., Fe, Pb, Zn) into a small portion of hypersaline liquid, whereas Au ± Cu partition into the vapor phase, which eventually cools and contracts to a low-salinity aqueous liquid, as proposed as an alternative by Heinrich et al. (2004) and Heinrich (2005, 2007). In both cases, the resulting epithermal fluid will lie on the liquid side of the solvus, because of the curvature of the critical curve to lower salinities at low temperatures (Fig. 3a). Subsequent near-surface boiling of this low-salinity aqueous solution and loss of H_2S will cause metal deposition at the low pressures and temperatures of the epithermal environment (see below for details).

Temperature-salinity characteristics of fluids: The two main parameters of fluid inclusions routinely obtained from microthermometric experiments are the temperature of homogenization and salinity. Homogenization temperature (Th) is the temperature at which a fluid inclusion transforms from a multiphase (heterogeneous) to one-phase (homogeneous) state (Diamond, 2003). In general, Th provides an estimate of the minimum temperature of entrapment. For coexisting liquid and vapor inclusions, a unique estimate of temperature and pressure of entrapment is possible using the well-known PVTX properties of the H_2O-NaCl (-CO_2) system (e.g., Roedder and Bodnar, 1980; Sterner and Bodnar, 1985; Sterner et al., 1988); in all other cases a correction is required. This correction concerns the temperature of formation, which may be independently estimated using different geothermometers (e.g., trace element- or stable isotope-based geothermometers). In porphyry systems, such a correction usually does not exceed 50° to 100°C for low-salinity aqueous fluids; however, for single-phase fluids, it may reach 200° to 250°C (Rusk et al., 2008b), implying that entrapment temperatures may be much higher than the measured Th. Being unable to determine or predict the true temperature of entrapment in many cases for the published fluid inclusion data, we use Th as the best proxy available for temperature of formation in the following text when discussing variations of physical parameters or element concentrations of fluid inclusions as a function of temperature. The second parameter, salinity, corresponds to the amount of solutes in aqueous solution, including electrolytes (e.g., NaCl, KCl) and nonelectrolytes (e.g., CO_2), and can be estimated based on temperature of final dissolution of solids (ice, hydrohalite, clathrate, or halite) and experimental phase equilibria in the NaCl-H_2O (-CO_2) model system (Bodnar and Vityk, 1994; Diamond, 1994).

Data base for this study: In this paper we compiled a large dataset of published fluid compositions, temperatures of homogenization, and salinity measurements, which includes 801 fluid inclusion assemblages[1] (with 2–17 inclusions per assemblage) and 469 single fluid inclusions from more than 30 deposits in porphyry Cu, Cu-Au, Mo, and Cu-Mo systems, Sn-W–mineralized granites, and various porphyry-related vein and epithermal deposits. Data are classified into the four main fluid inclusion types as follows: single-phase, 109 assemblages and 84 single inclusions; hypersaline liquid, 352 assemblages and 112 single inclusions; vapor-rich, 153 assemblages and 7 single inclusions; and low-to-intermediate salinity aqueous inclusions, 187 assemblages and 266 single inclusions (data sources in Table 1).

Figure 4 illustrates the homogenization temperatures and salinities of the four types of fluid inclusions in porphyry systems discussed in this paper. The largest amount of microthermometric data exists on hypersaline liquid inclusions, but their abundance is due mostly to the relative ease of obtaining microthermometric data compared to vapor-rich or single-phase inclusions. Values of Th for hypersaline liquid inclusions vary from ~250° to >700°C; their salinities (limited by the NaCl saturation curve in Fig. 4) range from 26 to >65 wt % NaCl equiv. The few data points that lie above the NaCl curve may result from (1) heterogeneous entrapment of a NaCl-saturated fluid, or (2) post-entrapment modification of the fluid inclusions (Becker et al., 2008). Due to similarities in their properties (Table 1), single-phase, vapor-rich, and low-to-moderate salinity aqueous inclusions partially overlap in the ranges of 350° to 420°C and 0 to 10 wt % NaCl equiv; this can create confusion regarding the definitions given by different authors to these inclusions (Table 2). However, single-phase, intermediate density inclusions, regarded as analogues of the parental magmatic fluid (Redmond et al., 2004; Audétat et al., 2008; Rusk et al., 2008; Landtwing et al., 2010), have, on average, higher salinities than vapor-rich inclusions, usually between 5 and 10 wt % NaCl equiv for identical Th intervals, between 350° and ~650°C (Fig. 4).

At temperatures of <320°C, corresponding to formation of retrograde assemblages in skarns, porphyry-related veins and replacement bodies, and epithermal deposits, the dominant inclusions are the low-to-intermediate salinity aqueous type. Hypersaline liquid inclusions at these temperatures are uncommon, but they may be produced in some cases by boiling of a low-salinity aqueous fluid at low pressure and temperature (e.g., Simmons and Browne, 1997). Low-density, vapor-rich inclusions also result from boiling of a moderate-salinity aqueous liquid; however they are not shown on the temperature-salinity plot in Figure 4, because of difficulties in obtaining the corresponding microthermometric data.

---

[1] The term "fluid inclusion assemblage" (FIA) was introduced by Goldstein and Reynolds (1994) for simultaneously trapped (cogenetic) fluid inclusions occupying an individual petrographic feature (e.g., crystal-growth zone, healed fracture). Working with FIAs rather than individual fluid inclusions allows the identification of a fluid inclusion population that is representative of a given hydrothermal event; the standard deviation of various physical parameters and composition of the fluids can also be determined. The geologic meaning of the data acquired can be better evaluated and data scatter can be attributed to natural variations or to various fluid processes.

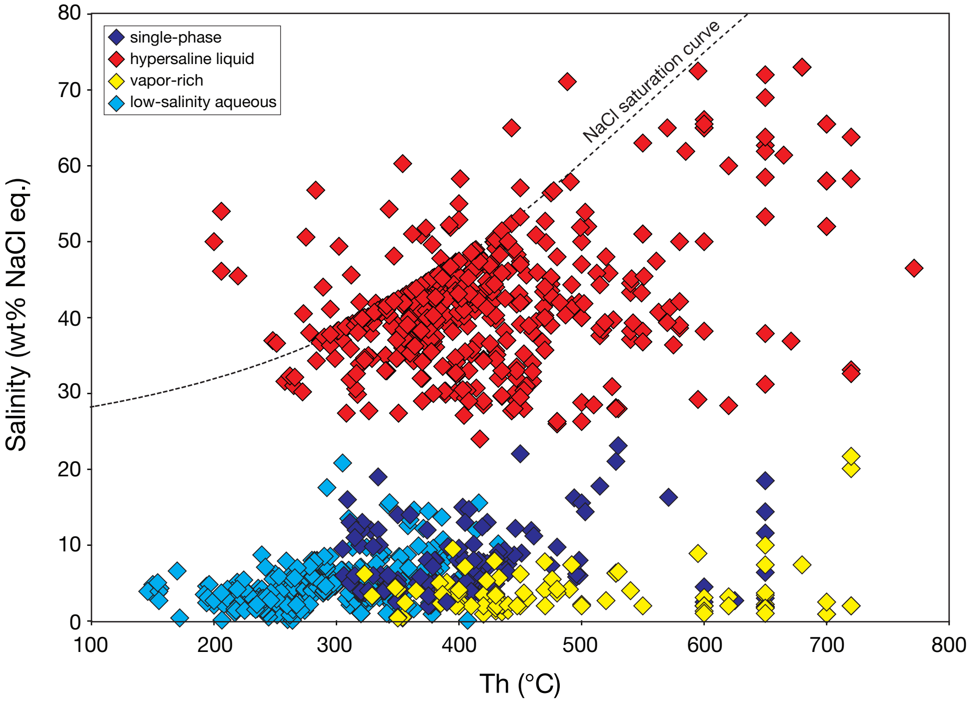

FIG. 4. Plot of salinity vs. temperature of homogenization for the four main fluid inclusion types in porphyry systems summarized in Table 1: single-phase: intermediate-density aqueous inclusions (with liquid/vapor ≈ 1 at room temperature), representing the single-phase magmatic fluid; hypersaline liquid: high-salinity liquid inclusions, usually containing saline aqueous liquid, vapor bubble, and halite, sometimes also other transparent and/or opaque daughter phases at room temperature; vapor-rich: high- and low-density vapor-rich inclusions containing >60% vapor at room temperature; low-salinity aqueous: liquid-rich low to intermediate salinity inclusions (<40% vapor at room temperature), free of daughter crystals. Almost all data points correspond to average values for fluid inclusion assemblages (FIAs), where several inclusions were measured (see Table 1 for data sources).

Composition of Ore Fluids in Porphyry Cu-Mo-Au Systems

Metal concentrations in ore fluids: Insights from fluid inclusion analyses

In the 1990s, LA-ICP-MS, PIXE, and SR-XRF analytical techniques were successfully applied to measure metal concentrations in individual fluid inclusions from magmatic-hydrothermal systems (e.g., Anderson et al., 1989; Ryan et al., 1991; Heinrich et al., 1992; Rankin et al., 1992; Wilkinson et al., 1994; Audétat et al., 1998; Günther et al., 1998). As a result, a large amount of data on metal concentrations in ore-bearing fluids from a variety of porphyry and associated deposits was generated. The first compilation of the data was reported by Williams-Jones and Heinrich (2005) in their review of vapor transport of metals; they compared the concentrations of metals in vapor discharged from volcanic fumaroles with data from fluid inclusions in magmatic-hydrothermal systems and concluded that the metal-transporting capacity of aqueous fluids and vapors at depth is much higher than that of low-pressure and hence low-density volcanic vapors. Later, Audétat et al. (2008) discussed the composition and metal content of fluids from 17 mineralized and barren magmatic-hydrothermal systems; they demonstrated that the metal content of magmatic aqueous fluids correlates positively with the type and amount of mineralization in the associated intrusions. Wilkinson et al. (2008) compared LA-ICP-MS analyses of single-phase and hypersaline liquid inclusions from the Chuquicamata and El Teniente, Chile, and Butte porphyry Cu deposits and suggested that both fluid types may be equally capable of transporting Cu, and that their relative mass proportion in the system will influence Cu mobility and spatial distribution. Recently, Rusk et al. (2011) reported analyses of single-phase, parental magmatic fluid from ten of the largest porphyry Cu, Cu-Mo, Mo, and Cu-Au deposits, pointing out that this fluid was trapped at near-magmatic temperatures and pressures (~600°C and 1.5–2.5 kbars), and was dominated by Na, K, and Cu, with subordinate Fe; Na/K ratios range between 1 and 4, and most of the Na/Cu ratios range from 1 to 200.

Our compilation of the concentrations of metals (Mn, Fe, Cu, Zn, As, Mo, Ag, Sb, Au, Pb) and major alkalis (Na, K) in the four fluid types in porphyry systems defined in this study is summarized in Table 1 and presented for selected metals in Figure 5. The general features of metal concentration patterns are discussed below.

For each fluid inclusion type, large variations in metal content have been observed, up to two orders of magnitude for most metals in the single-phase type and up to four orders of magnitude in the other three fluid types. For single-phase fluids trapped at near magmatic temperatures and having the most pristine magmatic signatures (i.e., prior to modification by cooling, fluid unmixing, wall-rock reaction, and mineral precipitation), these variations should reflect variability in

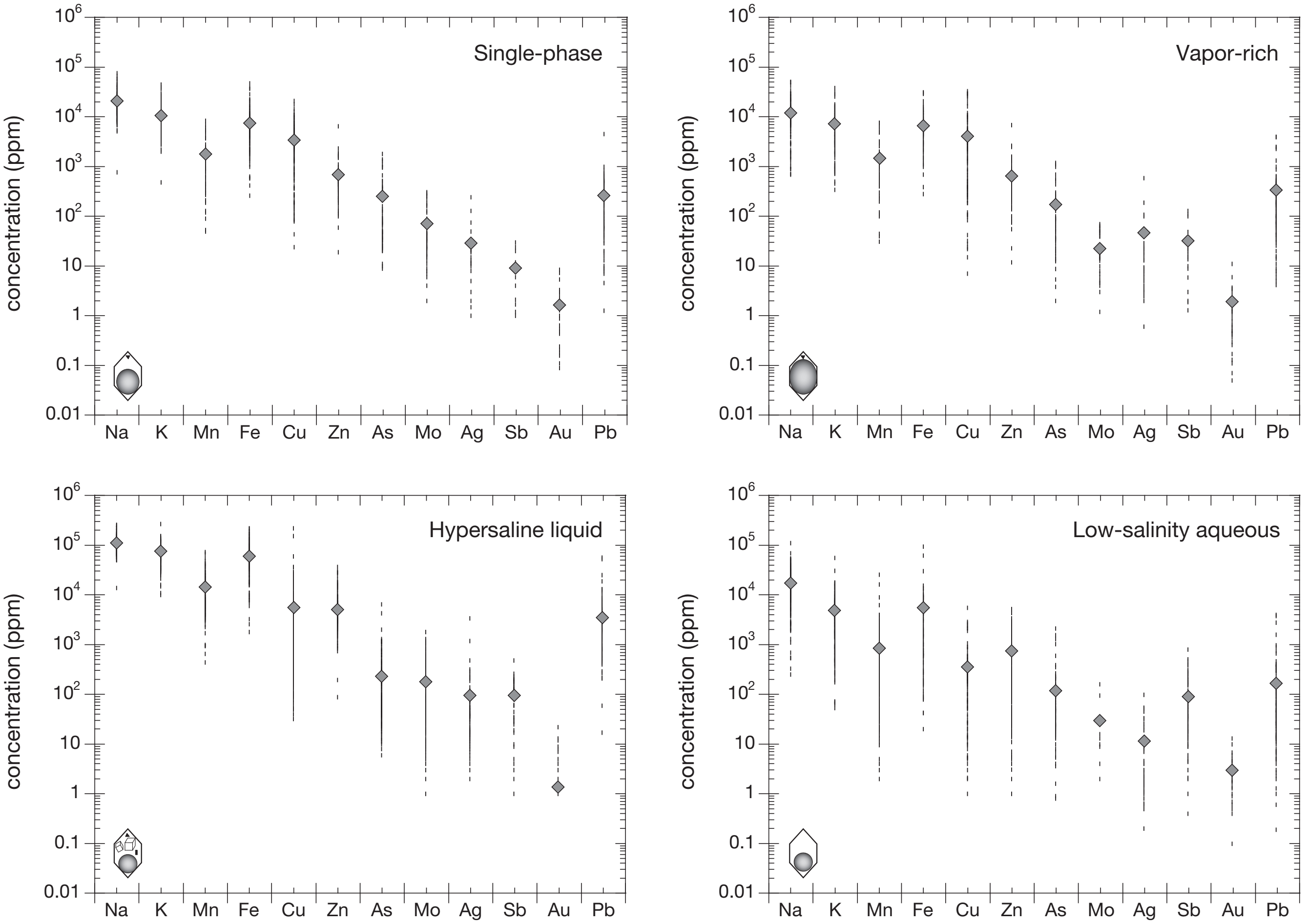

FIG. 5. Alkali (Na and K) and metal (Mn, Fe, Cu, Zn, As, Mo, Ag, Sb, Au, Pb) concentrations (in ppm) in single-phase, hypersaline liquid, vapor-rich and low salinity aqueous inclusions in porphyry systems. Average concentrations are shown by gray diamonds; vertical bars reflect data scatter. Elements are arranged on the horizontal axis by mass (see Table 1 for data sources).

chemical and physical parameters of the parental magma, including composition, depth and pressure, and redox state (Audétat and Simon, 2012). The larger variations for hypersaline liquid, vapor-rich, and low-salinity aqueous inclusions can be explained by metal fractionation upon unmixing and cooling plus mineral precipitation.

Copper exhibits the largest concentration range amongst the metals, varying more than three orders of magnitude. Its concentrations span from 10s to 10,000s ppm, with a maximum value of ~20,000 ppm in single-phase fluid inclusions, , from a few ppm to ~30,000 ppm in vapor-rich and hypersaline liquid inclusions, , and from ≤1 ppm to 5,500 ppm in low salinity aqueous inclusions (Fig. 5). Such variations likely reflect a combination of factors, such as magma characteristics, silicate melt-fluid partitioning, fluid unmixing, mineral precipitation, and, as recently demonstrated, very likely significant post-entrapment modifications, particularly in the vapor-rich inclusions (as discussed below). Molybdenum shows similar concentrations in single-phase and vapor-rich fluids (10s ppm on average), whereas in hypersaline liquid inclusions Mo attains several 100s ppm, with a maximum of 2,000 ppm. This was attributed to Mo enrichment in the hypersaline liquid as a result of fluid unmixing in the porphyry regime (e.g., Klemm et al., 2008) prior to molybdenite precipitation. Gold tenors in the different fluid types are highly variable—from 0.0 *n* to *n* ppm, uncommonly up to 20 ppm; in most cases, gold concentrations are below the limit of detection (LOD), and in the present compilation only significant values (>LOD) for Au are taken in account. Gold mean concentrations in single-phase, hypersaline liquid, and vapor-rich inclusions are similar, 1.6, 1.4, and 1.9 ppm, respectively. Low salinity aqueous fluids show the highest average content of Au, 3.0 ppm, as well as the highest Au concentration reported, 26 ppm (Table 1; Fig. 5). Silver has an average content of 10s ppm in all fluid types; however, in hypersaline liquid inclusions, Ag can attain several 1,000s ppm, with a maximum of 3,400 ppm. Lead and zinc have very similar behavior—their average concentration in single-phase, vapor-rich, and low salinity aqueous fluids is on the order of 100s ppm, and attains several 1,000s ppm in hypersaline liquids, with a maxima of 40,000 and 60,000 ppm for Zn and Pb, respectively. This is due to transport of these metals dominantly as highly soluble chloride complexes (discussed below).

Based on the mean concentrations calculated for different elements, the following relative abundance trends for the four fluid inclusion types can be established:

1. Single-phase inclusions: Na>K>Fe>Cu>Mn>Zn>Pb ≈ As>Mo>Ag>Sb>Au;
2. Hypersaline liquid inclusions: Na>K>Fe>Mn>Cu ≈ Zn ≈ Pb>As ≈ Mo>Ag ≈ Sb>Au;
3. Vapor-rich inclusions: Na>K ≈ Fe>Cu>Mn>Zn ≈ Pb>Ag ≈ Sb ≈ Mo>Au;
4. Low salinity aqueous inclusions: Na>K ≈ Fe>Mn ≈ Zn>Cu ≈ Pb>Sb ≈ As>Mo>Ag>Au.

Some of these trends may be explained by the relative solubility of different metal-controlling solid phases, coupled with the abundance of complexing ligands (Cl, S) in the different fluid types (see below). In addition, a positive correlation exists between the average concentration of metals in the pristine single-phase magmatic fluids and their average abundance in the crust (Fig. 6; Rudnick and Gao, 2003). Except for Fe and Mn, which are abundant elements in the Earth's crust, the absolute concentrations of all other ore-relevant metals in single-phase inclusion fluids are systematically one to three orders of magnitude higher than their average Clarke values in crustal rocks and magmas (Fig. 6). This agrees with aqueous fluid/silicate melt partitioning coefficients of 10 to 1,000 for most metals, as shown by experimental studies (e.g., Candela, 1989; Simon et al., 2008; Zajacz et al., 2008), supporting the magmatic origin of the single-phase fluid type.

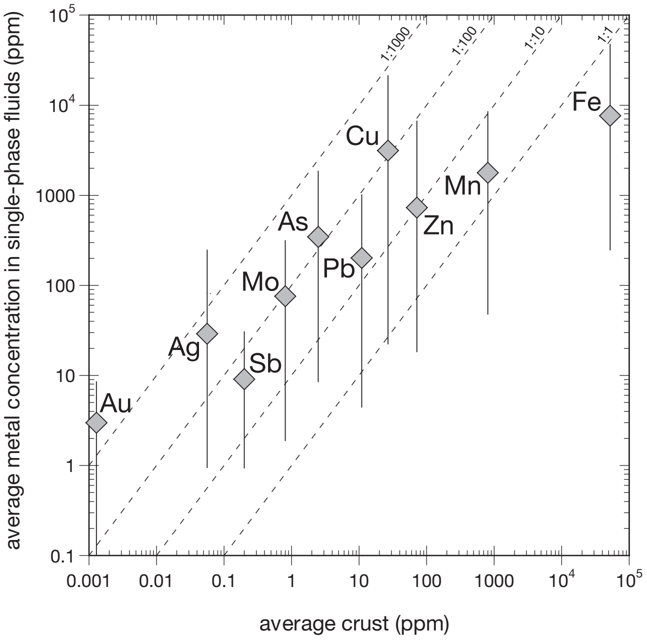

FIG. 6. Average metal concentrations (in ppm) in single-phase magmatic fluids from porphyry systems compared to their average crustal abundance (Clarke values; data from Rudnick and Gao, 2003). Vertical bars correspond to data scatter. Most metals, except Fe and Mn which are major elements in the crust, show one to three orders of magnitude higher concentrations in the juvenile magmatic single-phase fluid than their Clarke values (see text for discussion).

Metal concentrations as a function of fluid temperature and salinity

The compiled data are plotted versus Th and salinity in Figures 7 and 8 for Cu, Au, and accompanying metals (Mo, Ag, Zn, Pb, Fe, Mn). There is no clearly defined correlation between Th and metal content of the different fluid types. This may be due to: (1) potentially large differences between the Th values and the true entrapment temperature (particularly for single-phase and low salinity aqueous inclusions, as discussed above), and (2) the variability of factors other than temperature, which may strongly affect the solubilities of metals (e.g., fluid acidity, H_2S content; see below). However, several tendencies may be identified.

First, fluids of high-temperature inclusion types (single-phase, hypersaline liquid, and vapor-rich) exhibit comparable concentrations at Th >400°C for each element in the group Cu, Au, Mo, and Ag, within data scatter of ±1 order of magnitude; in contrast, Zn, Pb, Fe, and Mn in the hypersaline liquid inclusions systematically show one order of magnitude higher concentrations than the single-phase and vapor-rich inclusions. Second, local changes in temperature trends may be seen at Th ~400°C for some metals. Thus, at Th >400°C, Cu contents normally vary between 100 and 10,000 ppm; at 400° ± 25°C, Cu reaches a well-defined maximum of ~30,000 ppm in some hypersaline liquid and vapor-rich fluid inclusion assemblages (except for a few data points with Th values of ~600°–650°C; Fig. 7a); this behavior is not noted for the other metals. At Th <400°C, Cu, Zn, Pb, and Mn concentrations show a pronounced decrease with decreasing temperature; this tendency is most obvious for aqueous fluid inclusions, which exhibit more than 3 orders of magnitude decrease in Cu, Zn, Pb, and Mn between 400° and 200°C (from >1,000 ppm to a few ppm; Fig. 7). Third, in contrast to Cu, Zn, Pb, and Mn, the low salinity aqueous fluids with Th of 350° to 250°C show the highest gold concentrations, reaching 20 ppm in some inclusions. As mentioned above, this fluid type also shows the highest average Au concentration of ~3 ppm. In addition to the potential formation of highly soluble aqueous Au complexes with sulfur ligands (discussed below), such high concentrations might also reflect heterogeneous entrapment of gold nanoparticles from the fluid at temperatures of <350°C, as suggested by Wallier et al. (2006), Pudack et al. (2009), and Kouzmanov et al. (2010) for some intermediate and high sulfidation epithermal systems; gold transport and deposition as nanoparticles has also been proposed for some low sulfidation bonanza-grade epithermal veins (e.g., Saunders, 1990; Saunders and Schoenly, 1995).

Hypersaline liquid inclusions (salinity >26 wt % NaCl equiv) plot in distinct fields on the salinity versus metal concentration diagrams (Fig. 8), with Zn, Pb, Mn, Fe, and Ag typically an order of magnitude higher than in single-phase, vapor, or low-salinity aqueous inclusions. This is explained by the increasing stability of chloride species of the above-mentioned elements in salt-rich fluids (see below). Molybdenum, Cu, and Au show a more variable pattern. Some hypersaline liquid inclusions have Mo contents identical to single-phase and vapor inclusions (1–100 ppm), but a large number of hypersaline liquid inclusions have higher concentrations (100–2,000 ppm; Fig. 8). Gold does not show any dependence on

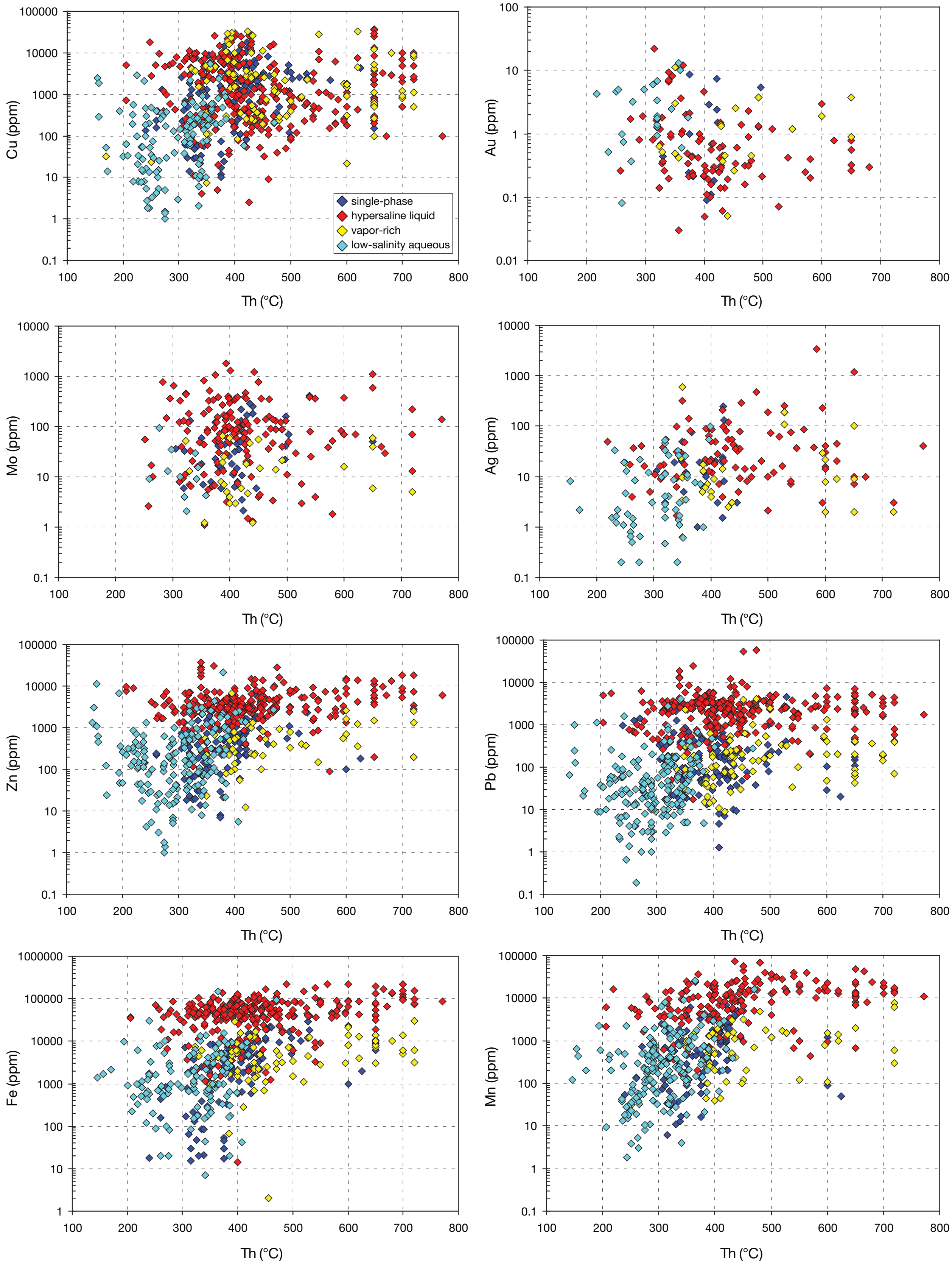

FIG. 7. Concentrations of metals (in ppm) in single-phase, hypersaline liquid, vapor-rich and low-salinity aqueous inclusions in porphyry systems as a function of temperature of homogenization (°C)(see Table 1 and Figure 4 for fluid types and data sources).

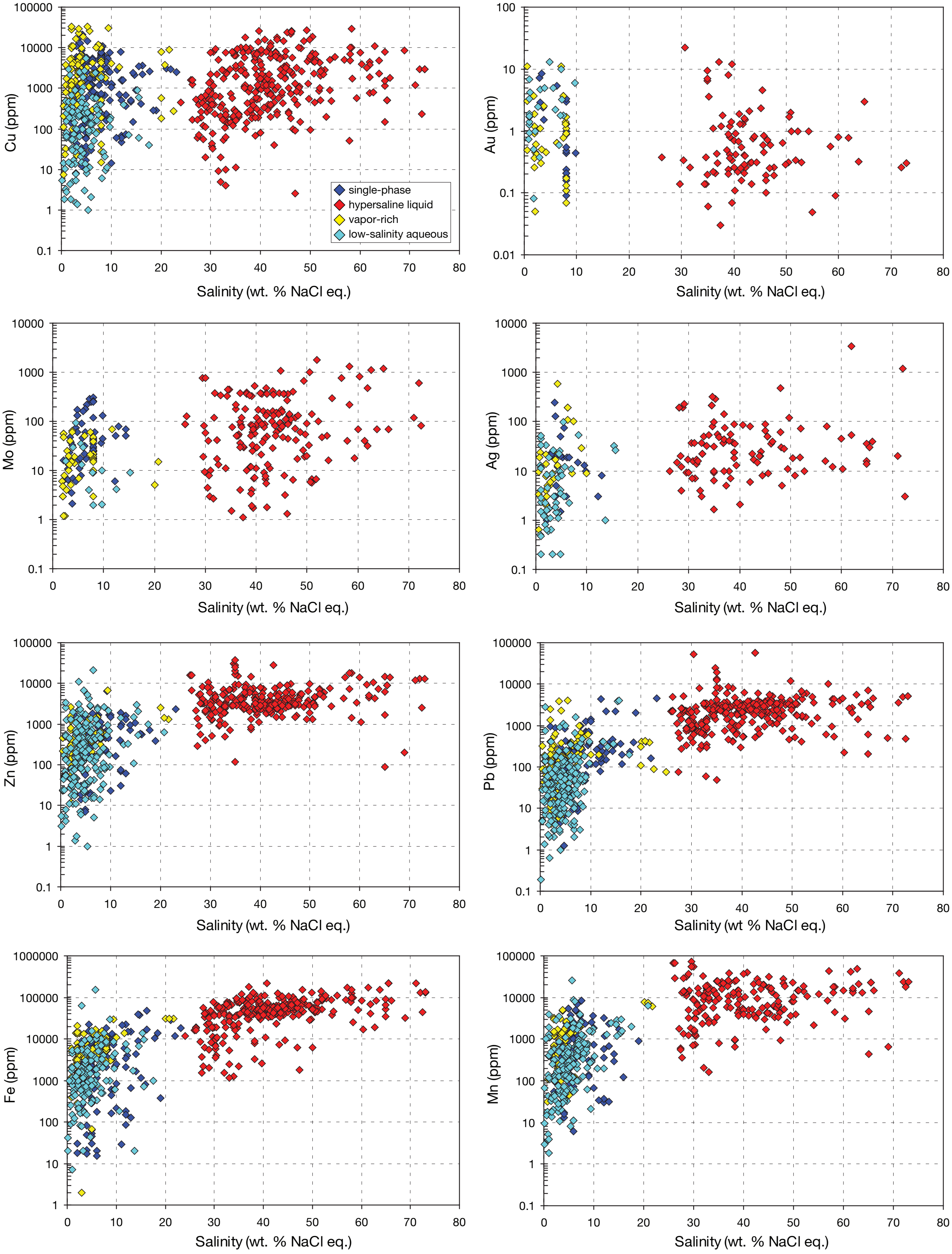

FIG. 8. Plots of metal concentrations (in ppm) in single-phase, hypersaline liquid, vapor-rich and low-salinity aqueous inclusions in porphyry systems as a function of apparent salinity (wt % NaCl equiv)(see Table 1 and Fig. 4 for fluid types and data sources).

salinity, consistent with the dominant presence of Au-sulfide complexes in most S-rich hydrothermal fluids (see below).

Single-phase and vapor inclusions systematically show higher Cu contents than those in aqueous fluids of the same salinity but lower temperature; this can be explained by decrease of the solubility of Cu sulfide minerals with cooling. However, recent studies suggest that the high Cu contents in vapor-rich and single-phase inclusions (up to 33,000 ppm; Table 1) are likely due to post-entrapment modifications. Lerchbaumer and Audétat (2012) conducted laboratory experiments on synthetic and natural coexisting vapor-rich and hypersaline liquid inclusions, subjected to re-equilibration with external fluids of different compositions. Their findings suggest that the Cu enrichment in the high-temperature vapor-like inclusions, reported in many studies, may be a result of post-entrapment Cu diffusion from the cooling external fluid into the S-rich inclusion fluid, previously trapped at higher temperature. Although the quantitative interpretation of this phenomenon both in natural and synthetic inclusions requires accurate knowledge of fluid composition, sulfur and copper aqueous speciation, and solution pH and their evolution over time and with temperature and pressure, the fundamental driving force of the diffusion is likely to be the low solubility of Cu-bearing sulfides, like chalcopyrite, in S-rich fluids with decreasing temperature (see below). The precipitation of Cu-bearing sulfides in the inclusion on cooling lowers the aqueous Cu^+ concentration in the inclusion. This creates a diffusion gradient between Cu^+ concentrations inside the S-rich inclusion and in the external fluid, which has lost most of its sulfur on cooling. This concentration gradient, coupled with elevated Cu^+ diffusion coefficients along the crystallographic c-axis of quartz (Lerchbaumer and Audétat, 2012, references therein), leads to Cu diffusion from the external fluid and its accumulation in the S-rich inclusion in the form of chalcopyrite or another Cu-bearing sulfide. The electrical charge balance in this diffusion process is likely to be maintained by H^+ and/or Na^+ diffusing out of the inclusion (Lerchbaumer and Audétat, 2012). Precipitation of copper sulfides from a saline H_2S-bearing fluid also creates additional acidity (see reactions 1a, b below), which further favors outward diffusion of H^+.

Because the solubility of Cu-S solids is far greater in S-poor salt-rich liquid phase than in the vapor (see below), S-rich vapor inclusions can accomodate more Cu than the coexisting hypersaline liquid inclusions. Thus, the elevated Cu contents in vapor-like inclusions from porphyry deposits may be due to post-entrapment modifications in many cases, depending on the thermal history of the host quartz and the chemical evolution of the surrounding fluid. Unfortunately, it is difficult to accurately estimate the degree of diffusion to determine the original Cu concentration in natural inclusions of fluid upon trapping. Gold and base metals, such as Zn, Fe, or Pb, are unlikely to be affected by such diffusion processes, because of the larger ionic radius and charge of their cations, yielding much lower diffusion coefficients than that of Cu^+ (Lerchbaumer and Audétat, 2012).

Sulfur content of ore fluids

In addition to metals, Guillong et al. (2008) and Seo et al. (2009) recently quantified by LA-ICP-MS the S contents of individual fluid inclusions from porphyry systems. Since then, Seo et al. (2011, 2012) produced a data set, including analyses of S and metals for a large number of single-phase, hypersaline liquid, and vapor-rich inclusion assemblages from the Bingham Canyon porphyry Cu-Au(-Mo) deposit. Using the same technique, Catchpole et al. (2011, in review) analyzed low to intermediate salinity aqueous inclusion assemblages from the polymetallic vein system at Morococha. The Bingham Canyon data show that the S content of most single-phase, vapor-rich, and hypersaline liquid inclusions ranges from 1,000 to 10,000 ppm, with a few inclusions attaining 30,000 ppm. At Morococha, low-salinity aqueous fluids usually have an order of magnitude lower S concentration, of 1,000s to 100s ppm. Catchpole et al. (2011) noted that in the case of Morococha, the low-to-intermediate salinity aqueous fluids have sufficient reduced S in solution to precipitate all available base metals in the fluid as sulfide minerals.

The S content of the four fluid inclusion types in porphyry systems is summarized in Table 1 and plotted in Figure 9. On average, the single-phase fluids exhibit the highest S concentrations (9,400 ppm), compared to hypersaline liquid (7,600 ppm), vapor-rich (6,300 ppm), and low salinity aqueous (2,700 ppm) inclusions (Table 1). This is in agreement with the elevated solubility of metal sulfides at high temperatures and its progressive decrease with cooling of the magmatic fluid (see below). In most cases the limit of detection is high ($\geq$1,000 ppm); rarely concentrations below 1,000 ppm have been determined (Fig. 9). There is no clear correlation between Th, fluid salinity, and S content of the different fluid inclusion types (Fig. 9a, b); there is also no apparent correlation between S and Fe, Mo, and Au of the four main fluid inclusion types (Fig. 9d-f). In contrast to these metals, the Cu content correlates positively with S content for many high-temperature and Cu- and S-rich inclusions, which plot along the 1:1 Cu/S line (Fig. 9c); the rest of the data shows an excess of S over Cu.

Interestingly, the 1:1 Cu/S plot on a ppm scale (Fig. 9c) corresponds to the 1:2 Cu/S molal ratio in the inclusion. Seo et al. (2009) initially interpreted this observation by the formation of stable volatile complexes of copper with a 1:2 Cu/S stoichiometry, which carry the major part of Cu and S in the vapor phase. However, this stoichiometry is also in agreement with that in chalcopyrite ($CuFeS_2$), which is the most likely solid phase observed in such inclusions (Sawkins and Scherkenbach, 1981; opaque mineral, Table 1). This Cu/S ratio suggests that all Cu in the inclusion is in the form of chalcopyrite, and points again to a diffusion of Cu into the inclusion driven by the precipitation of $CuFeS_2$ during post-entrapment cooling of the system. The fact that the Cu/S molal ratio never exceeds 2, within the existing data scatter (Fig. 9c), strongly suggests that the formation of chalcopyrite is the limiting factor of post-entrapment Cu enrichment. The lower Cu/S ratios (Fig. 9c) may be explained by an incomplete Cu diffusion depending on the fluid inclusion thermal history and external fluid composition and evolution. The absence of Fe-S correlation (Fig. 9d) is also consistent with the fact that Fe concentrations are typically a factor of 5 to 10 higher that those of Cu, so that the chalcopyrite formation has a minor effect on the total Fe content, most of which remains in solution in the inclusion fluid.

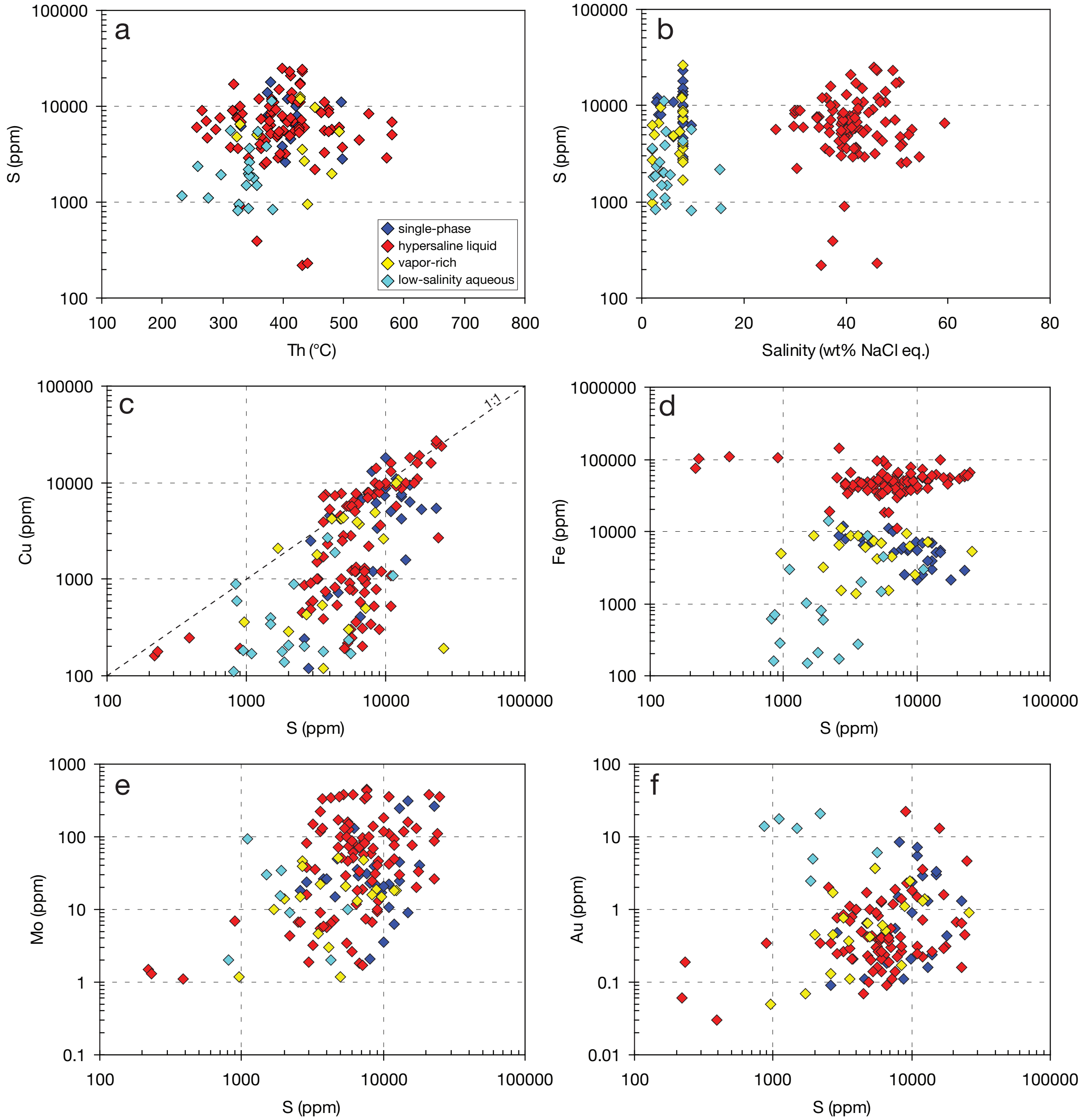

FIG. 9. Plots of sulfur concentration (in ppm) in single-phase, hypersaline liquid, vapor-rich and low salinity aqueous inclusions in porphyry systems as a function of temperature of homogenization (a), fluid salinity (b), Cu (c), Fe (d), Mo (e), and Au (f) content. Data from Guillong et al. (2008), Seo et al. (2009, 2011, 2012), and Catchpole et al. (2011, in review).

Vapor-liquid partitioning of sulfur and metals

Vapor-rich and hypersaline liquid inclusions commonly coexist in quartz and quartz-sulfide stockwork veins in porphyry deposits (Roedder, 1984, and references therein), forming trails of inclusions which homogenize at similar temperatures. Such fluid inclusion assemblages result from unmixing of homogeneous single-phase magmatic fluid (Fig. 3a; Henley and McNabb, 1978), and are formed by simultaneous entrapment of single vapor or hypersaline liquid inclusions along healed fractures (Roedder, 1971; Nash, 1976). Whereas the large metal transporting capacities of the hypersaline liquids have long been appreciated, the solubility of metals in low-density, salt-poor vapor was long overlooked due to the lack of robust analytical data on natural samples and experimental measurements. Results of PIXE, LA-ICP-MS, and, recently, SR-XRF analyses of vapor-liquid fluid inclusion assemblages demonstrate the following: (1) significant element fractionation between hypersaline liquid and vapor is widespread in magmatic-hydrothermal systems, regardless of pressure and temperature, and (2) the vapor phase has the ability to transport high concentrations of some metals at high pressure (Heinrich et al., 1992, 1999; Audétat et al., 1998; Cauzid et al., 2007; Seo et al., 2009).

Figure 10 summarizes recently published data on coexisting hypersaline liquid and vapor-rich inclusions formed in porphyry and skarn environments. The data are reported as distribution coefficients, $K_{metal} = C_{vap}/C_{liq}$, where C refers to the concentration (in ppm) of the metal in each of the two phases, vapor (vap) or liquid (liq). Sulfur, Cu, and As have average partitioning coefficients around 1 but the overall magnitude of this partitioning varies strongly between different datasets, especially for Cu (e.g., K_{Cu} ranges from ~0.1 to 100). Gold, where detectable, shows a clear preference for the vapor phase. Note that absolute concentrations in the vapor phase attain values of >10,000 and ≥10 ppm, respectively, for Cu and Au (Table 1), which is about two to four orders of magnitude higher than their average crustal abundances. Metals such as Mo, Bi, and Ag have K values between 0.1 and 1, with a few exceptions where they are enriched in the vapor phase. Metals such as Fe, Zn, and Pb, together with Na (and K, not shown), are clearly concentrated in the Cl-rich hypersaline liquid, with typical partitioning coefficients between 0.01 and 0.1. These trends are confirmed by experimental measurements and physical-chemical models (e.g., Pokrovski et al., 2005a; see below).

On the basis of their recent experiments under conditions where post-entrapment Cu diffusion in quartz-hosted fluid inclusions was limited or may be accurately evaluated, Lerchbaumer and Audétat (2012) estimated K_{Cu} values of 0.11 to 0.15 for typical vapor-liquid immiscibility conditions in porphyry systems. Such Cu vapor/liquid partition coefficients imply that hypersaline liquids likely carry more Cu than coexisting vapors. These values, together with other experimentally measured K_{Cu} values <1 in the majority of previous studies (see below), allow reconstruction of vapor/hypersaline liquid mass ratios in porphyry systems, which are estimated to be between ~4 and 9 (Lerchbaumer and Audétat, 2012). These results support the early models suggesting that the major transporting medium of Cu at porphyry depths is hypersaline liquid generated by phase separation (e.g., Henley and McNabb, 1978; Bodnar, 1995; Beane and Bodnar, 1995).

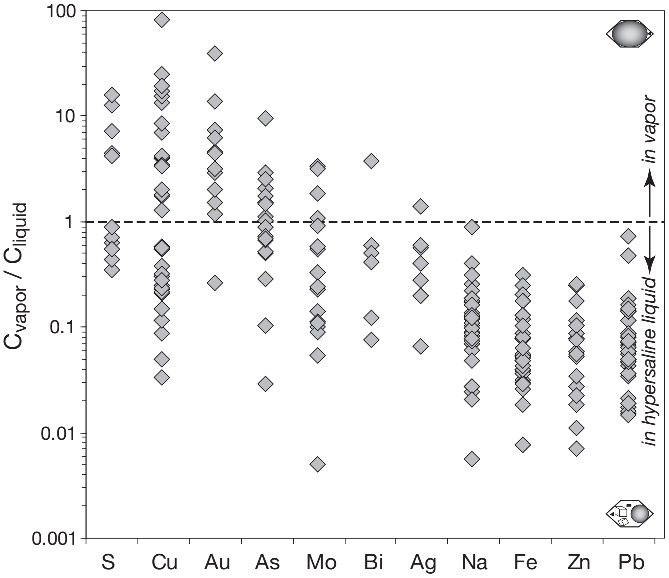

FIG. 10. Sulfur and metal concentration ratios (equivalent to vapor-liquid distribution coefficient) measured in coexisting vapor and hypersaline liquid inclusions from "boiling assemblages" in quartz from porphyry and related deposits. Data from Heinrich et al. (1999), Ulrich et al. (1999, 2001), Pettke et al. (2001), Audétat and Pettke (2003), Kehayov et al. (2003), Baker et al. (2004), Williams-Jones and Heinrich (2005), Klemm et al. (2007, 2008), and Seo et al. (2009).

Zn/Pb ratio in porphyry fluids as a potential tracer of fluid sources and fluid-melt partitioning

The whole dataset for Cu, Zn, and Pb compiled in Figures 7 and 8 shows large scatter of Cu/Zn and Cu/Pb ratios in all types of fluid inclusions, likely because of Cu precipitation, vapor-liquid partitioning, and/or post-entrapment diffusion. The only consistency in the dataset concerns the Zn/Pb ratio that varies over a narrow range, from 1 to 6 in high-temperature fluids (single-phase, hypersaline liquid, and vapor) from different deposits. It can be seen in Cu-Zn-Pb ternary diagrams (Fig. 11) that single-phase, hypersaline liquid, and vapor-rich inclusions form well-defined linear trends, corresponding to a constant Zn/Pb ratio of the mineralizing fluids for each of the deposits considered. These trends do not correspond to Cu precipitation trends; rather, they reflect differences in Cu, Zn, and Pb concentrations between the three major types of high-temperature fluids in porphyry systems. Single-phase fluids plot together with the vapor-rich inclusions toward the Cu-rich side of the trends, whereas hypersaline liquid inclusions show systematically lower Cu concentrations, as discussed above. Note that for two of the deposits, data provided by different analytical techniques are used, SX-XRF (Cline and Vanko, 1995) and LA-ICP-MS (Klemm et al., 2008) for Questa, New Mexico, and PIXE (Harris et al., 2003) and LA-ICP-MS (Ulrich et al., 2001) for Bajo de la Alumbrera, Argentina. For Butte, El Teniente, Chile, and Bingham Canyon, only published LA-ICP-MS data are used.

The Zn/Pb ratios in fluids from the five selected porphyry deposits are as follows: 6.0 ± 0.25, Butte; 4.0 ± 0.2, Questa; 3.0 ± 0.2, Bajo de la Alumbrera; 2.0 ± 0.1, El Teniente; and 1.1 ± 0.2, Bingham Canyon. The linear trend of data for each individual deposit in Figure 11 for the pristine single-phase magmatic fluid, and hypersaline liquid and vapor-rich inclusions produced by phase separation of the former fluid, confirms that phase unmixing and Cu-Au-Mo ore precipitation in the porphyry environment do not affect the initial Zn/Pb ratio of the fluid, which thus should reflect the original Zn/Pb ratio of the source magma.

Interestingly, Mo-rich deposits (Questa and Butte) display higher Zn/Pb ratios than Cu and Cu-Au deposits (El Teniente, Bingham Canyon, and Bajo de la Alumbrera). This observation does not correlate, however, with the magma chemistry and the expected magmatic fluid signatures. In fact, porphyry Mo deposits are broadly associated with evolved felsic magmas, commonly of rhyolitic composition, whereas porphyry Cu and Cu-Au deposits show spatial associations with intermediate-composition intrusions, commonly including interactions with mafic melts (Seedorff et al., 2005, and references therein). Large geochemical databases (e.g., http://earthref.org/GERM/ and http://georoc.mpch-mainz.gwdg.de/georoc) provide compilations of whole-rock data of various intrusion types from different tectonic settings. Thus, by comparing fractionated (dacitic to rhyolitic) with intermediate (andesitic)

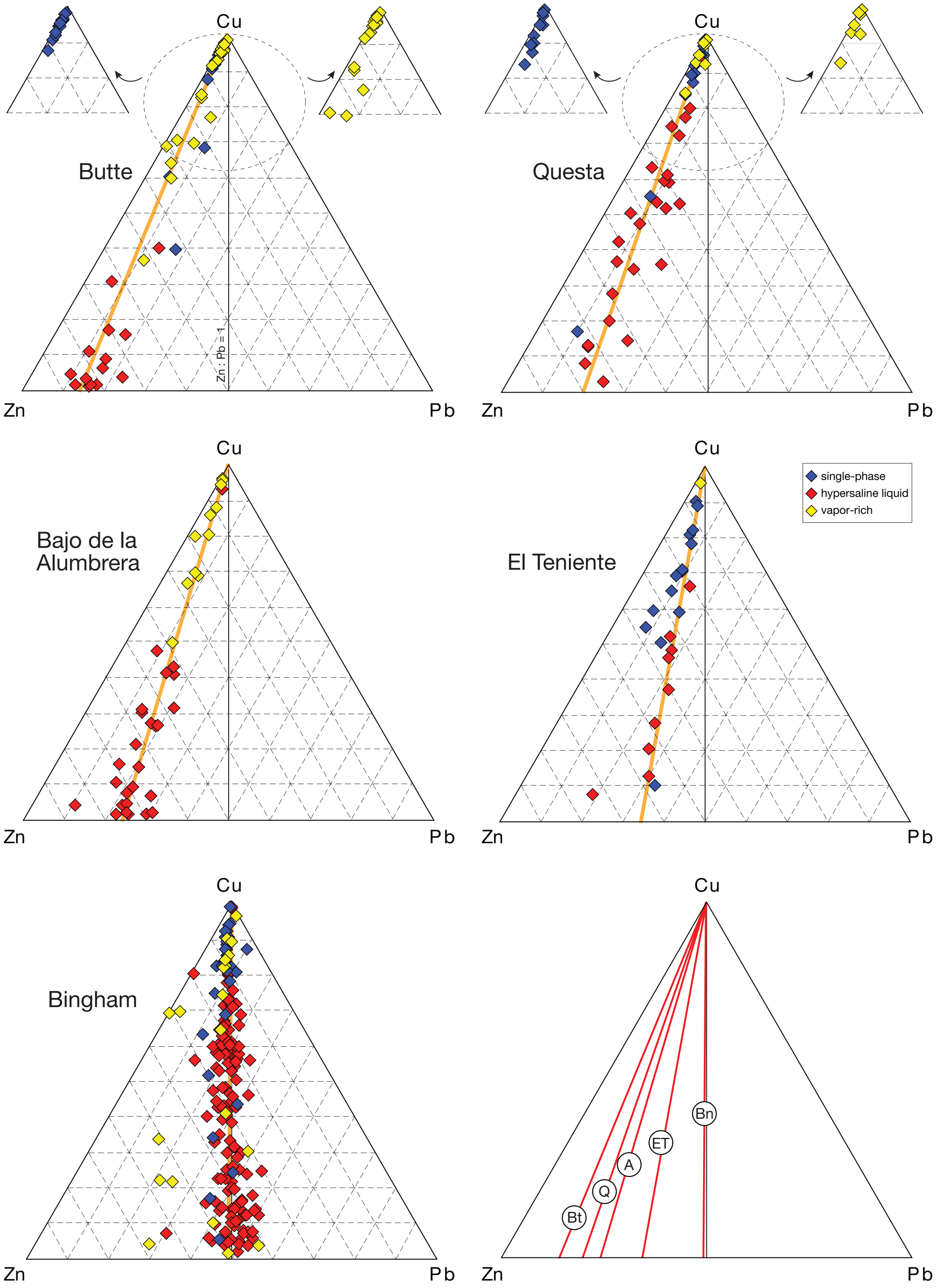

FIG. 11. Cu-Zn-Pb triangular plots of fluid compositions from selected porphyry Mo, Cu-Mo-Au, and Cu-Au deposits. Only compositions of high-temperature single-phase, hypersaline liquid, and vapor-rich inclusions are used. Linear trends marked by straight orange lines correspond to constant Zn/Pb ratio, at variable Cu/Zn and Cu/Pb for the different systems. The panel in the lower right corner summarizes the different Zn/Pb signatures of mineralizing fluids in the deposits, likely reflecting different Zn/Pb ratios in the source magmas (see text for discussion). Data used: Butte (Rusk et al., 2004); Questa (Cline and Vanko, 1995; Klemm et al., 2008); El Teniente (Klemm et al., 2007); Bingham (Landtwing et al., 2005, 2010; Seo et al., 2012); Bajo de la Alumbrera (Ulrich et al., 2001; Harris et al., 2003). Abbreviations: A = Alumbrera, Bn = Bingham, Bt = Butte, ET = El Teniente, Q = Questa.

magmas, it can be established that fractionated magmas are normally characterized by low Zn/Pb ratios (commonly 0.5–3) and intermediate magmas by higher and more variable Zn/Pb ratios (4–15). The few available fluid/melt partition coefficients, which are higher by a factor of 3 for Zn compared to Pb (Zajacz et al., 2008), could indeed explain the observed Zn/Pb ratios of ~3 in the fluids from Bajo de la Alumbrera, if the concentrations of the two elements in the silicate melt are similar. However, a large dataset on whole rocks and melt inclusion compositions from the Farallón Negro magmatic complex, host to the porphyry Cu-Au deposit at Bajo de la Alumbrera, indicates a Zn/Pb ratio between 2 and 5 in the silicate melt (Halter et al., 2004a, b). These Zn and Pb abundances in the melt would require a fluid/melt partition coefficient of Pb to be equal to or higher than that of Zn, to match the Zn/Pb ratio of 3 at Bajo de la Alumbrera (Fig. 11). Although we do not have a quantitative explanation of the origin of the Zn/Pb variations in the different deposits shown in Figure 11, more data on Pb and Zn speciation and partitioning in fluid-melt systems with different compositions are required to resolve this issue.

Metal Transport by Liquid and Vapor Phases in Porphyry Systems

Metal speciation, mineral solubility, and effect of major ligands in aqueous liquid and vapor

Past-century situation: Understanding metal transport and ore deposition mechanisms requires knowledge of the identity and stability of aqueous species as well as the solubility of minerals. Such data are acquired via laboratory experiments coupled with thermodynamic modeling. Numerous studies carried out from the 1960s to 1990s have provided a dataset on key metal complexes in aqueous solutions (reviews by Brimhall and Crerar, 1987; Barnes, 1997; Wood and Samson, 1998, and references therein). These data were integrated into thermodynamic equations, such as the Helgeson-Kirkham-Flowers (HKF) equation of state (Tanger and Helgeson, 1988; Shock et al., 1997; Sverjensky et al., 1997), the density model (Anderson et al., 1991), or the electrostatic model (Ryzhenko, 1981), enabling predictions of thermodynamic properties of aqueous metal complexes and solubility of minerals over a range of temperature and pressure (typically to 600°C and 5 kbar for fluid of densities above 0.4–0.5 g/cm^3), and salinities up to ~10 mol of NaCl equiv per kg of fluid (~50–60 wt %) (Helgeson et al., 1981; Oelkers et al., 2009). The resulting thermodynamic databases (e.g., SUPCRT; Johnson et al., 1992), coupled with user-friendly computer codes, allowed equilibrium calculations of mineral solubility, phase relationships, and chemical speciation in fluid-mineral systems (Oelkers et al., 2009, and references therein for a recent review).

Despite the different chemical properties of metals and diversity of ligands capable of binding them in aqueous solution, four main parameters have been shown to control mineral solubility: temperature, acidity, salinity, and S content of the fluid. The effect of pressure itself on the solubility in liquid and dense supercritical[2] fluid is rather small, at least within the range of depths relevant to the formation of porphyry deposits (<10 km). This is due to the low compressibility of liquid and supercritical water at densities of >0.4 to 0.5 g/cm^3, as recognized by the thermodynamic models cited above. However, the pressure effect is strong for the low-density vapor phase.

These achievements allow the major types of aqueous metal complexes to be identified (Table 3). Thus, in a typical hydrothermal fluid containing alkali chloride salts and S as sulfide and/or sulfate, metalloids such as As, Sb, Si, and B form uncharged hydroxide species. Molybdenum and W are likely to exist as oxyhydroxide anions and ion pairs with Na and K. The speciation of base and associated metals such as Cu, Fe, Zn, Pb, Cd, and Ag is largely dominated by chloride complexes (probably with the rare exception of some concentrated sulfate brines and low-temperature H_2S-rich liquids, in which these metals may also form sulfate and sulfide complexes, respectively). Gold and Pt form predominantly sulfide and/or chloride complexes depending on temperature, pH, and Cl and S contents. This relatively simple picture, consistent with the fundamental soft-hard classification of metals and ligands, allows a first-order estimation of metal solubility trends and ore precipitation mechanisms (Crerar et al., 1985). However, the exact composition (i.e., the number of ligands around the metal in the complex and its electric charge) and stability (i.e., thermodynamic formation constant) of the dominant complexes for many metals remained uncertain or were studied over small pressure and temperature ranges, prohibiting quantitative predictions. In addition, metal transport by a low-density vapor phase was almost unknown, owing to the lack of experimental data.

Major recent advances: In the past decade, there have been significant improvements in the knowledge of metal transport, particularly for porphyry-relevant metals such as Cu, Au, As, Sb, Mo, and Ag due to the following: (1) new systematic solubility studies using hydrothermal-reactor and synthetic-fluid inclusion techniques in model aqueous solutions (e.g., Stefánsson and Seward, 2003, 2004; Zotov et al., 2003; Tagirov et al., 2005, Ulrich and Mavrogenes, 2008; Zhang et al., 2012) and vapor-brine systems (Pokrovski et al., 2005a, 2008a), and (2) the development and application of spectroscopic methods (in particular, UV-visible and X-ray absorption spectroscopy) for in situ measurement of molecular structure of dissolved metal species, their solubility, and partitioning coefficients in model chemical systems relevant to porphyry deposits (e.g., Mavrogenes et al., 2002; Pokrovski et al., 2002a, 2006, 2008b, 2009a, b; Brugger et al., 2007; Testemale et al., 2009, 2011; Bazarkina et al., 2010; Etschmann et al., 2010; Minubayeva and Seward, 2010). The new data improved the accuracy of stability constants for major metal-bearing species in aqueous solution, better constrained their stoichiometry, and extended the data to a much larger temperature and pressure range. The current state of knowledge of speciation and solubility in hydrothermal liquid and vapor phases of the major groups of chemical elements typical for porphyry deposit environments is briefly summarized below.

---

[2] In this section, we use the term supercritical fluid for an aqueous phase above the critical point of pure water. The properties of this phase are further distinguished by its density as "dense supercritical fluid" (density > 0.4-0.5 g/cm^3) and "low-density supercritical fluid" (or "vapor" with density < 0.4-0.5 g/cm^3). This division is mostly imposed by the limitations of the available thermodynamic equations of state, as discussed in the text.

TABLE 3 Speciation of Metals in Aqueous Fluids and Hypersaline Liquids at Conditions Relevant to Porphyry Deposit Formation, as Inferred from Recent Experimental and Thermodynamic Studies

Metal	Major solid phases	Major aqueous species in saline aqueous fluid (200°-600°C, density >0.3-0.4 g/cm^3), at conditions of porphyry deposits [1]	Mean uncertainty in predicted metal concentration ($\log_{10}C_{metal}$)[2]	Key references[3]
As	Arsenopyrite, enargite, arsenian pyrite	$As(OH)_3$	>1.0	Pokrovski et al. (1996, 2002a, b)
Sb	Cu-Fe-Sn sulfosalts	$Sb(OH)_3$ [±$Sb(OH)_2Cl$, $Sb(OH)_3Cl^-$]	>1.0	Zotov et al. (2003) Pokrovski et al. (2006)
Zn	Sphalerite	$ZnCl_2$, $ZnCl_3^-$, $ZnCl_4^{2-}$ [±$Zn(HS)_2$, $Zn(HS)_3^-$]	1.0	Sverjenky et al. (1997) Wood and Samson, 1998) Tagirov and Seward, 2010)
Pb	Galena	$PbCl_2$, $PbCl_3^-$, $PbCl_4^{2-}$ [±$Pb(HS)_2$, $Pb(HS)_3^-$]	1.0	Sverjenky et al. (1997) Wood and Samson, 1998)
Fe	pyrite, magnetite, hematite, pyrrhotite	$FeCl_2$ [±$FeCl_4^{2-}$]	0.5 (1.0)	Sverjenky et al. (1997) Wood and Samson (1998) Testemale et al. (2009) Saunier et al. (2011)
Cu	Chalcopyrite, bornite, enargite	$CuCl_2^-$ [±$CuCl_3^{2-}$, $Cu(HS)_2^-$]	0.5	Akinfiev and Zotov (2001) Brugger et al. (2007) Akinfiev and Zotov (2010)
Ag	Argentite, sulfosalts	$AgCl_2^-$ [±$AgCl_3^{2-}$]	0.5	Akinfiev and Zotov (2001) Pokrovski et al. (2013)
Au	Native gold	$AuHS$, $Au(HS)_2^-$, $AuCl_2^-$ $Au(HS)H_2S$ (± polysulfide/sulfite)	0.5 (1.0)	Akinfiev and Zotov (2010) Pokrovski et al. (2009a, b)
Mo	Molybdenite	H_2MoO_4, $HMoO_4^-$, MoO_4^{2-} $NaHMoO_4$, $KHMoO_4$ (± sulfide/chloride)	> 2.0 (> 3.0)	Zotov et al. (1995) Shock et al. (1997) Ulrich and Mavrogenes (2008) Minubayeva and Seward (2010) Zhang et al. (2012)

[1] Species shown in brackets are subordinate or uncertain (see text)

[2] Estimated in terms of the variation of metal dissolved concentration in equilibrium with its major solid phase for typical porphyry fluid compositions at a given T, P, pH, and sulfur and oxygen fugacity, and using the range of published stability constants for the corresponding aqueous species from different studies; values in brackets are for the case where uncertain species are included in the calculations

[3] Major recent experimental or theoretical studies reporting thermodynamic data for aqueous complexes that were used in this study for calculating minerals solubility (numerous older references can be found therein)

Aqueous liquid and dense supercritical fluid: The aqueous speciation of metalloids (Si, B, Ge, As, Sb) is now well constrained. Among them, As and Sb are ubiquitous in porphyry systems and commonly accompany Au and Cu. Both As and Sb form soluble hydroxide species for which a robust dataset is available (Table 3). The stability of major chloride complexes of base and associated metals (Cu, Zn, Pb, Ag, Fe) is also known with reasonable accuracy, despite some disagreement about the exact stoichiometry of some metals (e.g., Fe, Zn, Ag; see Bazarkina et al., 2010; Saunier et al., 2011; Pokrovski et al., 2013, for details). Hydrogen sulfide and chloride complexes of Au are also well known from a number of recent experimental studies and thermodynamic compilations (Table 3), but there may be a significant contribution from species with other reduced sulfur forms in S-rich fluids (e.g., polysulfides; Pokrovski et al., 2009a; Pokrovski and Dubrovinsky, 2011). The current understanding of the speciation of Mo appears to be the poorest among the porphyry-relevant metals, owing to the lack of consistent data for oxyhydroxide species and its alkali metal ion pairs and suspected contributions of S- (e.g., Zhang et al., 2012) and Cl- (e.g., Ulrich and Mavrogenes, 2008) complexes.

Independent of information on aqueous speciation, thermodynamic properties of the metal-bearing minerals are also required to estimate their solubility. Whereas robust data are now available for the major sulfide minerals of base and associated metals (Fe, Cu, Ag, Mo, Zn, Pb, Cd), there is a lack of data for As- and Sb-bearing sulfide minerals forming in porphyry and epithermal environments, such as enargite, arsenian pyrite, and complex Sb sulfosalts. The resulting overall uncertainty in solubility predictions for each metal is reported in Table 3; it increases with increasing temperature (for all elements) and salt content in the fluid (for metals that form chloride complexes). For liquid phases and dense single-phase fluids (density >0.4 g/cm^3), the reported thermodynamic uncertainty for most metals (except Mo) is probably ≤1 order of magnitude in terms of metal concentration in equilibrium with its major mineral phase for moderate Cl and S contents in the fluid (<~30 wt % NaCl equiv, <1–2 wt % total dissolved S). Such uncertainty is relatively small compared to those associated with the natural variations of temperature, acidity, salinity, sulfur fugacity, and redox potential during porphyry and epithermal deposit formation. This allows at present semiquantitative thermodynamic modeling of ore-depositional mechanisms for moderate-temperature (<~500°C), moderate salinity (<30–40 wt % NaCl) aqueous solutions (e.g., Heinrich, 2005), and better constraints on some of these variables, which are difficult to obtain from natural samples (see below).

Vapor and low-density, single-phase fluids: In contrast to liquid and single-phase fluids, metal transport by low-density vapors is less well understood. Although the first direct experimental data on liquid-vapor partitioning coefficients for some porphyry ore-relevant metals (As, Sb, Cu, Zn, Pb, Fe, Cd, Au) have become available in the last decade (see below), the exact nature of vapor species and their molecular compositions, particularly in S-bearing systems, are still unknown. Scarce data are available about how total partitioning coefficients vary as a function of salt content other than NaCl (e.g., KCl, $CaCl_2$, $FeCl_2$), S content and speciation, and fluid acidity. The fundamental difference between the vapor phase and the liquid/single-phase fluids discussed above is the high compressibility of the former, resulting in large density variations with small pressure changes. Such changes are not accounted for by the widely used thermodynamic models, like the HKF equation-of-state, which are accurate for the dense aqueous phase, but not applicable to the vapor domain (i.e., density <0.3–0.4 g/cm^3; Plyasunov and Shock, 2001). Among the approaches currently used to describe the low-density, vapor-phase solubility of minerals and liquid-vapor partitioning are density (e.g., Pokrovski et al., 2005a, and references therein) and hydration models (e.g., Williams-Jones and Heinrich, 2005); however, they still remain largely empirical (see below). New models are currently under development that attempt unified descriptions of the liquid-vapor region (e.g., Akinfiev and Diamond, 2003), but they lack experimental data. In the last decade, molecular approaches based on quantum chemistry and molecular dynamics began to provide new insights into atomic structure and hydration energy of ore metal complexes (e.g., Au, Cu), helping to interpret spectroscopic signatures and solubility data and to allow a choice of the right speciation models to describe experimental results (e.g., Sherman, 2010; Pokrovski et al., 2013). Such approaches, albeit in their infancy, are expected to provide a direct link between the molecular properties of the dissolved species and their stability and solubility. Before discussing in detail the solubility and transport of porphyry ore metals in liquid and vapor phases, two issues intimately connected to hydrothermal fluid properties and metal distribution in porphyry systems are considered, the effect of CO_2 and the solubility of quartz.

Effect of CO_2: Carbon dioxide is a common volatile constituent in fluids associated with porphyry deposits, as shown by analyses of single-phase fluid inclusions from the deep high-temperature cores of Climax and Henderson, Colorado, Butte, Bingham Canyon, and El Salvador (Rusk et al., 2008c, 2011). These data indicate that CO_2 can be present at average concentrations of 10 wt % (~5 mol %), locally attaining 20 wt % (~10 mol %). However, the quantification of CO_2 contents in fluid inclusions from these systems is not routine, and requires detailed microthermometric measurements (e.g., Rusk et al., 2008b), and/or in situ spectroscopic methods such as Fourier transform infrared or Raman spectroscopy and involved calibration procedures (e.g., Wopenka and Pasteris, 1986; Dubessy et al., 1989; Burke et al., 2001; Frezzotti et al., 2012, and references therein). This explains, at least partly, the paucity of quantitative data for CO_2 in fluid inclusions from porphyry systems. Much more is known about CO_2 in magmatic rocks and silicate melts; Lowenstern (2001) provides a detailed review of CO_2 sources, contents, and behavior in magmas.

There are two key properties of CO_2 in magmatic systems that distinguish this compound from other volatiles such as water, Cl, and S: (1) low solubility of CO_2 in most types of silicate melts, and (2) absence of major mineral phases capable of retaining CO_2 in magmatic rocks. These properties are responsible for early degassing of CO_2 from magmas compared to water, Cl, and S (Lowenstern, 2001), and are likely to be the reason for the relatively modest CO_2 concentrations reported in fluids from porphyry systems compared to other types of Au deposits such as orogenic, Carlin-type, and intrusion-related gold, as well as mafic pegmatite-related Cu and PGE deposits, where CO_2 may attain >50 wt % of the fluid phase (e.g., Phillips and Evans, 2004; Hanley and Gladney, 2011). Under hydrothermal conditions characterized by water-salt-sulfur fluid systems, which are the subject of this paper, CO_2 may affect metal behavior in different ways, both direct and indirect.

First, the presence of CO_2 affects vapor-liquid equilibrium relationships as compared to a CO_2-free system. The PVTX properties of the H_2O-NaCl-CO_2 system are now reasonably well constrained, and physical-chemical models are available for predicting the densities of the vapor and liquid phases in this system (e.g., Bowers and Helgeson, 1983; Duan et al., 1995; Bakker, 2009). Phase separation conditions and exact phase compositions are, however, not sufficiently known to allow accurate modeling of the evolution of the CO_2-NaCl-H_2O system, in contrast to the volatile-free NaCl-H_2O system (Fig. 3; e.g., Driesner and Heinrich, 2007). Nevertheless, available data indicate that moderate quantities of CO_2 may significantly extend the vapor-liquid immiscibility domain and increase the pressure of phase separation. For example, the presence of 10 wt % CO_2 in a single-phase fluid containing 10 wt % NaCl at 400°C will raise the pressure of phase unmixing (i.e., the pressure below which two phases, an aqueous vapor and a saline liquid, exist) from 270 bar (in CO_2-free, 10 wt % NaCl-H_2O system) to ~500 bar (in the presence of CO_2; Bakker et al., 2009). This difference corresponds to >2 km depth at hydrostatic pressure or to ~1 km depth in a lithostatic regime. In the evolution path of the cooling and ascending magmatic fluid, this will allow earlier (i.e., greater depth) separation of the vapor phase and corresponding metal fractionation. Another effect of this phase separation is an increase in pH of the liquid phase due to preferential partitioning of acidic volatile components (CO_2 and also HCl, H_2S, and SO_2) into the vapor. As a numerical example illustrating this phenomenon, boiling of a 10 wt % NaCl + 5 wt % CO_2 aqueous solution from 350° to 320°C results in removal of 90% of CO_2 into the vapor phase, which will increase the pH of the liquid by over half an order of magnitude (from 5.0 in the initial solution to 5.5 after boiling). This may eventually lead to precipitation of some base metals remaining in the liquid phase (see below), depending on the efficiency of pH buffering via fluid-rock interaction. At the low-to-moderate temperatures (≤350°C) of epithermal environments this effect may be important, where water-silicate rock reactions are slow and vapor/liquid partition coefficients of CO_2 are high. In contrast, in higher-temperature (>400°C), salt-rich fluids of porphyry environments, the pH change of the liquid phase induced by removal of CO_2 is likely to be compensated for by rapid fluid equilibration with silicate rocks and an increase in salt content of the liquid phase, both favorable for sulfide mineral solubility (see below).

Second, CO_2 and particularly its anionic counterparts, bicarbonate (HCO_3^-) and carbonate (CO_3^{2-}) ions, may potentially act as ligands for so called hard metals such as rare earth elements (REE), Sn, Zr, U, Nb, and probably Fe (e.g., Seward and Barnes, 1997; Wood and Samson, 1998; Pokrovski, 2010, and references therein). Base metals, Ag, and Au are expected to be less affected by carbonate complexing, both because of their low chemical affinity with the hard carbonate ligand (e.g., Seward and Barnes, 1997) and the low abundance of carbonate ions in weakly acidic-to-neutral pH fluids in porphyry environments. For example, the concentration of bicarbonate and carbonate ions in an aqueous fluid of 10 wt % NaCl plus 5 wt % CO_2 at 400°C and 500 bars is <10 ppm at pH ~5, typical of that buffered by equilibrium with granitic or andesitic rocks. This concentration is negligible compared to the 100s to 1,000s ppm of Cu, Fe, or Sn in most fluids from magmatic-hydrothermal systems (see above).

Third, CO_2 (in large fractions) may lower the activity of H_2O in the fluid and thus affect solvation phenomena. Because most metal chloride and hydroxide complexes are strongly hydrated by water molecules, both in vapor and liquid phase (see below), lowering H_2O activity (~mole fraction) in the presence of CO_2 decreases the complex stability and thus metal solubility. Experimental studies on a few oxide and chloride solids in H_2O-CO_2 mixtures attest to this behavior over a wide range of T-P-X_{CO_2} conditions. For example, quartz solubility in a 20 wt % (10 mol %) CO_2-H_2O fluid at 600°C and 2 kbars is approximately two times lower than in pure water at the same pressure and temperature (Walther and Orville, 1983). A larger effect is observed for ionic compounds, AgCl for example, for which the solubility is lowered by a factor of three in the same CO_2-H_2O fluid compared to pure H_2O at 400°C and 1 kbar (Fig. 12; Akinfiev and Zotov, 1999). In contrast, for some nonpolar metal sulfide species (e.g., AuHS, Au(HS)H_2S), the presence of CO_2 might have the opposite effect due their preferential solvation in a CO_2-bearing solvent of low polarity and dielectric constant (Pokrovski et al., 2008a, 2009a). This hypothesis, however, awaits direct experimental confirmation. The solvation effect operates at large CO_2 fractions that change significantly the properties of the aqueous solvent. At the CO_2 contents of porphyry systems (typically ≤10 mol %; Rusk et al., 2008c), this effect on mineral solubility and the transport capacities of a fluid is expected to be minor compared to other factors (see below).

Solubility of quartz: Quartz is the ubiquitous gangue mineral associated with sulfide ore minerals in most porphyry deposits. In contrast to those minerals (see below), the simplicity and constancy of aqueous Si speciation over a wide pressure-temperature-composition range makes quartz solubility relatively insensitive to changes in acidity, salinity, redox potential, and S content. In aqueous fluids, the dominant solubility reaction for quartz is $SiO_2(s) + 2\ H_2O = Si(OH)_4$, which is a function of temperature and pressure; this solubility is known over a wide pressure and temperature range, from subduction zone fluids to the vapor phase, as a result of numerous studies (summarized by Walther and Helgeson, 1977; Manning, 1994; Newton and Manning, 2000, 2009, and references therein). The presence of CO_2 lowers the water activity, but has relatively little effect on SiO_2 solubility at CO_2 concentrations typical of porphyry fluids (less than a factor of 2). The presence of salt has a more complex effect due to a combination of changes in water activity and activity coefficients of aqueous silica. For example, at temperatures above 400°C and pressures below 1 to 2 kbars, moderate salt concentrations (up to 20 wt %) increase SiO_2 solubility by a factor of two to three compared to pure water and eliminates the retrograde solubility; by contrast, further salt addition leads to a solubility decrease (e.g., Fournier, 1999; Newton and Manning, 2000, and references therein). The effects of both CO_2 and salt are thus rather minor compared to the pressure and temperature effects themselves, which lead to orders of magnitude variations in quartz solubility.

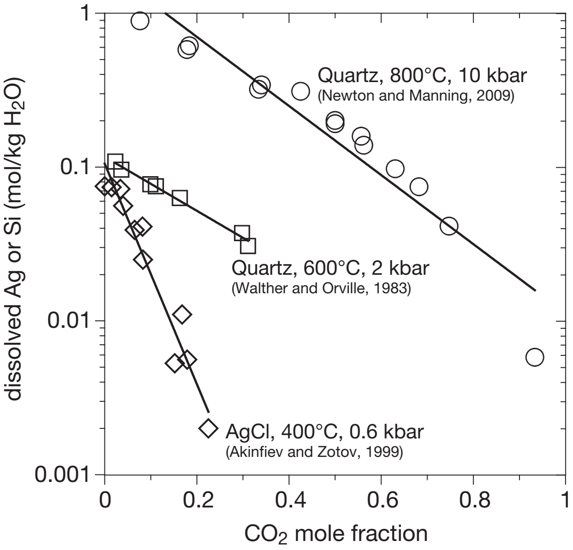

FIG. 12. Solubility of quartz and silver chloride in a H_2O-CO_2 fluid at indicated temperatures and pressures, as a function of the CO_2 mole fraction, according to published experimental data. Symbols stand for experimental data points from indicated references; straight lines show a linear fit to each dataset. Note the significant decrease of solubility with increasing CO_2 content.

Figure 13a shows quartz solubility in pure water as a function of temperature and pressure. An important property of quartz that affects rock permeability and fluid flow in porphyry deposits is its retrograde solubility in the temperature range of ~370° to 470°C at pressures below ~800 bars (Fig. 13a). This phenomenon is due to the change of the fluid density in this pressure and temperature range; water density at these conditions exhibits a pronounced drop (Fig. 13b), corresponding to the change from a liquid-like to vapor-like fluid, and the quartz solubility pattern closely matches the density curve. The fluid density is thus the major variable controlling the solubility of quartz, which is reflected in SiO_2 solubility equations over a wide range of pressure and

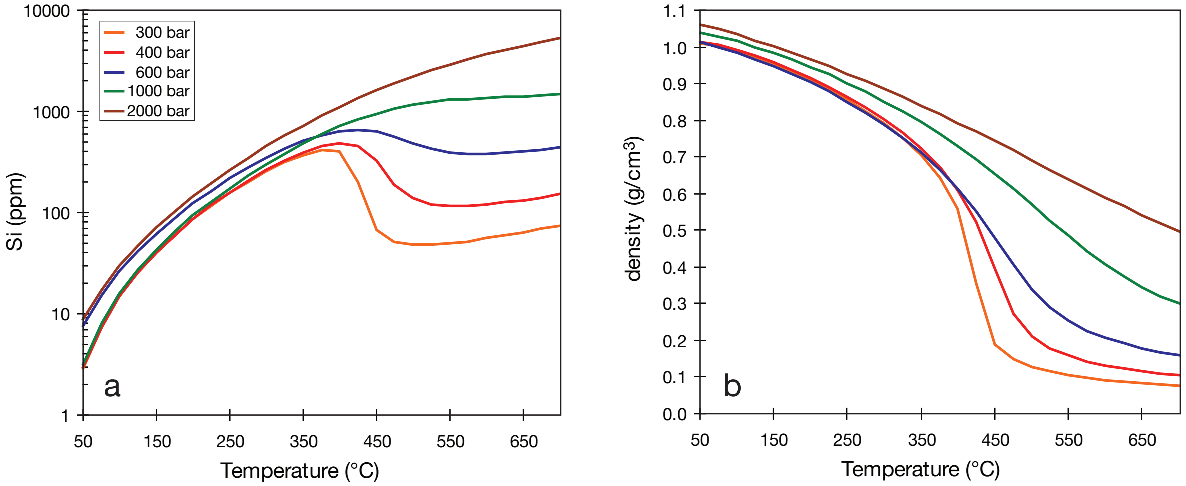

FIG. 13. Quartz solubility (silicon concentration) in pure water as a function of temperature (a) at different pressures calculated using the density equation of Manning (1994). Note the zone of retrograde solubility between ~370° and 470°C, at pressures below 800 bars. This pattern matches well the change of the fluid density from liquid-like to vapor-like in this domain (b), demonstrating that fluid density has a primary control on quartz solubility.

temperature (e.g., Manning et al., 1994). Note that the solubility pattern shown in Figure 13 is not unique for quartz; it has also been observed for other oxides, such as GeO_2 (Pokrovski et al., 2005b). Similar pressure and temperature (~density) dependencies are expected to hold for silicate minerals (e.g., Dolejs and Manning, 2010). From a physical-chemical point of view, such patterns are a combination of solvation (which is a direct function of the solvent density) and thermal disorder (which is a function of temperature) (see Pokrovski et al., 2005b, for details).

In contrast, experimental data for sulfide minerals are insufficient at present to establish predictive equations over such a wide range of densities as that available for quartz. In addition, dissolution and precipitation reactions of sulfides are much more complex than that of quartz; they involve volatile components (H_2S) and are acidity and redox dependent. Quantitative prediction of all these effects on sulfide mineral solubility is possible at present only for fluids with liquid-like densities (typically, >0.5 g/cm³), corresponding to the pressure and temperature domain of prograde quartz solubility (Fig. 13). These effects are discussed in the following section.

Solubility-controlling reactions of ore metals in aqueous solution

In this section, we discuss the main solubility-controlling reactions for Cu, Au and accompanying metals (Ag, Zn, Pb, Fe, Mo) in aqueous solution and dense supercritical fluid. Figure 14 shows the solubility of major ore minerals as a function of four key parameters—temperature, acidity, salinity, and S content—calculated using the available thermodynamic data for minerals and aqueous species cited in Table 3. Compared to these parameters, pressure has a minor effect on mineral solubility in the liquid-phase and dense supercritical-fluid domain, as discussed above, but it was included in the calculations to be consistent with the evolution of cooling and ascending magmatic fluids in porphyry systems. Two fundamental factors that control metal transport by the fluid phase are (1) the nature of the dissolved species (chloride *vs* sulfide *vs* oxyhydroxide), and (2) the chemical composition and stability of the major mineral phases. In most cases, chalcopyrite, pyrite, molybdenite, sphalerite, galena, argentite/acanthite, and native gold are the major mineral phases of Cu, Fe, Mo, Zn, Pb, Ag, and Au, respectively, allowing them be used as model minerals for identifying the major trends in metal behavior during fluid-rock interactions in porphyry systems. The amplitudes and trends in solubility are quite different among the metals considered (Fig. 14). For conditions typical of porphyry deposits, these trends are governed by the following reactions:

$$CuCl_2^- + FeCl_2^0 + 2H_2S = CuFeS_2(s) + 3H^+ + 0.5H_2 + 4Cl^- \quad (1a)$$

$$CuCl_2^- + FeS_2(s) + 0.5H_2 = CuFeS_2(s) + H^+ + 2Cl^- \quad (1b)$$

$$FeCl_2^0 + 2H_2S = FeS_2(s) + 2H^+ + 0.5H_2 + 2Cl^- \quad (2)$$

$$ZnCl_n^{2-n} + H_2S = ZnS(s) + 2H^+ + nCl^-,\ n = 2, 3, 4 \quad (3)$$

$$PbCl_n^{2-n} + H_2S = PbS(s) + 2H^+ + nCl^-,\ n = 2, 3, 4 \quad (4)$$

$$AgCl_2^- + 0.5H_2S = 0.5Ag_2S(s) + H^+ + 2Cl^- \quad (5)$$

$$Au(HS)_2^- + 0.5H_2 + H^+ = Au(s) + H_2S, \text{ in near-neutral and alkaline fluids} \quad (6a)$$

$$AuHS^0 + 0.5H_2 = Au(s) + H_2S, \text{ in acidic fluids} \quad (6b)$$

$$Au(HS)H_2S^0 + 0.5H_2 = Au(s) + 2H_2S, \text{ in acidic S-rich fluids and possibly vapors} \quad (6c)$$

$$AuCl_2^- + 0.5H_2 = Au(s) + H^+ + 2Cl^-, \text{ above 500°C in acidic saline fluids} \quad (6d)$$

$$HMoO_4^- + H^+ + 2H_2S + H_2 = MoS_2(s) + 4H_2O \quad (7a)$$

$$NaHMoO_4^0 + H^+ + 2H_2S + H_2 = MoS_2(s) + 4H_2O + Na^+ \quad (7b)$$

$$KHMoO_4^0 + H^+ + 2H_2S + H_2 = MoS_2(s) + 4H_2O + K^+ \quad (7c)$$

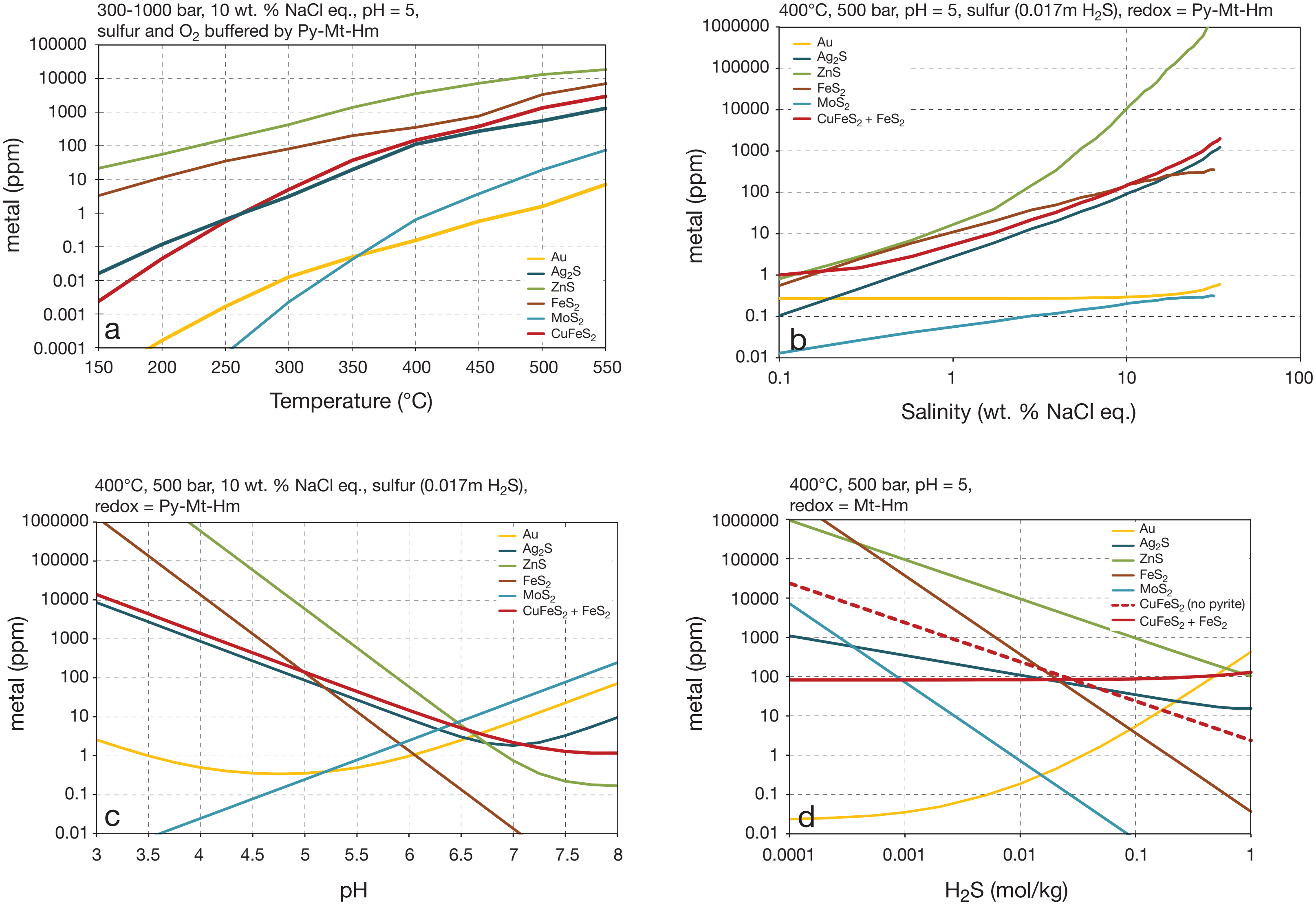

FIG. 14. Solubility of chalcopyrite, pyrite, sphalerite (± galena), molybdenite, argentite, and native gold (a), expressed as elemental metal concentrations, a) as a function of temperature in fluids with salinity of 10 wt % NaCl equiv at pH 5 in equilibrium with the pyrite-magnetite-hematite (py-mt-hm) buffer at pressure progressively decreasing from 1,000 bars at 500°C to 300 bars below 300°C; b) as a function of salinity at 400°C, 500 bars in equilibrium with pyrite-magnetite-hematite (py-mt-hm); c) as a function of pH at 400°C, 500 bars, 10 wt % NaCl, and in the py-mt-hm stability field; and d) as a function of H_2S concentration at 400°C, 500 bar, 10 wt % NaCl, and redox of the magnetite-hematite univariant. Calculations were performed using the HCh computer code (Shvarov, 2008). Thermodynamic properties of the minerals are taken from SUPCRT (Johnson et al., 1992); those of major fluid constituents and activity coefficient models are detailed in Pokrovski et al. (2009a, b). Stability constants of metals complexes are from references in Table 3.

The differences in aqueous speciation between base metals plus Ag (chlorides), Au (predominantly sulfides), and Mo (oxyhydroxides) yield contrasting solubility trends versus pH, H_2S, and salinity for these three groups of metals (Fig. 14). The only feature common to all metals is an increase in solubility with temperature, at least for Fe sulfide, Fe oxide, and silicate-buffered systems, which are a reasonable proxy for sulfur fugacity, redox, and pH, respectively, in rock-dominated porphyry environments (e.g., Giggenbach, 1997). However, the absolute dissolved concentrations of Cu, Fe, Zn, and Pb in equilibrium with relevant sulfide minerals are much higher than for Au and Mo, and the effect of temperature is most pronounced for Cu and Mo, yielding steeper solubility curves as a function of temperature (Fig. 14a).

For all metals except Au, solubility increases significantly with salinity (Fig. 14b), the largest increase being for Zn (and Pb, not shown), which are likely to form tri- and tetrachloride species (Table 3). Fluid acidity (pH) exerts a strong effect on ZnS and FeS_2 (and PbS, not shown) solubility. For example, with all other parameters being equal, a pH change from 4 to 5 yields a 100-fold decrease in solubility at a given temperature and salinity (Fig. 14c). This is likely the major factor leading to ZnS, PbS, and FeS_2 precipitation (see below). Copper and Ag also have elevated solubilities in acidic fluids, but are less affected by pH changes. In contrast to other metals, Mo solubility is very low under acidic conditions and increases with increasing pH. The effect of reduced sulfur is also fundamentally different for base metals and Mo in contrast with Au (Fig. 14d); high H_2S concentrations are not favorable for Zn, Fe, Ag, and Mo solubility, but are likely to be the major cause of efficient Au transport. Copper concentrations in equilibrium with the pyrite-chalcopyrite assemblage, ubiquitous in porphyry systems, is independent of H_2S content (as H_2S is not involved in reaction 1b), whereas in a pyrite-free system, the stoichiometric solubility of $CuFeS_2$ decreases with increasing H_2S (Fig. 14d). These different solubility trends provide a foundation for interpreting metal distribution in porphyry systems (see below).

Experimental insights into vapor-phase transport of metals in porphyry systems

One of the major advances in understanding porphyry Cu (-Mo-Au) systems over the past decade is the recognition that the vapor phase can transport significant quantities of metals (Figs. 5, 7, 8). This fact has motivated experimental and theoretical research that allows the physical and chemical factors affecting the metal vapor-phase transport and vapor-liquid partitioning to be constrained, as discussed in the following subsections.

Lessons from volcanic gases: Extensive work on volcanic gases sampled from fumarolic discharges since the mid-20th century suggests selective vapor transport of some metals in some places, particularly in ash-laden vapor plumes related to quiescently erupting volcanoes (summary by Hedenquist, 1995). However, the majority of vapor samples from atmospheric-pressured fumaroles of passively degassing volcanoes show low metal concentrations, typically less than a few ppm for base metals (Zn, Pb, Cu, Sn, Mo), Ag, and As, and less than a few ppb for Au (e.g., Hedenquist et al., 1994a; Hedenquist, 1995; Williams-Jones and Heinrich, 2005; and references therein). Such measured concentrations are in agreement with gas-sublimate equilibria in water-free systems, involving chloride, sulfide, oxide, or native metal gaseous species whose thermodynamic properties are available in large databases (e.g., JANAF; Chase, 1998; Ivtanthermo, 1983). The metal contents of the vapor from volcanic fumaroles associated with passively degassing volcanoes are, however, 2 to 5 orders of magnitude lower than those measured in vapor inclusions from porphyry deposits (Figs. 7, 8; Table 1). The main difference between the surficial volcanic vapors and hydrothermal vapors trapped at high pressure is the density, which increases by a factor of ~100 from the surface (d_{vapor}~0.001 g/cm^3 at <10 bars) to a few kilometers depth (d_{vapor}~0.01-0.4 g/cm^3 at 100–1,000 bars). Density appears to be the major parameter affecting mineral solubility in the vapor phase.

Hydration control on solid-phase solubility in vapor: Recent solubility studies of Au, Cu, Sn, Mo, and Ag oxides and chlorides in unsaturated water vapor (i.e., at pressures below the vapor-liquid saturation curve of water or H_2O-salt solution) confirm that the dominant control of metal solubility is water pressure, which is directly proportional to density (Archibald et al., 2001, 2002; Williams-Jones and Heinrich, 2005; Rempel et al., 2006; and references therein). They show that at water pressures of a few hundred bars, the solubility of a metal-bearing solid phase, such as oxide, chloride or native metal, is many orders of magnitude higher compared to the volatility of this solid in a dry H_2O-free system. This enhanced solubilization in the presence of water may be explained by solid-gas reactions:

$$CuCl(s) + n\ H_2O(gas) = CuCl \cdot nH_2O(gas) \quad (8a)$$

$$MoO_3(s) + n\ H_2O(gas) = MoO_3 \cdot nH_2O(gas) \quad (8b)$$

$$Au(s) + HCl(gas) + n\ H_2O(gas) = AuCl \cdot nH_2O(gas) + 0.5\ H_2(gas) \quad (8c)$$

where n is the apparent hydration number, which varies between ~1 and ~20, depending on the species, temperature, and pressure; in most cases, it increases systematically with pressure. These studies reveal three fundamental controls on vapor-phase transport of metals: (1) in the hydrothermal vapor phase, metals form complexes with the same ligands as in aqueous solution (chloride, sulfide, or hydroxide); (2) in contrast to the aqueous solution or hypersaline liquid, the major vapor species are uncharged (at least in unsaturated vapor below the water critical point), in agreement with the low dielectric constant of the vapor favoring ion association; and (3) as in aqueous solution, the metal complexes are solvated by water molecules; the higher the pressure the more metal that can be dissolved in the vapor phase in equilibrium with a metal-bearing solid or melt. The main limitation of this hydration approach is the relatively narrow temperature and pressure range of measurements (most were conducted at 250°–350°C at <200 bars), and large changes in apparent hydration numbers with pressure (e.g., $AuCl \cdot nH_2O$, $n = 3$-5; $MoO_3 \cdot nH_2O$, $n = 2$–4 in that small range; Archibald et al., 2001; Rempel et al., 2006); this makes practical application of these results difficult to conditions of porphyry deposits. An alternative to the hydration models discussed above may be an approach that relates solubility to vapor-phase density, which is shown to be extremely efficient in the case of quartz solubility (see above) and of vapor-liquid fractionation of various metals, as shown below.

Fluid density control on vapor-liquid partitioning in S-free systems: Further insights into vapor-phase transport have been provided by direct measurements of vapor-liquid partition coefficients of metals in model salt-water systems analogous to hypersaline liquid and vapor inclusions from porphyry deposits (Pokrovski et al., 2005a, 2008a, b; Pokrovski, 2010, and references therein). These works demonstrate that vapor-liquid distribution of elements obeys simple relationships involving the densities of the coexisting vapor and liquid phases. Figure 15 shows that the partition coefficient of each metal (K, which is the ratio of metal mass concentrations in the coexisting phases, C_{vapor}/C_{liquid}) is linearly proportional on a logarithmic scale to the ratio between the vapor and liquid densities, which are well known in the H_2O-NaCl system (e.g., Driesner and Heinrich, 2007). All lines tend to converge to the critical point, where the concentrations are identical in both phases and the partition coefficient is, by definition, equal to one. Such ray diagrams have long been known for salts and acids dissolved in water (e.g., Styrikovich et al., 1955; Alvarez et al., 1994; Palmer et al., 2004); they stem from classical thermodynamics and statistical mechanics that demonstrate that the hydration energy of the solute evolves linearly with the solvent density (Mesmer et al., 1988; Palmer et al., 2004). These relationships (Fig. 15) confirm the validity of this model for a variety of metals and metalloids over a wide temperature range; they support the findings in unsaturated vapor systems and demonstrate that water-solute interaction (or hydration) is a key factor controlling metal vapor-phase solubility and vapor-liquid partitioning. In S-free water-salt systems, where the speciation of metals and metalloids is dominated either by hydroxide or chloride complexes (Table 3), any significant deviation from a linear trend with an origin at the critical point should be regarded as an experimental or analytical artifact (Pokrovski, 2010). With the exception of arsenous, boric, and, probably, molybdic (not shown) acids, whose K values cluster around unity in liquid-vapor systems at >400°C, all other elements, from silica to rare earths being transported in the fluid or liquid phase in the form of chloride or hydroxide species, have no chance to enrich the vapor phase relative to the coexisting liquid (Fig. 15). All are concentrated in the liquid by a factor of 10 to 1,000 at conditions typical of vapor-hypersaline liquid separation in porphyry systems at temperatures between 300° and 500°C.

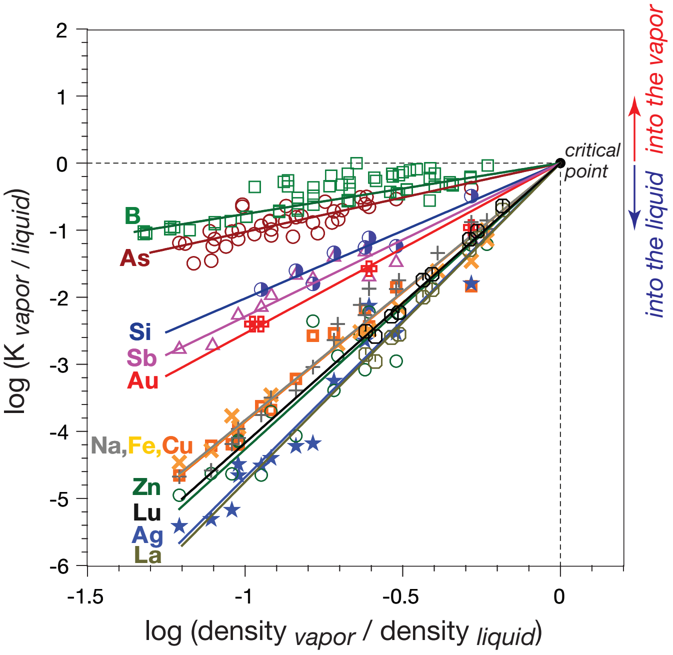

FIG. 15. Vapor-liquid partition coefficients (log $K_{vapor/liquid}$ = log [m_{vapor}/m_{liquid}] where *m* is the number of moles of the element per 1 kg of fluid in the corresponding phase) of different metals and metalloids at two-phase equilibrium in the system H_2O + NaCl ± KCl ± HCl; at ~200° to 600°C as a function of the vapor-to-liquid density ratio. Symbols stand for experimental data from the following sources: B = Styrikovich et al. (1960), Kukuljan et al. (1999), Liebscher et al. (2005), Foustoukos and Seyfried (2007); As^{III}, Si, Na, Zn, Fe^{II}, Cu^{I}, Ag^{I} and Au^{I} = Pokrovski et al. (2005a); Sb^{III} = Pokrovski et al. (2005a, 2008b); Lu and La = Shmulovich et al. (2002). Limited data for Mo^{VI} (Rempel et al., 2009) and Pb (Pokrovski et al., 2008b) plot close to As/B and Zn/Fe/Cu, respectively (omitted for clarity). Lines represent the regression through origin (i.e., critical point) of the experimental data for each element using the equation log K = *n* × log (d_{vapor}/d_{liquid}), where *n* is an empirical coefficient for each metal (Pokrovski et al., 2005a).

At magmatic temperatures (600°–800°C), limited experimental data from synthetic fluid inclusions for Au, Cu, Zn, and Ag in S-free systems involving Na, K, and Fe chloride saline liquids, silicate melts, and H_2O-HCl vapor phases, indicate density relationships similar to those established for lower temperature hydrothermal conditions (Fig. 15), although with absolute vapor-hypersaline liquid partition coefficients somewhat higher than 500°C for similar vapor/liquid density ratios (Fig. 16a). The difference, however, rarely exceeds an order of magnitude and may be explained by the increasing fraction of neutral, and thus more volatile, chloride species in the hypersaline liquid with increasing temperature (e.g., Pokrovski et al., 2008a) and/or possible formation of oxychloride or hydrogen-chloride species in the magmatic vapor phase (e.g., Simon et al., 2005). Both phenomena are due to the reinforcement of electrostatic interactions in aqueous complexes with increasing temperature and decreasing dielectric constant of the solvent. This enhances the stability of uncharged species and strengthens chemical bonds with hard ligands (e.g., O/OH versus Cl). Even at temperatures as high as 800°C, all principal porphyry-deposit metals (Au, Cu, Fe) are enriched in the liquid phase compared to the vapor (Fig. 16a). Note that both vapor and liquid densities change in regular and predictable fashion that may be reasonably approximated by the H_2O-NaCl system (Driesner and Heinrich, 2007) for natural vapor and hypersaline liquid compositions dominated by Na, K, and Fe chlorides. Consequently, these simple density trends provide an efficient and practical way of predicting vapor-liquid fractionation over the range of magmatic-hydrothermal conditions, with an uncertainty within an order of magnitude.

The presence of CO_2, which has a weak capacity for direct binding to most base and chalcophile metals, will affect the fluid properties mainly by enlarging the degree of immiscibility between the vapor and liquid, thus further enhancing the density contrast between these two phases. This effect is expected to lead to a larger contrast in the vapor-liquid partitioning for most metals and their further enrichment in the

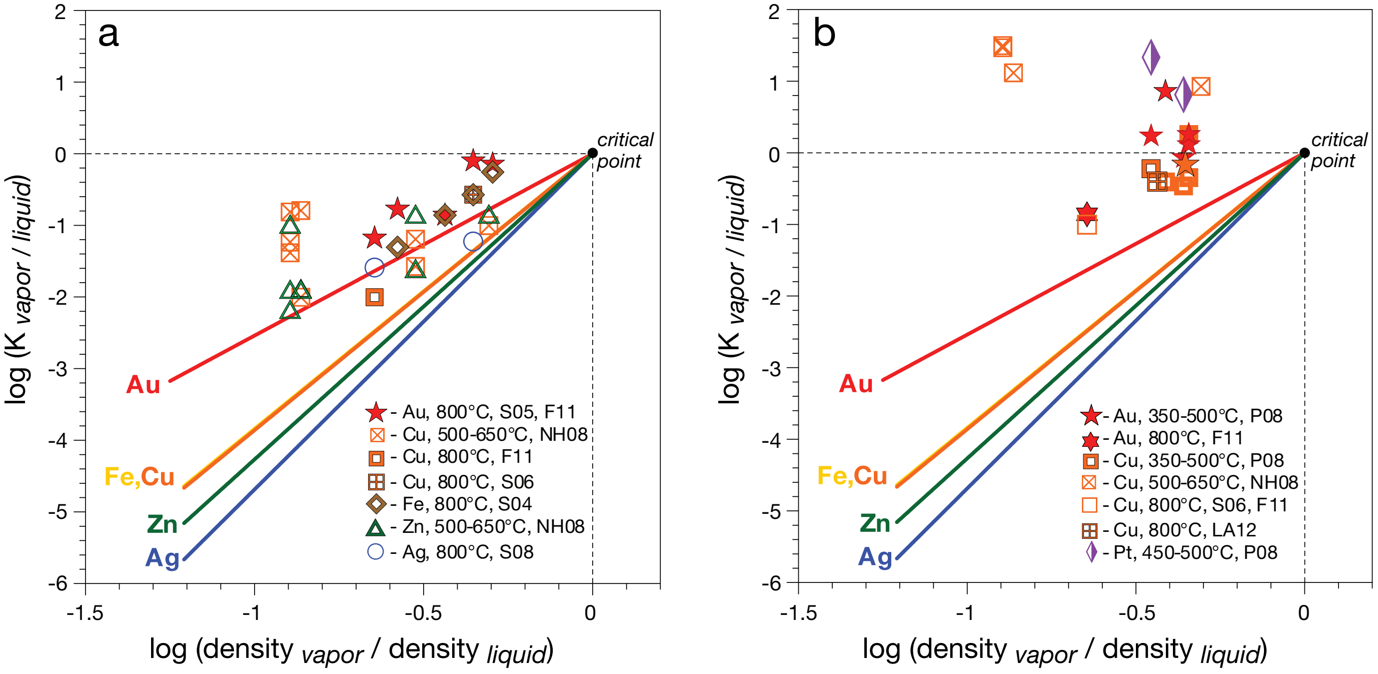

FIG. 16. (a) Vapor-liquid partition coefficients (log $K_{vapor/liquid}$ = log [m_{vapor}/m_{liquid}] of Au, Cu, Fe, Zn, and Ag in the two-phase model system H_2O + NaCl ± KCl ± HCl at magmatic temperatures (500°–800°C) as a function of the vapor-to-liquid density ratio. Symbols stand for experimental data from the following sources: NH08 = Nagaseki and Hayachi (2008), S04 = Simon et al. (2004), S05 = Simon et al. (2005), S06 = Simon et al. (2006), S08 = Simon et al. (2008), F11 = Frank et al. (2011). The straight lines through the critical point for the indicated elements represent the density-model predictions in the S-free system based on data below 500°C (Pokrovski et al., 2005a, 2008a). With the exception of a few nonsystematic outliers, most high-temperature data follow, within errors, a roughly linear log K vs log (d_{vap}/d_{liq}) dependence with an origin at the critical point, similar to that established at hydrothermal temperatures; the somewhat higher K values likely reflect the increasing fraction of neutral, and thus more volatile, metal chloride species with increasing temperature and/or possible formation of new oxy-chloride and hydrogen-chloride species in magmatic vapor phase. (b) The effect of sulfur on vapor-liquid partition coefficients (log $K_{vapor/liquid}$ = log [m_{vapor}/m_{liquid}] of Au, Cu and Pt in model two-phase salt-water sulfur-rich systems (H_2O-NaCl-KCl-HCl-$FeCl_2$-S-pyrrhotite-bornite) at acidic-to-neutral pH, 350° to 800°C, and 1 to 10 wt % sulfur in the vapor. Symbols stand for experimental data from the following sources: P08 = Pokrovski et al. (2008a), NH08 = Nagaseki and Hayachi (2008), S06 = Simon et al. (2006), F11 = Frank et al. (2011), LA12 = Lerchbaumer and Audétat (2012). Partitioning of Zn, Fe, and Ag is not affected within errors by the presence of sulfur (symbols are omitted for clarity). The straight lines for the indicated elements represent the density-model predictions in the S-free system (from Pokrovski et al., 2005a; see Fig. 16a).

dense liquid phase. The effect of S, which may selectively bind some metals, appears to be different.

Effect of sulfur on vapor-liquid partitioning in porphyry systems: Experimental data for S-free systems agree with observations on natural coexisting liquid and vapor inclusions for all metals and metalloids, except Au and Cu (Fig. 10). The most plausible explanation for Au and Cu enrichment in the vapor phase is the formation of volatile species with S, the second most important ligand after chloride; this effect has recently been demonstrated experimentally. With the addition of 1 to 2 wt % of S to the water-salt system at acidic-to-neutral pH and temperatures of 350° to 500°C, Cu and Au partition coefficients ($K_{vapor/liquid}$) at equilibrium increase by one to two orders of magnitude (Fig. 16b), attaining values in favor of the vapor for Au (K_{Au} > 1), whereas the volatility of Ag, Zn, Fe, and Pb is almost unaffected (Pokrovski et al., 2008a). Platinum exhibits partitioning similar to that for Au, largely in favor of the vapor phase (K~10; however no experimental data in S-free systems are available for comparison).

Synthetic fluid inclusion studies at higher temperatures (600°–800°C) also demonstrate an increase of *K* values for Cu in the presence of S, but exhibit large discrepancies. For example, Lerchbaumer and Audétat (2012) reported K_{Cu} values two orders of magnitude lower than those of Nagaseki and Hayashi (2008) in the same H_2O-NaCl-S system, with H_2S concentrations up to 5 to 10 wt % in the vapor phase (K_{Cu} ~0.1 vs. 10; Fig. 16b). Other experimental studies, both at hydrothermal (Pokrovski et al., 2008a) and magmatic (Simon et al., 2006; Frank et al., 2011) temperatures, reported vapor/liquid partitioning coefficients for Cu between 0.1 and 0.5 at dissolved S contents of 1 to 2 wt %, typical for porphyry systems (Seo et al., 2009). Although these K values are systematically less than one (with the exception of the study by Nagaseki and Hayashi, 2008), they are up to an order of magnitude higher than in S-free systems for the same conditions and data source (Fig. 16a).

Although the exact nature and stoichiometry of Au, Pt, and Cu complexes in the vapor phase remain unconstrained, it is likely that these metals form neutral hydrogen sulfide complexes. Such species might behave as regular gases, which enrich the vapor phase with a decrease in the vapor/liquid density ratio. The higher volatility of Au and Pt compared to Cu is consistent with the far greater stability of Au hydrogen sulfide species in aqueous solution, as discussed above. The low volatility of Zn, Fe, and Ag is a direct consequence of the larger stability of their chloride versus sulfide complexes in aqueous solution (Table 3).

Another important factor controlling the vapor-liquid distribution of these metals in S-rich systems is the fluid acidity (pH). Because neutral sulfide species have a far greater volatility than their charged counterparts (Pokrovski et al., 2002a, 2008a), Au (and Cu) are expected to be more volatile at acidic conditions under which $AuHS^0$ and probably $AuHSH_2S^0$ are more abundant in the liquid phase (reactions 6b, c). At pH >5, where $Au(HS)_2^-$ (reaction 6a) and $Cu(HS)_2^-$ form in the solution, K values for Au and Cu are systematically <1 (Pokrovski et al., 2008a). Phase separation of such a fluid will thus not favor Au and Cu fractionation into the vapor phase.

The effect of CO_2 on vapor-liquid partitioning of S-bound metals remains experimentally unconstrained. The scarce data for CO_2-free systems (Fig. 16b) suggest that partitioning of volatile Au- and Pt-bearing sulfide complexes into the vapor phase might be enhanced in the presence of CO_2, both due to an increase in the density contrast between liquid and vapor and specific solvation of neutral nonpolar molecules, such as Au-H_2S complexes, by nonpolar CO_2 (Pokrovski et al., 2008a). The selective solvation capacities of supercritical CO_2 are used in chemical engineering for synthesis and purification of organometallic and organic compounds at moderate temperatures (e.g., Erkey, 2000). However, this hypothesis awaits experimental confirmation for conditions applicable to porphyry systems.

Experimental data for the S-bearing systems discussed above explain vapor-liquid distributions of Au, Ag, and base metals observed in fluid inclusions from porphyry Cu (-Mo-Au) deposits; however, they still fail to reproduce the strong enrichment of Cu measured in vapor-like inclusions (K_{Cu} as high as 10–100; Fig. 10). Recent experiments on natural and synthetic fluid inclusions in quartz re-equilibrated with different fluid and melt compositions revealed rapid diffusion of Cu^+ through the quartz host, leading to large post-entrapment changes in Cu concentrations in the inclusion fluid (Li et al., 2009; Zajacz et al., 2009; Lerchbaumer and Audétat, 2012). These studies may thus explain the observed Cu enrichment in natural S-rich vapor inclusions through preferential diffusion of Cu^+ from the surrounding fluid into previously formed S-rich inclusion fluids (see above).

Discussion: Ore Deposition and Metal Distribution in Porphyry Cu (-Mo-Au) Systems

Ore formation and metal distribution in porphyry systems result from a combination of processes, ultimately leading to decreases in the solubility of metals in the hydrothermal fluid and their precipitation. In this section, we apply thermodynamic modeling to interpret the metal contents of natural fluid inclusions from porphyry systems, discuss the major processes controlling metal precipitation, and identify factors that cause the observed metal zoning in porphyry-centered districts.

Comparison of metal concentrations measured in ore fluids with thermodynamic predictions

The majority of previous studies devoted to thermodynamic modeling of porphyry deposits focused on the major-element composition of fluid inclusions by considering the PVTX properties of NaCl-KCl-CO_2-H_2O systems (e.g., Bodnar and Sterner, 1984; Sterner et al., 1988; Bodnar and Vityk, 1994; Heinrich, 2007), mineral assemblages, alteration sequences, and sulfidation state (e.g., Reed, 1997; Einaudi et al., 2003), as well as Au, plus Fe, Cu, Zn, and Pb sulfide solubility and metal precipitation in model aqueous fluids (e.g., Hemley and Hunt, 1992; Hezarkhani et al., 1999; Heinrich et al., 2004; Heinrich, 2005). These studies provided constraints on fluid properties and major element composition, temperature, and pressure of deposition, minerals that control the redox and sulfur state of the fluid, and general trends in the behavior of some metals during fluid evolution. The large dataset of metal concentrations in natural fluid inclusions compiled in this study, together with an improved knowledge of aqueous metal speciation and dissolved species stability, allows more detailed and direct comparisons of natural metal contents with thermodynamic predictions. This approach provides new insights into depositional mechanisms and metal fractionation in the porphyry and epithermal environments.

Figure 17 shows the calculated solubility of major metal-bearing ore minerals as a function of temperature and salinity under redox and acidity conditions typical of porphyry systems, as inferred from mineral associations and wall-rock alteration patterns. The assemblage pyrite-magnetite-hematite was chosen as a proxy for the redox state and H_2S fugacity (Einaudi et al., 2003) and the pH was constrained between 4 and 5 assuming buffering by aluminosilicate assemblages common in porphyry deposits over a wide temperature range (Meyer and Hemley, 1967; Reed, 1997). Significant deviations from these conditions will be directly reflected in differences between calculated and measured metal concentrations. The main trends for the principal metals in porphyry deposits are highlighted below.

Zinc, lead, and silver: Calculations show that for Zn, Pb, and Ag at 400°C, the great majority of single-phase fluids and hypersaline liquids are undersaturated with respect to ZnS, PbS, and Ag_2S minerals at pH ≤5 (Fig. 17a-c). These results accord well with the observed paucity of Zn, Pb, and Ag

FIG. 17. Comparison of the calculated Zn, Pb, Ag, Mo, Cu, and Au dissolved concentrations in the fluid in equilibrium with the corresponding major ore minerals, sphalerite (a), galena (b), argentite (c), molybdenite (d), chalcopyrite (e and f) and native gold (g and h) as a function of temperature (all metals) and salinity (for Cu and Au); metal concentrations analyzed in the four types of fluid inclusions are shown in Figures 7 and 8. The data points of the different inclusion types are shown as contours of different color for simplicity. The calculations were performed at NaCl concentrations of 3, 10, and 40 wt % at pH 5 and buffered by the pyrite-magnetite-hematite assemblage (unless indicated in the legend). Arrows illustrate the effect of pH (and redox for Mo) change on the calculated solubilities (see text for discussion). Abbreviations: MH = magnetite-hematite; NNO = nickel-nickel oxide.

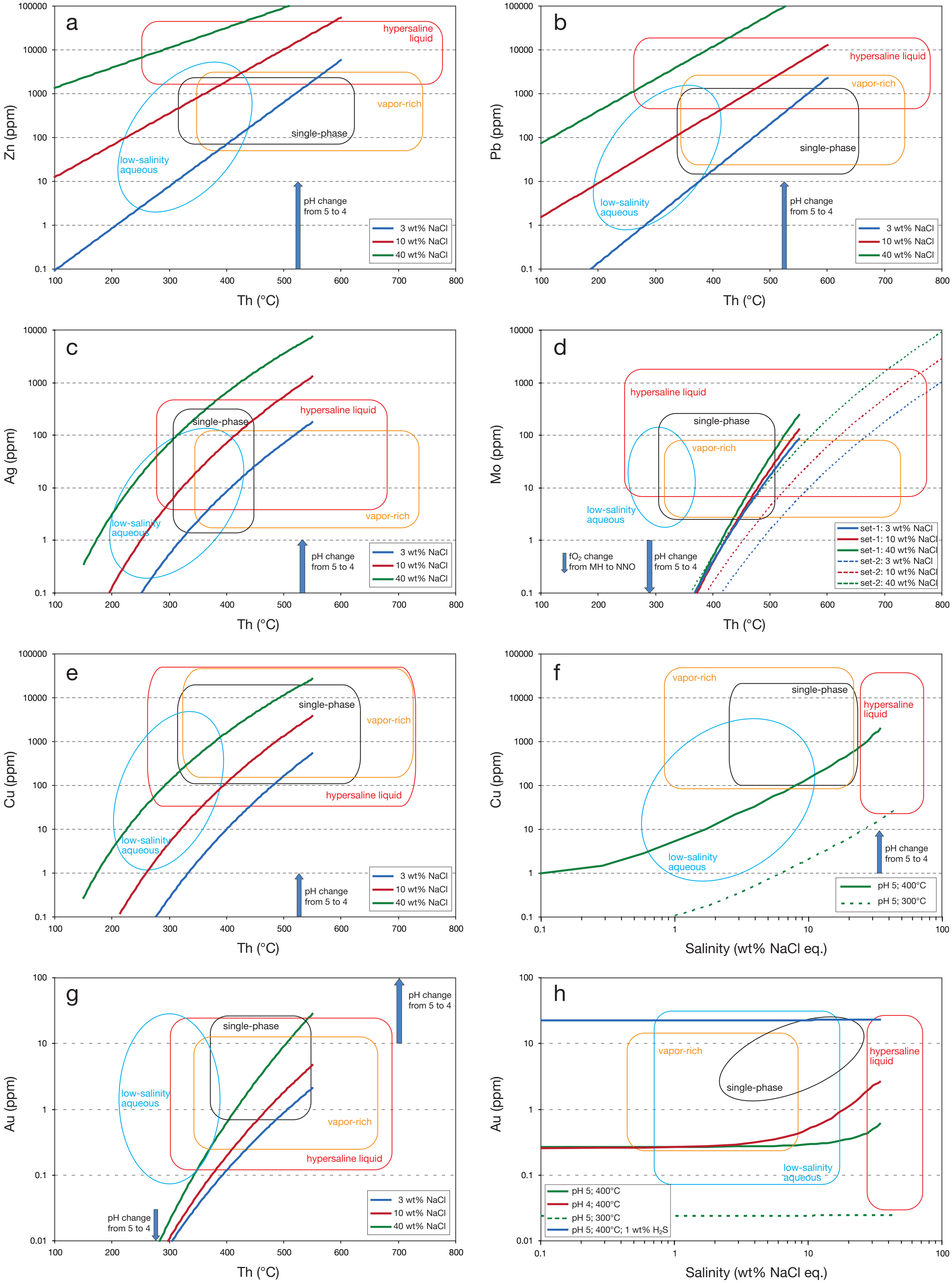
a
Zn (ppm)
100000
10000
1000
100
10
1
0.1
Th (°C)
100 200 300 400 500 600 700 800
hypersaline liquid
vapor-rich
single-phase
low-salinity aqueous
pH change from 5 to 4
3 wt% NaCl
10 wt% NaCl
40 wt% NaCl
b
Pb (ppm)
hypersaline liquid
vapor-rich
single-phase
low-salinity aqueous
pH change from 5 to 4
3 wt% NaCl
10 wt% NaCl
40 wt% NaCl
c
Ag (ppm)
10000
1000
100
10
1
0.1
single-phase
hypersaline liquid
vapor-rich
low-salinity aqueous
pH change from 5 to 4
3 wt% NaCl
10 wt% NaCl
40 wt% NaCl
d
Mo (ppm)
hypersaline liquid
single-phase
vapor-rich
low-salinity aqueous
fO_2 change from MH to NNO
pH change from 5 to 4
set-1: 3 wt% NaCl
set-1: 10 wt% NaCl
set-1: 40 wt% NaCl
set-2: 3 wt% NaCl
set-2: 10 wt% NaCl
set-2: 40 wt% NaCl
e
Cu (ppm)
single-phase
vapor-rich
hypersaline liquid
low-salinity aqueous
pH change from 5 to 4
3 wt% NaCl
10 wt% NaCl
40 wt% NaCl
f
Cu (ppm)
vapor-rich
single-phase
hypersaline liquid
low-salinity aqueous
pH change from 5 to 4
pH 5; 400°C
pH 5; 300°C
Salinity (wt% NaCl eq.)
0.1 1 10 100
g
Au (ppm)
100
10
1
0.1
0.01
pH change from 5 to 4
single-phase
low-salinity aqueous
vapor-rich
hypersaline liquid
pH change from 5 to 4
3 wt% NaCl
10 wt% NaCl
40 wt% NaCl
h
Au (ppm)
vapor-rich
single-phase
hypersaline liquid
low-salinity aqueous
pH 5; 400°C
pH 4; 400°C
pH 5; 300°C
pH 5; 400°C; 1 wt% H_2S
Salinity (wt% NaCl eq.)

mineralization in typical porphyry deposits, and explain the constancy of the Zn/Pb ratios in the evolving magmatic-hydrothermal fluid (Fig. 11). Fluid saturation with these minerals occurs at lower salinities (<10 wt % NaCl equiv) and temperatures (<350°C) typical for low-to-intermediate salinity aqueous fluids. These observations are consistent with the occurrence of Pb-, Zn-, and Ag-bearing minerals in more distal, marginal to epithermal, settings. The most efficient mechanism for the precipitation of Zn and Pb, at both high and low temperatures, is the neutralization of an acidic fluid (pH ~3-5); this may occur, for example, by interaction with carbonate or other sedimentary rocks. This effect leads to a pH increase of 2 to 3 units (e.g., pH ~6–7 of an evolved fluid in equilibrium with calcite), yielding a 10,000-fold decrease of both ZnS and PbS solubility (Fig. 17a, b; reactions 3, 4). This solubility decrease explains the abundance of Pb and Zn mineralization in skarns and carbonate-replacement deposits (Fig. 1), very likely caused by pH increase resulting from reaction with carbonate rocks.

Copper: Calculated chalcopyrite solubility (in the presence of pyrite) between pH values of 4 and 5 agrees relatively well above 450° to 500°C with data for metals in single-phase and hypersaline fluids (Fig. 17e). This observation explains the ubiquitous presence of $CuFeS_2$ over the wide temperature range of porphyry systems, and accounts for the large decrease of Cu/Zn and Cu/Pb ratios during the evolution of magmatic fluids (Fig. 11); in contrast to Cu, both Zn and Pb remain in the hypersaline liquid and vapor phase. At 350° ± 50°C, the calculated Cu solubility is an order of magnitude lower on average than Cu contents measured in single-phase and hypersaline liquid inclusions (Fig. 17e, f). This discrepancy may, however, be reconciled if the true entrapment temperatures were ~50°C higher than homogenization temperatures and/or if there was post-entrapment Cu enrichment of some inclusions due to preferential Cu^+ diffusion, as discussed above. The solubility of $CuFeS_2$ in moderate-salinity solutions below 300°C is 100 to 1,000 times lower than the Cu concentrations found in aqueous fluid inclusions from porphyry-related vein and epithermal deposits (Fig. 17f). To efficiently transport Cu to the epithermal environment, such fluids should be acidic (pH ~3) and probably somewhat reduced. These properties may be consistent with fluid origin from condensation of an HCl- and H_2S-bearing vapor produced from phase separation of a magmatic fluid (Heinrich et al., 2004; Heinrich, 2005). They are also consistent with a single-phase H_2S/SO_2-bearing fluid that cools above the solvus (Fig. 3; Hedenquist et al., 1998) and becomes acidic as a result of SO_2 disproportionation to sulfuric acid and H_2S with decreasing temperature (see below). In the latter case, to maintain the high acidity favorable for Cu solubility, such a fluid should either flow through previously leached rocks characterized by residual vuggy quartz without neutralization potential or be focused in fractures to limit its interaction with Na- and K-bearing silicates, as the latter would cause neutralization of acidic components.

Gold: In most high-temperature (>400°C), single-phase fluids and hypersaline liquids in which Au is predominantly transported as $AuCl_2^-$ (reaction 6d), the calculated Au solubility over a wide salinity range matches the average concentration found in the majority of inclusions of the corresponding types (Fig. 17g, h). Below 400°C, by contrast, the predicted total Au concentrations in equilibrium with pyrite are two to three orders of magnitude lower than those measured in low-salinity aqueous fluids (typically 1–10 ppm; Fig. 17g). In order to be able to transport such high Au contents, this type of fluid would require 10 to 50 times more H_2S than that allowed by equilibrium with an excess of pyrite and hematite/magnetite. Such H_2S concentrations may originate from a condensed Fe-deficient, but S- and Au-rich vapor phase, produced by intersection of the V-L solvus by the single-phase fluid on ascent, at high pressure and temperature (Heinrich, 2005; fluid path 4 in Fig. 3, as discussed above). However, such an H_2S-rich aqueous solution would not be able to transport Cu as well as Fe, Ag, Pb, and Zn ($CuFeS_2$ stoichiometric solubility at 300°C would indicate <1 ppm Cu and 1 ppm Fe in an aqueous solution of 5 wt % NaCl and 1 wt % H_2S at pH~4). The inability of such a H_2S-rich fluid to transport base metals disagrees with the high concentrations of these elements measured in low to intermediate salinity aqueous fluid inclusions (Figs. 5, 7, 8). Knowledge of the exact chemical speciation and amount of S is likely to be the key to resolving these discrepancies. For example, the recent discovery of polysulfide forms, such as S_3^-, in S-rich acidic fluids might account both for enhanced Au transport as direct complexes with S_3^- and increased solubility of other metal sulfide minerals in such solutions due to the consumption of H_2S to form S_3^- (Pokrovski and Dubrovinsky, 2011; Pokrovski and Dubessy, 2012).

Molybdenum: Calculated molybdenite solubility is consistent between two independent datasets within better than one order of magnitude; one study used thermodynamic data for molybdic acid, its anions, and ion pairs with alkali metals (reactions 7a-c; Zotov et al., 1995; Shock et al., 1997) and the other was based on extrapolations to lower temperatures of direct MoS_2 solubility measurements at 600° to 800°C, interpreted in terms of thiomolybdate-sodium species (Zhang et al., 2012). However, at conditions applicable to porphyry deposits, both datasets predict MoS_2 solubilities up to 3 to 4 orders of magnitude lower than Mo contents in natural fluid inclusions at T_h <450°C (Fig. 17d). Neither acidic (pH < 3-4) nor reduced and H_2S-rich fluids (arrows, Fig. 17d) are able to transport Mo; corrections of T_h to true temperature of entrapment are also insufficient to account for this discrepancy. A possible explanation may be the existence of other important Mo complexes (e.g., oxychlorides, sulfides, or polysulfides), which have not been included in experiments conducted on simple model systems; another cause may be an overestimation of H_2S contents resulting from omission of other S species, which may form at the expense of H_2S (e.g., S_3^-). Both factors will tend to increase MoS_2 solubility (reactions 7a-c).

Major hydrothermal controls on ore formation in porphyry systems

During their evolution in porphyry systems, magmatic-hydrothermal fluids undergo five major processes that cause metal redistribution and deposition: decompression, phase separation (or boiling), cooling, interaction with rocks, and mixing with external waters. These processes are interconnected and one may overprint or act in parallel with another.

The improved knowledge of both natural metal concentrations and their chemical speciation in the liquid and vapor phases may help to better estimate the effect of each of these processes on the different metals, and potentially lead to an improvement in exploration strategies. Below we discuss major consequences of each of these processes on metal transport and deposition.

Decompression: All ascending fluids, magmatic and otherwise, undergo pressure decrease. Although the most direct result of decompression is phase separation (see next subsection) and temperature decline, pressure decrease in a single-phase fluid may also affect mineral solubility. However, the quantification of this effect on solubilities of sulfide minerals is difficult because of lack of experimental data, particularly in low-density vapor and supercritical fluid. Robust data are only available for quartz, which shows a sharp decrease in solubility with decreasing pressure at a given temperature (Fig. 13; Fournier, 1999). This property, together with retrograde solubility of quartz in the temperature range ~370° to 470°C at pressures below ~800 bars, affects the formation of veins and fluid flow by changing permeability due to quartz dissolution or precipitation. For example, at Bingham Canyon, Cu deposition occurred by cooling and decompression in a narrow temperature and pressure interval (425°–350°C, 200–140 bars) coupled with the retrograde quartz solubility, which generated secondary vein permeability by quartz dissolution with temperature decrease (Landtwing et al., 2005).

Pressure is also suggested to have a major influence on Cu/Au ratios in many porphyry deposits, likely because its evolution is easier to trace than those of other parameters. For example, Murakami et al. (2010) compiled Cu/Au ratios for 50 porphyry-style Cu-Au ± Mo deposits and noted that there is a large variation in the values, from 10^3 to 10^6, and these appear to correlate with the depth and pressure of ore deposition. According to the authors, deep-seated porphyry Cu ± Mo deposits are expected to be deficient in Au and to have Cu/Au ratios higher than that of their primary magmatic-hydrothermal input fluid. This may be explained by earlier precipitation of chalcopyrite relative to gold from a cooling moderate-salinity fluid, consistent with the solubility trends discussed above. Landtwing et al. (2010) proposed that deposit-scale variation of Cu/Au ratios in the Bingham Canyon ore is due to different fluid paths, under slightly different pressure regimes, of a common input fluid in the central part and periphery of the stock, leading to the inverted-cup morphology of the orebody. According to their model, in the central zone of the orebody, characterized by denser fracturing and higher permeability (Gruen et al., 2010), the magmatic fluid expanded due to the transition from lithostatic to hydrostatic pressure, and ore deposition occurred at lower pressure than on the periphery, dominantly from a vapor-like fluid that was enriched in S, Au, and Cu compared to the single-phase magmatic fluid, and to a lesser degree from minor condensing brine. In the deeper peripheral zones, by contrast, this same magmatic fluid cooled at higher pressure and thus underwent less phase separation. An analogous mechanism might explain the similar Cu/Au zonation observed in other porphyry Cu-Au deposits (e.g., Batu Hijau, Indonesia; Arif and Baker, 2004). However, because the pressure and temperature decrease and associated changes occur together, it is challenging to identify the contribution of pressure itself on metal distribution. Furthermore, robust thermodynamic modeling of the pressure effect in complex vapor-liquid systems is difficult (see above).

Phase separation: The second key process is phase immiscibility, which is caused by pressure decrease as the fluid ascends toward the surface (Fig. 3); this is recorded in various parts of magmatic-hydrothermal systems by coexisting liquid- and vapor-rich fluid inclusions (Fig. 1; Table 1). In the deep porphyry environment, phase separation results in condensation of a minor amount of hypersaline liquid from the dominant low-salinity vapor phase (Fig. 3, path 4), whereas in the epithermal environment, phase separation occurs by boiling of the dominant aqueous liquid via generation of vapor bubbles. The effect of phase separation on metal transport and deposition in these two cases is different.

As shown above, phase separation in porphyry deposits at high temperature and pressure results in a contrasting fractionation of ore-forming elements, with As, S, Au (and partly Cu) enriched in the vapor phase compared to Fe, Zn, Pb, and Ag (Figs. 10, 15, 16). This enrichment was believed to be a prerequisite for the generation of fluids that could form epithermal Au-Cu deposits (Heinrich, 2005), with contraction of the supercritical phase to an acidic S-bearing liquid capable of transporting Cu and Au at relatively low temperatures. Such conditions may be met in high-sulfidation Cu-Au deposits (Hedenquist et al., 1993, 1998; Heinrich et al., 2004), which are spatially associated with magmatic intrusions and underlying porphyry deposits. Sulfur is likely to play an important role in the distribution of the Cu and Au between liquid and vapor phases, particularly considering the fact that the mass of the vapor produced during magmatic fluid separation exceeds that of the hypersaline liquid (typical vapor/hypersaline liquid mass ratios are 4–9; e.g., Hedenquist et al., 1998; Pudack et al., 2009; Landtwing et al., 2010; Lerchbaumer and Audétat, 2012).

The effect of phase separation in the porphyry environment on the behavior of Mo is less clear. For some porphyry Mo deposits it has been suggested that vapor-liquid separation may cause pre-enrichment of Mo in the hypersaline liquid, prior to molybdenite deposition by cooling (Klemm et al., 2008). However, limited fluid-inclusion analyses (Fig. 10; Seo et al., 2009, 2012) and laboratory experiments in S-free systems (Rempel et al., 2009) suggest that a significant portion of the Mo may also partition into the vapor phase. In contrast to Cu and Au, however, a S-rich vapor phase is expected to precipitate all Mo when it cools and condenses, because of predicted extremely low MoS_2 solubility at temperatures below 400°C (Figs. 14a, 17d), whereas Au and Cu will remain in the fluid. However, in both high and low-sulfidation epithermal systems, Mo can be locally abundant (up to >0.1 wt %), thus implying existence of other, not studied yet, Mo complexes, capable of transporting Mo at conditions relevant to epithermal environment.

In the low-temperature and pressure (<~100 bar) epithermal environment, the density of the vapor phase is too low for significant metal partitioning into the vapor phase (Fig. 15). The main effect of boiling of a liquid under such conditions is the removal of H_2S and CO_2 from the liquid phase. This process leads to the breakdown of Au hydrogen-sulfide complexes and causes gold precipitation in veins, such as gold-rich, bonanza-grade veins, corresponding to the depth at which boiling occurred below the paleowater table (e.g., Saunders and Schoenly, 1995; Simmons et al., 2005). In addition, boiling results in the pH of the liquid increasing due to the loss of CO_2, which, in turn, may lead to precipitation of base metal and Ag sulfides such as galena, sphalerite, chalcopyrite, pyrite, and argentite (see above).

Cooling: Temperature is likely the most direct factor that influences mineral solubility and, thus, metal transport and precipitation, as indicated by a number of porphyry deposit case studies. Landtwing et al. (2005) used fluid inclusion studies to demonstrate that cooling of a magmatic-hydrothermal fluid over a small temperature interval (425°–350°C) was the main cause of Cu ± Au deposition at Bingham Canyon (Fig. 18a); similar conclusions were reached for other porphyry Cu-Au and Cu-Mo systems, such as Bajo de la Alumbrera (Ulrich et al., 2001) and Butte (Rusk et al., 2004). Recently, Catchpole et al. (2011, in review) reported similar findings for porphyry Cu-related base metal veins at Morococha, where the magmatic fluid evolved to an aqueous liquid that formed polymetallic mineralization in the epithermal environment at temperatures of 380° to 250°C (Fig. 18b). They observed that Cu concentrations decreased by more than three orders of magnitude where the temperature decreased by 150°C. This observation agrees well with thermodynamic calculations of chalcopyrite solubility in a low-salinity (<5 wt % NaCl), S-rich (1,000–5,000 ppm S), and acidic (pH ~3) fluid characteristic of that at Morococha. Similar temperature-dependent trends were also established for Zn, Pb, Ag, and Mn (Catchpole et al., in review). These two examples (Fig. 18) demonstrate that both in deep porphyry and shallower epithermal environments, cooling below 400°C of a single-phase fluid initially containing ~10,000 ppm (1 wt %) Cu is an efficient mechanism of ore formation. These observations from ore deposits are consistent with the general temperature dependences of sulfide mineral solubility (Fig. 14a).

Cooling of a magmatic fluid is also accompanied by large changes in sulfur speciation, which in turn affect H_2S concentration and acidity, according to the following reaction:

$$4\ SO_2 + 4\ H_2O = H_2S + 3\ HSO_4^- + 3\ H^+ \qquad (9)$$

This reaction does not lead to significant redox changes since it is independent of oxygen fugacity, whereas it is strongly pH-dependent, and its extent will depend on the degree of fluid interaction with surrounding silicate rocks. Where pH is buffered by silicate rocks (albite, K-feldspar, and muscovite; pH ~5) during fluid flow and cooling, reaction (9) shifts to the right with decreasing temperature due to consumption of H^+ by the rock, and SO_2 breakdown proceeds to 99% completion at temperatures below 400°C.

The behavior of metals in two extreme cases of rock equilibration is quite different; a model magmatic fluid containing 10 wt % NaCl equiv, 1 wt % H_2S, 1 wt % SO_2, 10,000 ppm Fe, 5,000 ppm Cu, 300 ppm Mo and an excess of metallic Au (Fig. 19) was cooled numerically in or out of equilibrium with

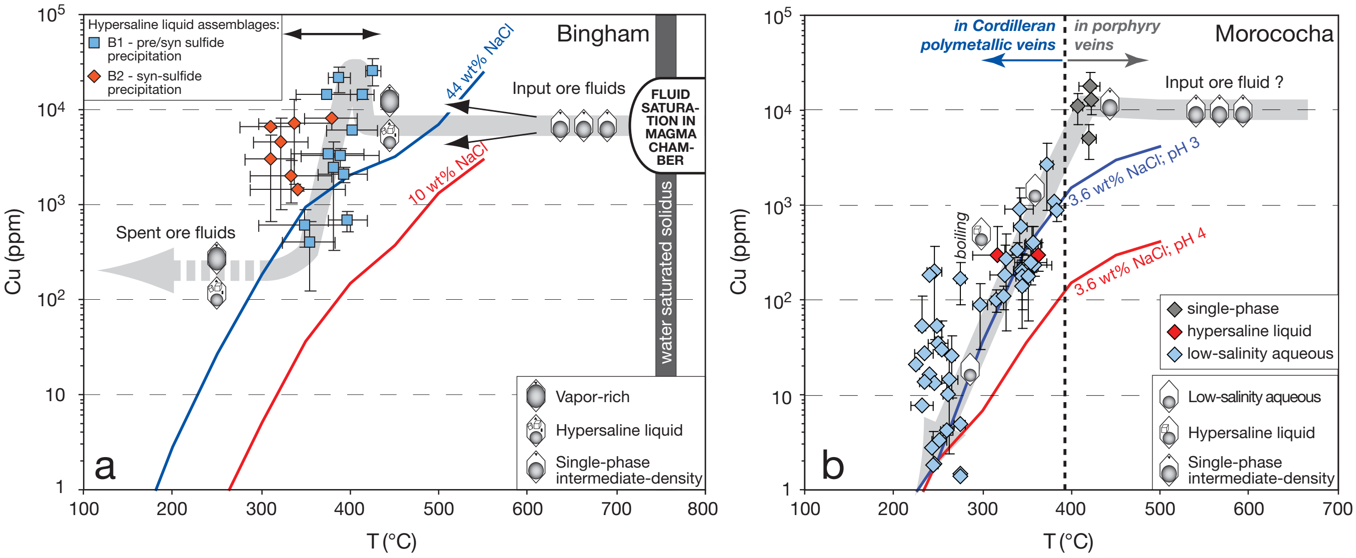

FIG. 18. Concentrations of Cu measured in fluid inclusions as a function of homogenization temperature in (a) the Bingham porphyry Cu-Mo-Au deposit and (b) the porphyry copper-related base metal vein system in Morococha, central Peru. Modified from Heinrich et al. (2005), Landtwing et al. (2005), and Catchpole et al. (in review). Each point represents a fluid inclusion assemblage, with 1σ error bars. Gray arrows correspond to fluid evolution paths. In both systems, the magmatic input fluid of intermediate density has initial concentration of ~10,000 ppm Cu (1 wt %). At Bingham, phase separation is associated with massive Cu precipitation in the porphyry environment at temperatures of 420° to 350°C, whereas at Morococha, a temperature decrease from 400° to 250°C caused a three orders of magnitude decrease in Cu concentration in the low-to-intermediate salinity aqueous fluids that formed polymetallic veins which overprinted the porphyry Cu-Mo system. Chalcopyrite solubility curves (this study) are reported for comparison as follows: in Bingham, for fluids with salinity of 10 and 40 wt % NaCl equiv at pH 5, in equilibrium with the pyrite-magnetite-hematite assemblage; and in Morococha, for fluids with salinity of 3.6 wt % NaCl equiv, 0.1 m H_2S, pH 3 and 4, and oxygen fugacity of hematite-magnetite assemblage. Acidic fluids (pH <3), likely produced by condensation of a vapor phase, are necessary to account for the observed Cu concentrations in low-salinity aqueous inclusions.

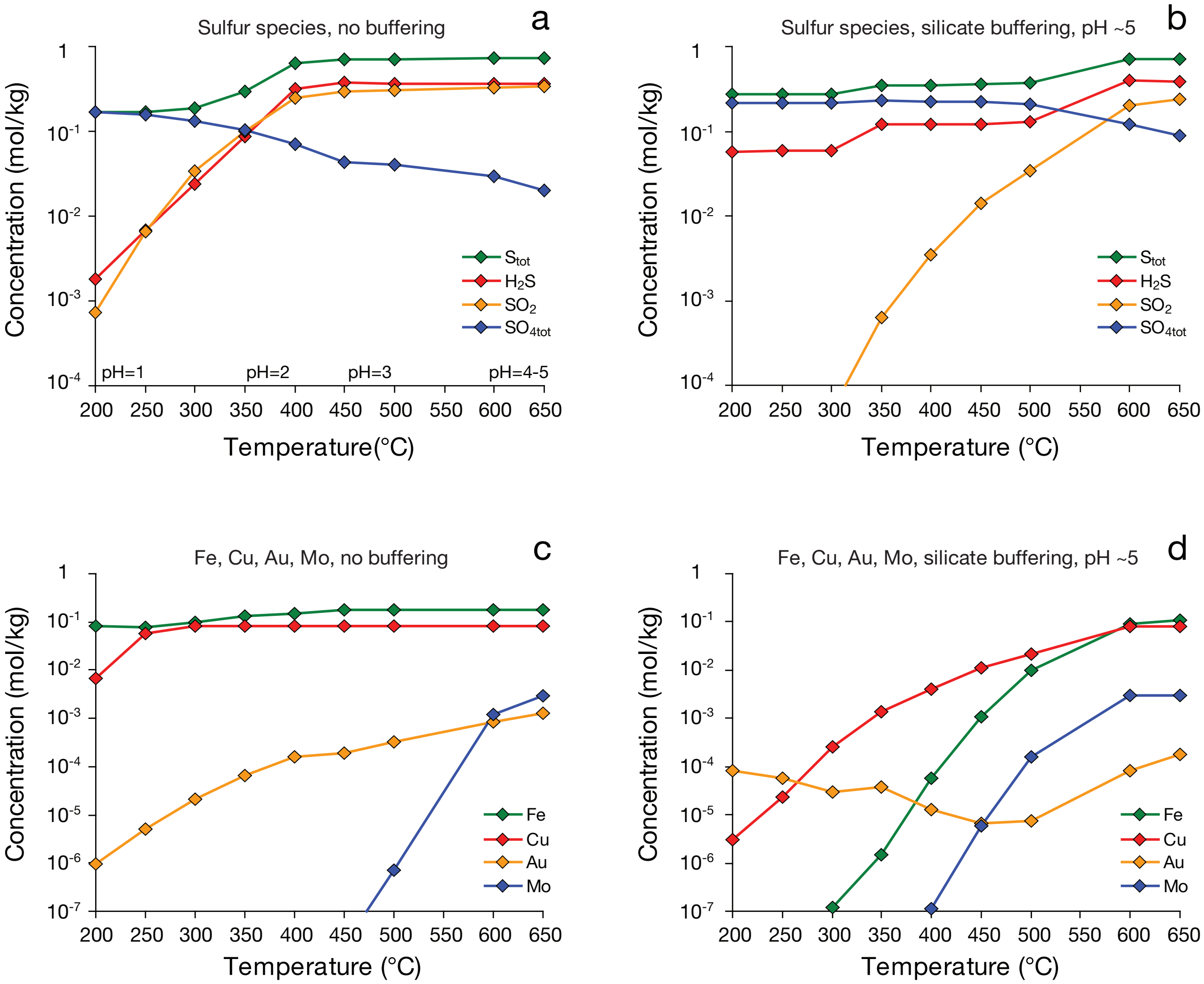

FIG. 19. Concentrations of principal sulfur forms (a, b) and Fe, Cu, Mo and Au (c, d) as a function of temperature in a model magmatic fluid initially containing 10 wt % NaCl equiv, 1 wt % H_2S, 1 wt % SO_2, 10,000 ppm Fe, 5,000 ppm Cu, 300 ppm Mo and an excess of metallic Au. Thermodynamic properties for S-species were taken from the SUPCRT database (Johnson et al., 1992; Sverjensky et al., 1997), whereas those of metal species are from references in Table 3. Panels (a) and (c) show the situation where the fluid cools in a closed system and is not allowed to react with alkali silicate minerals. Note the acidification of such a fluid on cooling; this is shown by pH values close to the temperature axis on panel (a), due to generation of sulfuric acid from the SO_2 disproportionation reaction (reaction 9). These acidic pH values favor Fe, Cu and Au transport as chloride complexes to temperatures as low as 300°–250°C; below these temperatures a significant portion of the Fe and Cu, Au and S precipitates as pyrite, chalcopyrite, covellite, native Au, and native S. Significant Mo transport by such a fluid is limited to >550°C. Panels (b) and (d) show the same fluid, cooling in contact with an excess of the quartz-muscovite/andalusite–K-feldspar assemblage that buffers the solution pH between 4.5 and 5.0 over the complete investigated temperature range. Note a sharp decrease of SO_2 concentrations below ~400°C, and high H_2S contents persisting down to 200°C. These contents, coupled with near-neutral pH, are unfavorable for Cu and Fe solubility below 400°–350°C, but are favorable for significant Au transport in the range from 600° to 200°C, to conditions of formation of Au epithermal deposits; by contrast, Mo mobility in the fluid phase is significant only above 450° to 500°C. These two contrasting scenarios are likely to encompass the range of conditions that natural fluids undergo (see text for details).

an assemblage of quartz+muscovite/andalusite+K-feldspar. The initial fluid composition corresponds to typical salt, S, and metal contents found in single-phase fluid inclusions from major porphyry deposits (see above), and is similar to that adopted in previous modeling studies (e.g., Heinrich, 2005). In the absence of fluid neutralization by silicate rocks (Fig. 19a), reaction (9) causes acidification of the cooling fluid, which is very favorable for Cu and Fe mobility (Fig. 14). Thus, large metal concentrations (in the form of chloride complexes) may be carried without significant loss by such a fluid to temperatures as low as 200°C (Fig. 19c). In contrast, where pH of the fluid is neutralized by interaction with aluminosilicate rocks, >90% of the initial Cu and Fe will precipitate from the solution between 600° and 400°C in the form of magnetite (at 500°–600°C) and pyrite + chalcopyrite (at <500°C). This agrees with observed Cu-Fe mineralization in high-temperature porphyry stages (potassic alteration). Depending on the fluid-rock ratio and fluid flow paths and velocities, neutralization of this acidic fluid may be delayed until further ascent and cooling. For this reason, in many porphyry deposits the bulk of the Cu mineralization (mainly as chalcopyrite and bornite) precipitates at temperatures close to 400°C, where reaction (9) moves strongly to the right, and at lower temperatures than the initial quartz veining that accompanies the potassic alteration (e.g., Landtwing et al., 2005). However, such a neutralized fluid will be unable to carry significant amounts of Cu and Fe (and Pb, Zn, Ag) to the low-temperature epithermal environment. The effective transport of these metals to such settings by S-rich fluids is thus only possible if the pH of the acidic fluid does not change as it ascends through the rock, which requires the buffering capacity of the rock to already have been altered by an earlier acidic fluid. Such an early acidic fluid prepares a favorable conduit for one or more subsequent pulses of fluid rich in metals, both by consuming the neutralization capacity of the rock and creating additional permeability due to partial mineral dissolution. This effect allows Cu and Fe to be transported further and deposited later in pyrite-chalcopyrite veins associated with a phyllic overprint of potassic alteration (e.g., Hedenquist et al., 1998; Pudack et al., 2009). In addition, a portion of the Cu initially precipitated during the potassic stage may be redissolved by a subsequent acidic fluid and redeposited in the upper and cooler levels of the system, e.g., within the phyllic zone or shallower advanced argillic lithocap overlying the porphyry environment (Brimhall, 1977; Sillitoe, 2010; Fig. 1).

The behavior of Au upon the disproportionation of SO_2 is more complex, because of the change of dominant Au species from chloride (reaction 6d) to sulfide (reactions 6a-c) with a decrease in the temperature and an increase in the progress of reaction (9) to the right. With an excess of S over metals, a magmatic fluid will be able to carry Au at concentrations of >10 ppm to low temperatures (~250°C), buffered or not with rocks and without reaching saturation with the metal (Fig. 19); this is despite the large differences in Au speciation and solubility-controlling factors between acidic and neutral fluids. The interplay between the initial fluid redox, S, Cl, and major metal concentrations may have different effects on Au behavior in different deposits (e.g., Heinrich, 2005). This uncertainty is superimposed on another major unknown of Au aqueous chemistry; the existence or not of dissolved S-bearing complexes other than H_2S, such as SO_2 or polysulfides (Pokrovski et al., 2008a, 2009a).

In contrast to all other metals, the capacity for Mo transport will be decreased sharply upon SO_2 disproportionation, because an increase in the H_2S content and acidity both decrease MoS_2 solubility (Figs. 14c, d, 17d, 19d). Fluid neutralization by reaction with aluminosilicate rocks may help maintain significant Mo concentrations (>~10s ppm) in the fluid down to ~500°C (Fig. 19d). This effect might explain the higher temperature of molybdenite formation compared to that of Cu and Au (~400°C) in some Mo-dominated porphyry deposits (e.g., Henderson; Seedorff and Einaudi, 2004). However, in typical porphyry Cu-Au deposits, Mo generally postdates the main stage of Cu-Fe sulfide precipitation and/or can be more distal from the intrusion than Cu (e.g., Sillitoe, 1979, 2010; Seedorff et al., 2005; Rusk et al., 2008b; Seo et al., 2012). A quantitative physical-chemical interpretation of this distribution pattern is not obvious. Seo et al. (2012) suggested that small differences in redox potential and acid/base balance of the magmatic source might lead to the temporal and spatial separation of Mo from Cu in porphyry Cu-Au deposits such as Bingham Canyon (Porter et al., 2012). However, the available thermodynamic data on Mo species (see above), coupled with a realistic range of redox and acidity parameters for porphyry systems and associated magmatic rocks, underestimate by many orders of magnitude (e.g., Fig. 19a, b) the Mo concentrations measured in natural fluid inclusions (100s ppm; Figs. 5, 7, 8). Either variations in source-magma chemistry, fluid-magma interaction, and metal and S contents are much larger than those inferred from available geologic observations and analyses, or as yet unknown Mo-bearing species control the transport of this metal, both in liquid and vapor phases. The latter issue is expected to be resolved by future experimental work.

Fluid-rock interaction: The fourth major process accompanying the evolution of a magmatic-hydrothermal fluid is its interaction with surrounding rocks, leading to changes of pH, redox state, and sulfide content, and thus mineral alteration and metal precipitation. In porphyry and related settings, fluid-rock interaction is expressed as alteration zonation centered on the fluid source and propagating into the surrounding rocks (Figs. 1, 2). As highlighted above, the stronger the neutralizing capacity of the rock, the more efficient will be the metal precipitation. A particularly good example is provided by the skarn environment with its commonly observed metal zonation from proximal Cu ± Au to distal Zn-Pb zones, resulting from a combination of temperature decrease and neutralization of the fluid by the carbonate wall rocks. Carbonate sediment-hosted Au deposits may form in the distal portions of porphyry systems (e.g., the Bingham Canyon district; Cunningham et al., 2004; Fig. 1), likely due to rock decarbonitization and the resulting pH increase.

The redox state of the fluid may also change during alteration processes. For example, intermediate-composition calc-alkaline magmatic rocks typically contain a significant fraction of iron as FeO, which tends to reduce SO_2 to H_2S in the magmatic fluid during temperature decrease (Giggenbach, 1992; Einaudi et al., 2003). Although the typical redox changes in porphyry systems have a relatively modest effect on Fe, Cu, and Au mineral solubility (e.g., an f_{O_2} change by an order of magnitude will change FeS_2, $CuFeS_2$, and Au solubility by only a factor of 2–3), the interaction with an Fe(II)-bearing rock may act as a sink for hydrogen sulfide by precipitation of pyrite ± pyrrhotite, and lower the sulfidation state of the fluid when temperature decreases to <300°C (Einaudi et al., 2003). This H_2S consumption will shift reactions (6a-c) to the right, leading to precipitation. This explains the common presence of chalcopyrite in biotite sites in porphyry deposits, and high porphyry Cu and Au grades in deposits associated with mafic rocks, such as Oyu Tolgoi, Mongolia, and Resolution, Arizona (Sillitoe, 2010).

Fluid mixing: The fifth major phenomenon is mixing of two fluids with distinct temperature, salinity, acidity, and/or redox properties. This process may contribute to ore formation in some near-surface crustal settings such as seafloor hydrothermal systems and Mississippi Valley-type deposits (Franklin et al., 2005; Leach et al., 2005). However, in porphyry deposits there is little evidence for incursion of external waters into the deep porphyry orebody, either before or during Cu and Au precipitation. It is widely accepted, based on stable isotope (e.g., Hedenquist et al., 1998; Watanabe and Hedenquist, 2001; Harris and Golding, 2002) and fluid inclusion (e.g., Ulrich et al., 2001; Pudack et al., 2009) studies that fluids that cause potassic alteration cores and large phyllic alteration overprints have a dominantly magmatic fluid component (Hedenquist et al., 1998; Seedorff and Einaudi, 2004; Rusk et al., 2008b). As emphasized by Seedorff et al. (2008), field evidence and hydrological modeling suggest that dense brines such as saline formation waters or re-circulated magmatic hypersaline liquid (Fig. 2) may access the deep, central, and peripheral high-temperature parts of the hydrothermal systems, causing deep sodic-calcic alteration during heating. However, the influence of such potential fluid mixing on Cu and Au precipitation in porphyry orebodies has not been evaluated.

In summary, cooling of a magmatic fluid during ascent and depressurization, accompanied by water-rock interaction, is likely to be the major cause of most metal deposition in porphyry systems. Fluid immiscibility is a major process that may occur at different levels in magmatic-hydrothermal systems and strongly affect sulfur, and precious and base-metal behavior. Large-scale mixing with meteoric and sedimentary-basin fluids is a relatively uncommon phenomenon during metal precipitation, and is not expected to be a major cause of ore formation in the porphyry environment. These general tendencies determine the metal zoning in magmatic-hydrothermal systems and may provide clues for prospecting, if the major events in fluid evolution are identified from geologic as well as fluid inclusion, mineralogic or stable isotope studies.

Conclusions

This paper compiles recent data on fluid compositions from porphyry Cu (-Mo-Au) and associated deposits as recorded by fluid inclusions, quantitatively analyzed by new microanalytical techniques such as LA-ICP-MS, PIXE, and SR-XRF. The resulting data, together with the known properties of the H_2O-NaCl system, reveal four major genetic types of inclusions in the porphyry environment that reflect the temperature and pressure evolution of a magmatic metal-bearing fluid: (1) single-phase fluid of moderate salinity containing metals and volatiles (CO_2, H_2S, SO_2) exsolved from the magma, (2) aqueous low-density vapor and (3) hypersaline high-density liquid, both produced by unmixing of the single-phase fluid on cooling and decompression when it crosses the two-phase vapor-liquid boundary of the salt-water system in porphyry and skarn environments, and (4) low-salinity aqueous fluids generated by condensation of the single-phase or vapor-type fluids and their eventual mixing with meteoric waters in the epithermal environment—the shallow parts of porphyry systems.

The metal contents of the single-phase magmatic fluid at the base of the porphyry environment show patterns controlled by metal abundances in crustal silicate magmas, coupled with elevated fluid/melt metal partitioning coefficients; this results in the single-phase fluid having the following general composition: Fe (~10,000 ppm) > Cu (~4,000 ppm) ≈ Mn (~2,000 ppm) > Zn (~700 ppm) ≈ Pb (~300 ppm) > Mo (~80 ppm) > Ag (~30 ppm) > Au (~1 ppm), with typical variations within about an order of magnitude around these mean values. For the metals of economic interest in porphyry Cu-Au and related deposits (Cu, Au, Mo ± Zn, Pb), these concentrations are one to three orders of magnitude higher than their average crustal abundances, resulting in a high potential of magmatic-hydrothermal fluids to form porphyry and related deposits.

Metal concentrations in the aqueous vapor and hypersaline liquid inclusions are controlled by vapor-liquid partitioning coefficients, which depend on the vapor and liquid densities and chemical metal speciation. Thus, Fe, Mn, Zn, Pb, and Ag, which form chloride complexes in both phases, are generally enriched in the saline chloride liquid, whereas Au, which preferentially forms hydrogen sulfide complexes, is systematically enriched in the vapor phase. Metalloids, like As and Sb, and Mo show, on average, similar concentrations in the liquid and vapor phase, consistent with the volatile properties of their oxyhydroxide species revealed by experiments in model systems. Copper contents exhibit the largest variation relative to the other metals, with vapor-liquid distribution coefficients from 0.01 to 100. This is likely to be due in part to post-entrapment modification of the primary single-phase and vapor-rich fluid inclusions caused by diffusion of Cu through quartz to the inclusion fluid from the evolving hydrothermal fluid, as shown by recent laboratory measurements. These data, combined with other recent experiments on vapor-liquid partitioning, strongly suggest that the true vapor-liquid distribution of Cu during phase separation is intermediate between that of base metals and metalloids, with Cu contents on average an order of magnitude higher in the hypersaline liquid phase than in the vapor in porphyry systems.

Metal concentrations in the low-salinity aqueous fluids are generally one to two orders of magnitude lower than those in the high-temperature single-phase, vapor-rich, and hypersaline liquid inclusions, and decrease with decreasing temperature. This reflects the decrease of sulfide mineral solubility with fluid cooling and mixing with external waters in the epithermal environment. The only exception among these metals is Au, whose concentrations in low-salinity aqueous fluids are similar to those in higher temperature porphyry fluids (~1–10 ppm). This observation may be explained by the selective transport of Au by the vapor phase, which condenses into an H_2S-rich aqueous solution on cooling and carries large amounts of Au as S-bearing complexes.

The metal contents measured in natural fluid inclusions may be interpreted in light of the present-day knowledge of the solubility of ore minerals and the speciation of metals in hydrothermal solutions under the conditions typical of porphyry systems. The available thermodynamic data on the stability of sulfide minerals and the main aqueous chloride, sulfide, and hydroxide species of metals allow predictions of mineral solubilities in the liquid and dense supercritical fluids as a function of key parameters such as temperature, pressure, salinity (Cl content), acidity (pH), S concentration, and redox potential. When these parameters are constrained to the typical range of porphyry systems, based on temperatures and pressures and major fluid components recorded in fluid inclusions and alteration mineral patterns, calculations of mineral solubilities generally reproduce well the Cu, Ag, Fe, Zn, and Pb concentrations measured in the different types of fluid inclusions. In contrast, thermodynamic predictions for Au in epithermal fluids, and, more particularly, Mo in both epithermal and porphyry fluids underestimate the contents of these metals compared to natural compositions. This situation points to gaps in existing speciation models of both metals and S, likely due to neglecting some important species.

This comparison of natural data and physical chemistry provides useful constraints on the mechanisms and processes controlling metal transport and deposition in the porphyry and epithermal environments. Modeling shows that cooling of a magmatic fluid, accompanied by water-rock interaction, is likely to be the major cause of most metal deposition in porphyry systems, resulting in the formation of Cu ± Au ± Mo ore shells, centered on the porphyry stock. Outward base-metal zoning consists of Cu-Zn, Zn-Pb-Ag, Pb-Ag, and As-Sb-Hg-Au zones, in order of increasing distance from the porphyry center; this matches well the observed metal zonation in many porphyry districts around the world. Changes in S speciation on cooling, caused by SO_2 disproportionation, are likely to control the fractionation of Au from Cu during fluid evolution on ascent. Efficient neutralization through water-rock interaction is also a major driving force for Zn, Pb, and, in part, Au and Ag deposition in more distal portions of porphyry systems. Fluid immiscibility is a major process that may occur at different levels in magmatic-hydrothermal systems and strongly affects the behavior of S and Au versus other metals by contrasting fractionation between the resulting vapor and liquid phases. Large-scale mixing with meteoric and sedimentary-basin fluids is a relatively uncommon phenomenon and is not expected to be a major cause of ore formation in the porphyry environment.

Challenges

Despite significant progress in understanding the composition and properties of ore-forming fluids in porphyry systems, much remains to be done. The necessary work spans analytical, experimental, and theoretical fields of research whose major near-future challenges are briefly outlined below.

Analytical challenges

A number of analytical challenges regarding fluid inclusions, which are the only direct samples of ore-forming fluids, remain to be addressed. Among the elements in ore fluids, S is one of the most poorly understood and quantified components. Because the S concentration and redox state of the fluid phase commonly control the metal supply, mineralization efficiency, and ore grade in porphyry and associated epithermal systems, systematic S analyses of fluid inclusions are needed. Although this is now analytically possible, only a few studies have actually analyzed S contents in individual fluid inclusions using LA-ICP-MS techniques (Guillong et al., 2008; Seo et al., 2009, 2011, 2012; Catchpole et al., 2011, in review). Such total S analyses should be coupled with in situ spectroscopic determination of the speciation of S, using in situ micro-Raman spectroscopy (e.g., Giuliani et al., 2003), and potentially X-ray absorption spectroscopy (e.g., Métrich et al., 2009).

Further in situ measurement of Cl/Br, $^{87}Sr/^{86}Sr$ and Pb-isotope ratios via LA-ICP-MS analyses of individual fluid inclusions can improve our understanding of component sources in porphyry systems as well as the chronology of ore formation (Pettke et al., 2010, 2011, 2012; Seo et al., 2011). An interesting finding of the present study is the potential to use Zn/Pb ratios in high-temperature fluids from porphyry systems for tracing magmatic processes and magma-host rock interaction involved in ore fluid generation. A better appreciation of possible fluid-inclusion post-entrapment modifications, such as selective metal diffusion (e.g., Lerchbaumer and Audétat, 2012), is also essential for robust interpretation of ore fluid compositions. Many elements may be powerful geochemical tracers, such as REE, but are not yet routinely analyzed in fluid inclusions, even if they are present at concentrations easily detectable by in situ techniques such as LA-ICP-MS.

In contrast to porphyry-style deposits, for which a large fluid-composition data set is available, the information on ore-forming fluid compositions in low pressure and temperature environments dominated by aqueous-type fluids, such as epithermal and Carlin-type Au deposits, is still fragmentary. In such settings, a recently developed method, combining near-infrared microscopy with LA-ICP-MS (Kouzmanov et al., 2010), allows direct analyses of the actual metal-precipitating fluids in inclusions hosted by opaque ore minerals, such as enargite, wolframite, stibnite, sphalerite, tetrahedrite, and pyrite. This opens up new potential for fluid inclusion research in ore deposits, enabling direct determination of PTX characteristics of the fluids that precipitated ore minerals, in addition to information provided by the commonly used optically transparent gangue minerals; this will allow verification of the broadly accepted assumption that gangue and associated ore minerals are cogenetic. For example, Simmons et al. (1988) reported microthermomic data of sphalerite-, pyrargyrite-, quartz-, and calcite-hosted fluid inclusions from the Santo Niño intermediate-sulfidation epithermal vein at Fresnillo, Mexico, and demonstrated that ore minerals in this system precipitated from chemically distinct fluid compared to those that precipitated the gangue minerals ("brine fluids" with salinity of 8.5–12 wt % NaCl equiv vs. dilute fluids with salinity of ~2 wt % NaCl equiv, respectively), suggesting episodicity of ore-forming pulses in the hydrothermal system.

Experimental challenges

The novel analytical directions outlined above should be coupled with speciation and solubility experiments in geologically relevant model systems under controlled laboratory conditions that nature does not offer to geologists. One of the major remaining gaps in this field is S speciation in high-temperature fluids (aqueous and silicate melts). The recent discovery of a new polysulfide sulfur form in S-rich fluids, the trisulfur ion S_3^-, which is stable in aqueous fluids over a wide temperature and pressure range (Pokrovski and Dubrovinsky, 2011; Pokrovski et al., 2011; Jacquemet et al., 2012; Pokrovski and Dubessy, 2012), might affect our interpretation of S transport in porphyry systems, its isotopic fractionation, and S control on metal mobility. In situ spectroscopy approaches (Raman, XAS) are necessary to better constrain the stability field of S_3^- and other intermediate S forms (e.g., SO_2) and quantify their effect on Au, Cu, and Mo mineral solubility and metal transport via direct complexing.

Another essential experimental need is to improve our knowledge of the speciation and solubility of certain porphyry-related metals, such as Mo, for which large discrepancies persist. Better knowledge of aqueous speciation and mode of occurrence in host sulfide phases of trace elements, such as Pt, Bi, Se, and Te that commonly accompany the major ore metals, is also required. Another experimental challenge will be to better understand the effect of CO_2, a major volatile in magmatic-hydrothermal systems, on metal transport. Recent studies (e.g., Pokrovski et al., 2008a; Hanley and Gladney, 2011) point to enhanced transport of Cu, Au, Pd, and Ni by such CO_2-rich fluids, but there is no sound physical-chemical interpretation of this potentially important phenomenon, since experimental data on metal sulfide solubility in CO_2-rich fluids are lacking. Finally, a recent direction in hydrothermal research related to porphyry deposits is the use of nontraditional stable isotopes of metals (Cu, Fe, Mo) in an attempt to trace metal and fluid sources and evolution (e.g., Graham et al., 2007; Hannah et al., 2007; Mathur et al., 2009, 2010). However, interpretation of these new analytical data requires knowledge of equilibrium and kinetic isotope fractionation factors among different minerals and between minerals and fluids, which can only be acquired via experimental measurements. For example, such data may provide better constraints on timing and conditions of iron sulfide mineral formation under hydrothermal conditions (e.g., Saunier et al., 2011, and references therein).

Theoretical challenges

A major challenge in ore-deposit research continues to be interpretation of pertinent experimental data for mineral solubility and metal speciation in the framework of physical-chemical equations of state and development of theoretical approaches enabling predictions over a wide range of conditions relevant to porphyry deposits, from the single-phase fluid to hypersaline liquid or low-density vapor phase. These equations should be integrated in user-friendly databases and computer codes (e.g., Oelkers et al., 2009). These data, coupled with physical hydrology models based on heat and fluid flow plus rock permeability, will allow integrated reactive transport models of fluid paths and three-dimensional ore distribution (Driesner and Geiger, 2007; Ingebritsen et al., 2010; Ingebritsen and Appold, 2012), which can contribute to better exploration and extraction strategies.

Acknowledgments

This work was supported by the Swiss National Science Foundation (grant 20021-127123 to K.K.) and l'Agence Nationale de la Recherche (grant SOUMET-ANR 2011 Blanc SIMI 5-6/009-01 to G.S.P). We thank J.W. Hedenquist for inviting us to write this contribution, his patience while waiting for both initial and revised manuscript, and his invaluable comments and suggestions. R.H. Sillitoe is acknowledged for permission to use one of his published figures and for his detailed comments on the manuscript, T. Driesner for sharing numerical data on the NaCl-H_2O system, and J.P. Richards and B. Rusk for thoughtful reviews that greatly improved the clarity of the paper.

REFERENCES

Akinfiev, N.N., and Diamond, L.W., 2003, Thermodynamic description of aqueous nonelectrolytes at infinite dilution over a wide range of state parameters: Geochimica et Cosmochimica Acta, v. 67, p. 613–627.

Akinfiev, N.N., and Zotov, A.V., 1999. Thermodynamic description of equilibria in mixed fluids (H_2O-non-polar gas) over a wide range of temperature (25–700°C) and pressure (1-5000 bars): Geochimica et Cosmochimica Acta, v. 63, p. 2025–2041.

——2001, Thermodynamic description of chloride, hydrosulphide, and hydroxide complexes of Ag(I), Cu(I), and Au(I) at temperatures of 25–500°C and pressures of 1–2000 bar: Geochemistry International, v. 39, p. 990–1006.

——2010, Thermodynamic description of aqueous species in the system Cu-Ag-Au-S-O-H at temperatures of 0–600°C and pressures of 1–3000 bar: Geochemistry International, v. 48, p. 714–720.

Allan, M.M., Morrison, G.W., and Yardley, B.W.D., 2011, Physicochemical evolution of a porphyry-breccia system: A laser ablation ICP-MS study of fluid inclusions in the Mount Leyshon Au deposit, Queensland, Australia: Economic Geology, v. 106, p. 413–436.

Alvarez, J., Corti, H.R., Fernandez-Prini, R., and Japas, M.L., 1994, Distribution of solutes between coexisting steam and water: Geochimica et Cosmochimica Acta, v. 58, p. 2789–2798.

Anderson, A.J., Clark, A.H., Ma, X.P., Palmer, G.R., Macarthur, J.D., and Roedder, E., 1989, Proton-induced X-ray and gamma-ray emission analysis of unopened fluid inclusions: Economic Geology, v. 84, p. 924–939.

Anderson, G.M., Castet, S., Schott, J., and Mesmer, R.E., 1991, The density model for estimation of thermodynamic parameters of reactions at high temperature and pressure: Geochimica et Cosmochimica Acta, v. 55, p. 1769–1779.

Archibald, S.M., Migdisov, A.A., and Williams-Jones A.E., 2001, The stability of Au-chloride complexes in water vapor at elevated temperatures and pressures: Geochimica et Cosmochimica Acta, v. 65, p. 4413–4423.

——2002, An experimental study of the stability of copper chloride complexes in water vapor at elevated temperatures and pressures: Geochimica et Cosmochimica Acta, v. 66, p. 1611–1619.

Arif, J., and Baker, T., 2004, Gold paragenesis and chemistry at Batu Hijau, Indonesia: Implications for gold-rich porphyry copper deposits: Mineralium Deposita, v. 39, p. 523–535.

Arribas, A., 1995, Characteristics of high-sulfidation epithermal deposits, and their relation to magmatic fluid: Mineralogical Association of Canada Short Course Series, v. 23, p. 419–454.

Arribas, A.J., Hedenquist, J. W., Itaya, T., Okada, T., Concepción, R.A., and Garcia, J.S.J., 1995, Contemporaneous formation of adjacent porphyry and epithermal Cu-Au deposits over 300 ka in northern Luzon, Philippines: Geology, v. 23, p. 337–340.

Audétat, A., and Pettke, T., 2003, The magmatic–hydrothermal evolution of two barren granites: a melt and fluid inclusion study of the Rito del Medio and Canada Pinabete plutons in northern New Mexico (USA): Geochimica et Cosmochimica Acta, v. 67, p. 97–121.

Audétat, A., and Simon, A.C., 2012, Magmatic controls on porphyry copper genesis: Society of Economic Geologists Special Publication 16, p. 553–572.

Audétat, A., Günther, D., and Heinrich, C.A., 1998, Formation of a magmatic–hydrothermal ore deposit: insights with LA-ICP-MS analysis of fluid inclusions: Science, v. 279, p. 2091–2094.

——2000a, Magmatic–hydrothermal evolution in a fractionating granite: A microchemical study of the Sn-W-F–mineralized Mole granite (Australia): Geochimica et Cosmochimica Acta, v. 64, p. 3373–3393.

——2000b, Causes for large-scale metal zonation around mineralized plutons: fluid inclusion LA-ICP-MS evidence from the Mole granite, Australia: Economic Geology, v. 95, p. 1563–1581.

Audétat, A., Pettke, T., Heinrich, C.A., and Bodnar, R.J., 2008, The composition of magmatic–hydrothermal fluids in barren versus mineralized intrusions: Economic Geology, v. 103, p. 877–908.

Babcock, R.C., Jr., Ballantyne, G.H., and Phillips, C.H., 1995, Summary of the geology of the Bingham district: Arizona Geological Society Digest, v. 20, p. 316–335.

Baker, T., Van Achterberg, E., Ryan, C., and Lang, J.R., 2004, Composition and evolution of ore fluids in a magmatic-hydrothermal skarn deposit: Geology, v. 32, p. 117–120.

Bakker, R.J., 2009, Package FLUIDS. Part 3: correlations between equations of state, thermodynamics and fluid inclusions: Geofluids, v. 9, p. 63–74.

Ballard, J.R., Palin, J.M., Williams, I.S., Campbell, I.H., and Faunes, A., 2001, Two ages of porphyry intrusion resolved for the super-giant Chuquicamata copper deposit of northern Chile by ELA-ICP-MS and SHRIMP: Geology, v. 29, p. 383–386.

Barnes, H.L., 1979, Solubility of ore minerals, *in* Barnes, H.L., ed., Geochemistry of hydrothermal ore deposits, 2nd ed.: New York, John Wiley & Sons, p. 404–460.

——1997, Geochemistry of hydrothermal ore deposits, 3rd ed., Barnes H.L., ed., New York, John Wiley & Sons, 972 p.

Barra, F., 2011, Assessing the longevity of porphyry Cu-Mo deposits: examples from the Chilean Andes: *in* Barra, F., Reich, M., Campos, E., and Tornos, F., eds., Let's talk ore deposits: SGA Biennial Meeting, 11th, 26–29 September 2011, Antofagasta, Chile, Proceedings, p. 145–147.

Baumgartner, R., Fontboté, L., and Vennemann, T., 2008, Mineral zoning and geochemistry of epithermal polymetallic Zn-Pb-Ag-Cu-Bi mineralization at Cerro de Pasco, Peru: Economic Geology, v. 103, p. 493–537.

Bazarkina, E.F., Pokrovski, G.S., Zotov, A.V., Hazemann, J-L., 2010, Structure and stability of cadmium chloride complexes in hydrothermal fluids: Chemical Geology, v. 276, p. 1–17.

Beane, R.E., 1982, Hydrothermal alteration in silicate rocks, in Titley, S.R.,ed., Advances in geology of the porphyry copper deposits, southwestern North America: Tucson, University of Arizona Press, p. 117–137.

Beane, R.E., and Bodnar, R.J., 1995, Hydrothermal fluids and hydrothermal alteration in porphyry copper deposits: Arizona Geological Society Digest, no. 20, p. 83–93.

Beane, R.E., and Titley, S.R., 1981, Porphyry copper deposits: hydrothermal alteration and mineralization: Economic Geology 75th Anniversary Volume, p. 235–269.

Becker, S.P., Fall, A., and Bodnar, R.J., 2008, Synthetic fluid inclusions. XVII. PVTX properties of high salinity H_2O-NaCl solutions (> 30 wt % NaCl): Application to fluid inclusions that homogenize by halite disappearance from porphyry copper and other hydrothermal ore deposits: Economic Geology, v. 103, p. 539–554.

Bethke, P.M., Rye, R.O., Stoffregen, R.E., and Vikre, P.G., 2005, Evolution of the magmatic-hydrothermal acid-sulfate system at Summitville, Colorado: Integration of geological, stable-isotope, and fluid-inclusion evidence: Chemical Geology, v. 215, p. 281–315.

Beuchat, S., Moritz, R., and Pettke, T., 2004, Fluid evolution in the W-Cu-Zn-Pb San Cristobal vein, Peru: Fluid inclusion and stable isotope evidence: Chemical Geology, v. 210, p. 201–224.

Bodnar, R.J., 1995, Fluid-inclusion evidence for a magmatic source for metals in porphyry copper deposits: Mineralogical Association of Canada Short Course Series, v. 23, p. 139–152.

Bodnar, R.J., and Sterner, S.M., 1985, Synthetic fluid inclusions in natural quartz. II. Application to PVT studies: Geochimica et Cosmochimica Acta, v. 49, p. 1855–1859.

Bodnar, R.J., and Vityk, M.O., 1994, Interpretation of microthermometric data for H_2O-NaCl fluid inclusions, *in* DeVivo, B., and Frezzotti, M.L., eds., Fluid inclusions in minerals: Blacksburg, Virginia Tech, p. 117–130.

Bodnar, R.J., Reynolds, T.J., and Kuehn, C.A., 1985, Fluid inclusion systematics in epithermal systems: Reviews in Economic Geology, v. 2, p. 73–97.

Bowers, T.S., and Helgeson H.C.,1983, Calculation of the thermodynamic and geochemical consequences of nonideal mixing in the system H_2O-CO_2-NaCl on phase relations in geologic systems: equation of state for H_2O-CO_2-NaCl fluids at high pressures and temperatures: Geochimica et Cosmochimica Acta, v. 47, p. 1247–1275.

Brimhall, G.H., Jr., 1977, Early fracture-controlled disseminated mineralization at Butte, Montana: Economic Geology, v. 72, p. 37–59.

Brimhall, G.H., and Crerar D.A., 1987, Ore fluids: magmatic to supergene: Reviews in Mineralogy and Geochemistry, v. 17, p. 235–321.

Brugger, J., Etschmann, B., Liu, W., Testemale, D., Hazemann, J.L., Emerich, H., Van Beek, W., and Proux, O., 2007, An XAS study of the structure and thermodynamics of Cu(I) chloride complexes in brines up to high temperature (400°C, 600 bar): Geochimica et Cosmochimica Acta, v. 71, p. 4920–4941.

Burke, E.A.J., 2001, Raman microspectrometry of fluid inclusions: Lithos, v. 55, p. 139–158.

Burnham, C.W., 1979, Magmas and hydrothermal fluids, *in* Barnes, H.L., ed., Geochemistry of hydrothermal ore deposits, 2nd ed.: New York, John Wiley & Sons, p. 71–136.

Candela, P.A., 1989, Felsic magmas, volatiles, and metallogenesis: Reviews in Economic Geology, v. 4, p. 223–233.

Catchpole, H., Kouzmanov, K., Fontboté, L., Guillong, M., and Heinrich, C.A., 2011, Fluid evolution in zoned Cordilleran polymetallic veins—insights from microthermometry and LA-ICP-MS of fluid inclusions: Chemical Geology, v. 281, p. 293–304.

Cauzid, J., Philippot, P., Martinez-Criado, G., Ménez, B., and Labouré, S., 2007, Contrasting Cu-complexing behaviour in vapour and liquid fluid inclusions from the Yankee Lode tin deposit, Mole Granite, Australia: Chemical Geology, v. 246, p. 39–54.

Chang, Z., Hedenquist, J.W., White, N.C., Cooke, D.R., Roach, M., Deyell, C. L., Garcia, J., Jr., Gemmell, J.B., McKnight, S., and Cuison, A.L., 2011, Exploration tools for linked porphyry and epithermal deposits: Example from the Mankayan intrusion-centered Cu-Au district, Luzon, Philippines: Economic Geology, v. 106, p. 1365–1398.

Chase, M.W., Jr., 1998, NIST-JANAF Thermochemical Tables, 4th ed., Journal of Physical and Chemical Reference Data, Monograph no. 9.

Chivas, A.R., O'Neil, J.R., and Katchan, G., 1984, Uplift and submarine formation of some Melanesian porphyry copper deposits: Stable isotope evidence: Earth and Planetary Science Letters, v. 68, p. 326–334.

Cline, J.S., and Bodnar, R.J., 1991, Can economic porphyry copper mineralization be generated by a typical calc-alkaline melt?: Journal of Geophysical Research, v. 96, p. 8113–8126.

——1994, Direct evolution of brine from a crystallizing silicic melt at the Questa, New Mexico, molybdenum deposit: Economic Geology, v. 89, p. 1780–1802.

Cline, J.S., and Vanko, D.A., 1995, Magmatically generated saline brines related to molybdenum at Questa, New Mexico, USA: Mineralogical Association of Canada Short Course Series, v. 23, p. 153–174.

Cooke, D. R., Hollings, P., and Walsh, J. L., 2005, Giant porphyry deposits: Characteristics, distribution, and tectonic controls: Economic Geology, v. 100, p. 801–818.

Corbett, G.J., and Leach, T.M., 1998, Southwest Pacific rim gold-copper systems: Structure, alteration, and mineralization. Society of Economic Geologists Special Publication 6, 237 p.

Crerar, D., Wood, S., and Brantley, S., 1985, Chemical controls on solubility of ore-forming minerals in hydrothermal solutions: Canadian Mineralogist, v. 23, p. 333–352.

Cunningham, C.G., Austin, G.W., Naeser, C.W., Rye, R.O., Ballantyne, G.H., Stamm, R.G., and Barker, C.E., 2004, Formation of a paleothermal anomaly and disseminated gold deposits associated with the Bingham Canyon porphyry Cu-Au-Mo system, Utah: Economic Geology, v. 99, p. 789–806.

Deckart, K., Clark, A.H., Cuadra, P., and Fanning, M., 2012, Refinement of the time-space evolution of the giant Mio-Pliocene Río Blanco-Los Bronces porphyry Cu-Mo cluster, Central Chile: new U-Pb (SHRIMP II) and Re–Os geochronology and ^{40}Ar/^{39}Ar thermochronology data: Mineralium Deposita, DOI 10.007/s00126-012-0412-9.

Deen, J.A., Rye, R.O., Munoz, J.L., and Drexler, J.W., 1994, The magmatic hydrothermal system at Julcani, Peru—evidence from fluid inclusions and hydrogen and oxygen isotopes: Economic Geology, v. 89, p. 1924–1938.

Deyell, C.L., Leonardson, R., Rye, R.O., Thompson, J.F.H., Bissig, T., and Cooke, D.R. 2005a, Alunite in the Pascua-Lama high-sulfidation deposit: Constraints on alteration and ore deposition using stable isotope geochemistry: Economic Geology, v. 100, p. 131–148.

Deyell, C.L., Rye, R.O., Landis, G.P., and Bissig, T., 2005b, Alunite and the role of magmatic fluids in the Tambo high-sulfidation deposit, El Indio-Pascua belt, Chile: Chemical Geology, v. 215, p. 185–218.

Diamond, L.W., 1994, Salinity of multivolatile fluid inclusions determined from clathrate hydrate stability: Geochimica et Cosmochimica Acta, v. 58, p. 19–41.

——2003, Glossary: Terms and symbols used in fluid inclusion studies: Mineralogical Association of Canada Short Course Series, v. 32, p. 363–372.

Dilles, J.H., and Einaudi, M.T., 1992, Wall-rock alteration and hydrothermal flow paths about the Ann-Mason porphyry copper deposit, Nevada –a 6-km vertical reconstruction: Economic Geology, v. 87, p. 1963–2001.

Dilles, J.H., Solomon, G.C., Taylor, H.P., and Einaudi, M.T., 1992, Oxygen and hydrogen isotope characteristics of hydrothermal alteration at the Ann-Mason porphyry copper deposit, Yerington, Nevada: Economic Geology, v. 87, p. 44–63.

Dilles, J.H., Farmer, G.L., and Field, C.W., 1995, Sodium-calcium alteration by non-magmatic saline fluids in porphyry copper deposits: Results from Yerington, Nevada: Mineralogical Association of Canada Short Course Series, v. 23, p. 309–338.

Dilles, J.H., Einaudi, M.T., Proffett, J., and Barton, M.D., 2000, Overview of the Yerington porphyry copper district: Magmatic to nonmagmatic sources of hydrothermal fluids: Their flow paths and alteration effects on rocks and Cu-Mo-Fe-Au ores: Society of Economic Geologists Guidebook Series, v. 32, p. 55–66.

Dolejs, D., and Manning, C.E., 2010, Thermodynamic model for mineral solubility in aqueous fluids: theory, calibration and application to model fluid-flow systems: Geofluids, v.10, p. 20–40.

Driesner, T., 2007, The system H_2O-NaCl. Part II: Correlations for molar volume, enthalpy, and isobaric heat capacity from 0 to 1000°C, 1 to 5000 bar, and 0 to 1 X_{NaCl}: Geochimica et Cosmochimica Acta, v. 71, p. 4902–4919.

Driesner, T., and Geiger, S., 2007, Numerical simulation of multiphase fluid flow in hydrothermal systems: Reviews in Mineralogy and Geochemistry, v. 65, p. 187–212.

Driesner, T., and Heinrich, C.A., 2007, The system H2O–NaCl. Part I: Correlation formulae for phase relations in temperature-pressure-composition space from 0 to 1000°C, 0 to 5000 bar, and 0 to 1 XnaCl: Geochimica et Cosmochimica Acta v. 71, p. 4880–4901.

Duan, Z., Moller N., and Weare J., 1995, Equation of state for NaCl-H_2O-CO_2 system—prediction of phase equilibria and volumetric properties. Geochimica et Cosmochimica Acta, v. 59, p. 2869–2882; http://www.geochem-model.org/programs.htm.

Dubessy, J., Poty, B., and Ramboz, C., 1989, Advances in C-O-H-N-S fluid geochemistry based on micro-Raman spectrometric analysis of fluid inclusions: European Journal of Mineralogy, v. 1, p. 517–534.

Eastoe, C.J., 1978, Fluid inclusion study of the Panguna porphyry copper deposit, Bougainville, Papua New Guinea: Economic Geology, v. 73, p. 721–748.

Einaudi, M.T., 1982, Description of skarns associated with porphyry copper plutons, southwestern North America, in Titley, S.R., ed., Advances in geology of the porphyry copper deposits, southwestern North America: Tucson, University of Arizona Press, p. 139–183.

Einaudi, M.T., Hedenquist, J.W., and Inan, E.E., 2003, Sulfidation state of fluids in active and extinct hydrothermal systems: Transitions from porphyry to epithermal environments: Society of Economic Geologists Special Publication 10, p. 285–313.

Emmons, W.H., 1927, Relations of disseminated copper ores in porphyry to igneous intrusions: American Institute of Mining and Metallurgical Engineers Transactions, v. 75, p. 797–809.

Erkey C., 2000, Supercritical carbon dioxide extraction of metals from aqueous solutions: a review: Journal of Supercritical Fluids, v. 17, 259–287.

Etschmann, B.E., Liu, W., Testemale, D., Mueller, H., Rae, N.A., Proux, O., Hazemann, J.L., and Brugger, J., 2010, An in situ XAS study of copper(I) transport as hydrosulfide complexes in hydrothermal solutions (25-592 degrees C, 180-600 bar): Speciation and solubility in vapor and liquid phases: Geochimica et Cosmochimica Acta, v. 74, p. 4723–4739.

Fifarek, R.H., and Rye, R.O., 2005, Stable-isotope geochemistry of the Pierina high-sulfidation Au-Ag deposit, Peru: influence of hydrodynamics on SO_4^{2-}-H_2S sulfur isotopic exchange in magmatic-steam and steam-heated environments: Chemical Geology, v. 215, p. 253–279.

Fournier, R.O., 1999, Hydrothermal processes related to movement of fluid from plastic into brittle rock in the magmatic-epithermal environment: Economic Geology, v. 94, p. 1193–1211.

Foustoukos, D.I., and Seyfried, W.E., 2007, Trace element partitioning between vapor, brine and halite under extreme phase separation conditions: Geochimica et Cosmochimica Acta, v. 71, p. 2056–2071.

Frank, M.R., Simon, A.C., Pettke, T., Candela, P.A., and Piccoli, P.M., 2011, Gold and copper partitioning in magmatic-hydrothermal systems at 800°C and 100 MPa: Geochimica et Cosmochimica Acta, v. 75, p. 2470–2482.

Franklin, J.M., Gibson, H.L., Jonasson, I.R., and Galley, A.G., 2005, Volcanogenic massive sulfide deposits: Economic Geology 100th Anniversary Volume, p. 523–560.

Frezzotti, M.L., Tecce, F., and Casagli, A., 2012, Raman spectroscopy for fluid inclusion analysis: Journal of Geochemical Exploration, v. 112, p. 1–20.

Garwin, S., 2002, The geologic setting of intrusion-related hydrothermal systems near the Batu Hijau porphyry copper-gold deposit, Sumbawa, Indonesia: Society of Economic Geologists, Special Publication 9, p. 333–366.

Giggenbach, W.F., 1992, Magma degassing and mineral deposition in hydrothermal systems along convergent plate boundaries: Economic Geology, v. 87, p. 1927–1944.

——1997, The origin and evolution of fluids in magmatic-hydrothermal systems, *in* Barnes, H. L., ed., Geochemistry of hydrothermal ore deposits, 3rd ed.: New York, John Wiley & Sons, p. 737–796.

Giuliani, G., Dubessy, J., Banks, D., Vinh, H. Q., Lhomme, T., Pironon, J., Garnier, V., Trinh, P.T., Long, P.V., Ohnenstetter, D., and Schwarz, D., 2003, CO_2-H_2S-COS-S_8-AlO(OH)-bearing fluid inclusions in ruby from marble-hosted deposits in Luc Yen area, North Vietnam: Chemical Geology, v. 194, p. 167–185.

Goldstein, R.H., and Reynolds, T.J., 1994, Systematics of fluid inclusions in diagenetic minerals: Society for Sedimentary Geology Short Course Series, v. 31, 199 p.

Graham, S., Pearson, N., Jackson, S., Griffin, W., and O'Reilly, S.Y., 2007, Tracing Cu and Fe from source to porphyry: in situ determination of Cu and Fe isotope ratios in sulfides from the Grasberg Cu-Au deposit: Chemical Geology, v. 207, p. 147–169.

Gray, J.E., and Coolbaugh, M.F., 1994, Geology and geochemistry of Summitville, Colorado—an epithermal acid sulfate deposit in a volcanic dome: Economic Geology, v. 89, p. 1906–1923.

Gruen, G., Heinrich, C.A., and Schroeder, K., 2010, The Bingham Canyon porphyry Cu-Mo-Au deposit. II. Vein geometry and ore shell formation by pressure-driven rock extension: Economic Geology, v.105, p. 69–90.

Guillong, M., Latkoczy, C., Seo, J.H., Günther, D., and Heinrich, C.A., 2008, Determination of sulfur in fluid inclusions by laser ablation ICP-MS: Journal of Analytical Atomic Spectrometry, v. 23, p. 1581–1589.

Günther, D., Audétat, A., Frischknecht, R., and Heinrich, C.A., 1998, Quantitative analysis of major, minor and trace elements in fluid inclusions using laser ablation inductively coupled plasma mass spectrometry: Journal of Analytical Atomic Spectrometry, v. 13, p. 263–270.

Gustafson, L.B., and Hunt, J. P., 1975, The porphyry copper deposit at El Salvador, Chile: Economic Geology, v. 70, p. 857–912.

Gysi, M., and Herbort, T., 2006, The epithermal Au-Ag ore deposit of Rodu-Frasin (Romania). With special focus on melt inclusions trapped in quartz phenocrysts and on fluid inclusions trapped in epithermal vein quartz, quartz phenocrysts and porphyry type vein quartz: Unpublished MSc thesis, ETH Zurich, 115 p.

Halter, W.E., Bain, N., Becker, K., Heinrich, C.A., Landtwing, M., von Quadt, A., Bissig, T., Clark, A.H., Sasso, A.M., and Tosdal, R.M., 2004a, From andesitic volcanism to the formation of a porphyry Cu-Au mineralizing magma chamber: The Farallon Negro Volcanic Complex, northwestern Argentina: Journal of Volcanology and Geothermal Research, v. 136, p. 1–30.

Halter, W.E., Heinrich, C.A., and Pettke, T., 2004b, Laser-ablation ICP-MS analysis of melt inclusions in an andesitic complex II: Magma genesis and implications for ore-formation: Contributions to Mineralogy and Petrology, v. 147, p. 385–396.

——2005, Magma evolution and the formation of porphyry Cu-Au ore fluids: evidence from silicate and sulfide melt inclusions: Mineralium Deposita, v. 39, p. 845–863.

Hanley, J.J., and Gladney, E.R., 2011, The presence of carbonic-dominant volatiles during the crystallization of sulfide-bearing mafic pegmatites in the North Roby zone, Lac des Iles Complex, Ontario: Economic Geology, v. 106, p. 33–54.

Hannah, J.L., Stein, H.J., Wieser, M.E., de Laeter, J.R., and Varner, M.D., 2007, Molybdenum isotope variations in molybdenite: Vapor transport and Rayleigh fractionation of Mo: Geology, v. 35, p. 703–706.

Harris, A.C., and Golding, S.D., 2002, New evidence of magmatic-fluid-related phyllic alteration: Implications for the genesis of porphyry Cu deposits: Geology, v. 30, p. 335–338.

Harris, A.C., Kamenetsky, V.S., White, N.C., van Achterbergh, E., and Ryan, C.G., 2003, Melt inclusions in veins: Linking magmas and porphyry Cu deposits: Science, v. 302, p. 2109–2111.

Harris, A.C., Golding, S.D., and White, N.C., 2005, Bajo de la Alumbrera copper-gold deposit: Stable isotope evidence for a porphyry-related hydrothermal system dominated by magmatic aqueous fluids: Economic Geology, v. 100, p. 863–886.

Harris, A.C., Dunlap, W.J., Reiners, P.W., Allen, C.M., Cooke, D.R., White, N.C., Campbell, I.H., and Golding, S.D., 2008, Multimillion year thermal history of a porphyry copper deposit: Application of U-Pb, $^{40}Ar/^{39}Ar$ and (U-Th)/He chronometers, Bajo de la Alumbrera copper-gold deposit, Argentina: Mineralium Deposita, v. 43, p. 295–314.

Hayba, D.O., Bethke, P.M., Heald, P., and Foley, N.K., 1985, Geologic, mineralogic, and geochemical characteristics of volcanic-hosted epithermal precious-metal deposits: Reviews in Economic Geology, v. 2, p. 129–167.

Hedenquist, J.W., 1995, The ascent of magmatic fluid: Discharge versus mineralization: Mineralogical Association of Canada Shortcourse Series, v. 23, p. 263–289.

Hedenquist, J.W., and Aoki, M., 1991, Meteoric interaction with magmatic discharges in Japan and the significance for mineralization: Geology, v. 19, p. 1041–1044.

Hedenquist, J.W., and Lowenstern, J.B., 1994, The role of magmas in the formation of hydrothermal ore deposits: Nature, v. 370, p. 519–527.

Hedenquist, J.W., and Richards, J.P., 1998, The influence of geochemical techniques on the development of genetic models for porphyry copper deposits: Reviews in Economic Geology, v. 10, p. 235–256.

Hedenquist, J.W., Simmons, S.F., Giggenbach, W.F., and Eldridge, C.S., 1993, White Island, New Zealand, volcanic-hydrothermal system represents the geochemical environment of high-sulfidation Cu and Au ore deposition: Geology, v. 21, p. 731–734.

Hedenquist, J.W., Aoki, M., and Shinohara, H., 1994a, Flux of volatiles and ore-forming metals from the magmatic-hydrothermal system of Satsuma Iwojima volcano: Geology, v. 22, p. 585–588.

Hedenquist, J.W., Matsuhisa, Y., Izawa, E., White, N.C., Giggenbach, W.F., and Aoki, M., 1994b, Geology, geochemistry, and origin of high-sulfidation Cu-Au mineralization in the Nansatsu district, Japan: Economic Geology, v. 89, p. 1–30.

Hedenquist, J.W., Arribas, A., Jr., and Reynolds, T.J., 1998, Evolution of an intrusion-centered hydrothermal system: Far Southeast-Lepanto porphyry and epithermal Cu-Au deposits, Philippines: Economic Geology, v. 93, p. 373–404.

Heinrich, C.A., 2005, The physical and chemical evolution of low-salinity magmatic fluids at the porphyry to epithermal transition: A thermodynamic study: Mineralium Deposita, v. 39, p. 864–889.

——2007, Fluid–fluid interactions in magmatic-hydrothermal ore formation: Reviews in Mineralogy and Geochemistry, v. 65, p. 363–387.

Heinrich, C.A., Ryan, C.G., Mernagh, T.P., and Eadington, P.J., 1992, Segregation of ore metals between magmatic brine and vapor—a fluid inclusion study using PIXE microanalysis: Economic Geology, v. 87, p. 1566–1583.

Heinrich, C.A., Günther, D., Audédat, A., Ulrich, T., and Frischknecht, R, 1999, Metal fractionation between magmatic brine and vapour, and the link between porphyry-style and epithermal Cu-Au deposits: Geology, v. 27, p. 755–758.

Heinrich, C.A., Driesner, T., Stefánsson, A., and Seward, T.M., 2004, Magmatic vapor contraction and the transport of gold from porphyry to epithermal ore deposits: Geology, v. 39, p. 761–764.

Heinrich, C.A., Halter, W., Landtwing, M.R., and Pettke, T., 2005, The formation of economic porphyry copper (-gold) deposits: constraints from microanalysis of fluid and melt inclusions: Geological Society, London, Special Publication 248, p. 247–263.

Helgeson, H.C., Kirkham, D.., and Flowers, G.C., 1981, Theoretical prediction of the thermodynamic behavior of aqueous-electrolytes at high-pressures and temperatures. 4. Calculation of activity-coefficients, osmotic coefficients, and apparent molal and standard and relative partial molal properties to 600°C and 5 Kb: American Journal of Science, v. 281, p. 1249–1516.

Hemley, J.J., and Hunt, J.P., 1992, Hydrothermal ore-forming processes in the light of studies in rock-buffered systems: II. Some general geological applications: Economic Geology, v. 87, p. 23–43.

Henley, R.W., and McNabb, A., 1978, Magmatic vapor plumes and groundwater interaction in porphyry copper emplacement: Economic Geology, v. 73, p. 1–20.

Hezarkhani, A., Williams-Jones, A.E., and Cammons, C.H., 1999, Factors controlling copper solubility and chalcopyrite deposition in the Sungun porphyry copper deposit, Iran: Mineralium Deposita, v. 34, p. 770–783.

Ingebritsen, S.E., and Appold, M.S., 2012, The physical hydrology of ore deposits: Economic Geology, v. 107, p. 559–584.

Ingebritsen, S.E., Geiger, S., Hurwitz, S., and Driesner, T., 2010, Numerical simulation of magmatic hydrothermal systems: Reviews of Geophysics, v. 48, RG1002.

Ivtanthermo, 1983, Tables of thermodynamic properties of individual substances: IVTANTHERMO database, Moscow, Russia.

Jacquemet, N., Guillaume, D., Zwick, A., and Pokrovski, G.S., 2012, In situ Raman spectroscopy identification of the S$^{3-\text{ion}}$ in gold-bearing fluids from synthetic fluid inclusions [abs.]: Geo-Raman X: Nancy, France, Journal of Conference Abstracts, p. 207–208.

Jannas, R.R., Bowers, T.S., Petersen, U., and Beane, R.E., 1999, High sulfidation deposit types in the El Indio district, Chile: Society of Economic Geologists Special Publication 7, p. 219–266.

John, E.C., 1978, Mineral zones in the Utah copper orebody: Economic Geology, v. 73, p. 1250–1259.

Johnson, J.W., Oelkers, E.H., and Helgeson, H.C., 1992, SUPCRT92: A software package for calculating the standard molal thermodynamic properties of minerals, gases, aqueous species, and reactions from 1 to 5000 bar and 0 to 1000°C: Computers & Geosciences, v. 18, p. 899–947.

Kamenetsky, V.S., van Achterbergh, E., Ryan, C.G., Naumov, V.B., Mernagh, T.P., and Davidson, P., 2002, Extreme chemical heterogeneity of granite-derived hydrothermal fluids: An example from inclusions in a single crystal of miarolitic quartz: Geology, v. 30, p. 459–462.

Kamenetsky, V.S., Naumov, V.B., Davidson, P., van Achterbergh, E., and Ryan, C.G., 2004, Immiscibility between silicate magmas and aqueous fluids: a melt inclusion pursuit into the magmatic-hydrothermal transition in the Omsukchan Granite (NE Russia): Chemical Geology, v. 210, p. 73–90.

Kehayov, R., Bogdanov, K., Fanger, L., von Quadt, A., Pettke, T., and Heinrich, C.A., 2003, The fluid chemical evolution of the Elatsite porphyry Cu-Au-PGE deposit, Bulgaria, *in* Eliopoulos, D.G., ed., Mineral exploration and sustainable development: Proceedings of 8th Biennial SGA meeting, Athens, Greece, August 2003, p. 1173–1176.

Kirkham, R.V., 1971, Intermineral intrusions and their bearing on the origin of porphyry copper and molybdenum deposits: Economic Geology, v. 66, p. 1244–1249.

Klemm, L.M., Pettke, T., Heinrich, C.A., and Campos, E., 2007, Hydrothermal evolution of the El Teniente deposit, Chile: Porphyry Cu-Mo ore deposition from low-salinity magmatic fluids: Economic Geology, v. 102, p. 1021–1045.

Klemm, L.M., Pettke, T., and Heinrich, C.A., 2008, Fluid and source magma evolution of the Questa porphyry Mo deposit, New Mexico, USA: Mineralium Deposita, v. 43, p. 533–552.

Kostova, B., Pettke, T., Driesner, T., Petrov, P., and Heinrich, C.A., 2004, LA-ICP-MS study of fluid inclusions in quartz from the Yuzhna Petrovitsa deposit, Madan ore field, Bulgaria: Schweizerische Mineralogische und Petrographische Mitteilungen, v. 84, p. 25–36.

Kotzeva, B.G., Guillong, M., Stefanova, E., and Piperov, N.B., 2011, LA-ICP-MS analysis of single fluid inclusions in a quartz crystal (Madan ore district, Bulgaria): Journal of Geochemical Exploration, v. 108, p. 163–175.

Kouzmanov, K., Bailly, L., Ramboz, C., Rouer, O., and Beny, J.M., 2002, Morphology, origin and infrared microthermometry of fluid inclusions in pyrite from the Radka epithermal copper deposit, Srednogorie zone, Bulgaria: Mineralium Deposita, v. 37, p. 599–613.

Kouzmanov, K., Pettke, T., and Heinrich, C.A., 2010, Direct analysis of ore-precipitating fluids: combined IR microscopy and LA-ICP-MS study of fluid inclusions in opaque ore minerals: Economic Geology, v. 105, p. 351–373.

Kukuljan, J.A., Alvarez, J.L., and Fernández-Prini, R., 1999, Distribution of $B(OH)_3$ between water and steam at high temperatures: Journal of Chemical Thermodynamics, v. 31, p. 1511–1521.

Kurosawa, M., Shimano, S., Ishii, S., Shima, K., and Kato, T., 2003, Quantitative trace element analysis of single fluid inclusions by proton-induced X-ray emission (PIXE): Application to fluid inclusions in hydrothermal quartz: Geochimica et Cosmochimica Acta, v. 67, p. 4337–4352.

Kurosawa, M., Ishii, S., and Sasa, K., 2010, Trace-element compositions of single fluid inclusions in the Kofu granite, Japan: Implications for compositions of granite-derived fluids: Island Arc, v. 19, p. 40–59.

Kwak, T.A.P., 1986, Fluid inclusions in skarns (carbonate replacement deposits): Journal of Metamorphic Geology, v. 4, p. 363–384.

Landtwing, M.R., Pettke, T., Halter, W.E., Heinrich, C.A., Redmond, P.B., Einaudi, M.T., and Kunze, K., 2005, Copper deposition during quartz dissolution by cooling magmatic-hydrothermal fluids: The Bingham porphyry: Earth and Planetary Science Letters, v. 235, p. 229–243.

Landtwing, M.R., Furrer, C., Redmond, P.B., Pettke, T., Guillong, M., and Heinrich, C.A., 2010, The Bingham Canyon porphyry Cu-Mo-Au deposit III. Zoned copper-gold ore deposition by magmatic vapor expansion: Economic Geology, v. 105, p. 91–118.

Lattanzi, P., 1991, Applications of fluid inclusions in the study and exploration of mineral deposits: European Journal of Mineralogy, v. 3, p. 689-701.

——1994, Fluids in ore deposits, *in* de Vivo, B., Frezzotti, M.L., eds., Fluid inclusions in minerals: Methods and applications: Virginia Polytechnic Institute and State University, International Mineralogical Association Working Group Short Course Volume, p. 297–307.

Leach, D.V., Sangster, D.F., Kelley, K.D., Large, R.R., Garven, G., Allen, C.R., Gutzmer, J., and Walters, S., 2005, Sediment-hosted lead-zinc deposits: A global perspective: Economic Geology 100th Anniversary Volume, p. 561–607.

LeFort, D., Hanley, J., and Guillong, M., 2011, Subepithermal Au-Pd mineralization associated with an alkalic porphyry Cu-Au deposit, Mount Milligan, Quesnel Terrane, British Columbia, Canada: Economic Geology, v. 106, p. 781–808.

Lerchbaumer, L., and Audétat, A., 2012, High Cu concentrations in vapor-type fluid inclusions: An artifact?: Geochimica et Cosmochimica Acta, v. 88, p. 255–274.

Li, Y., Audétat, A., Lerchbaumer, L., and Xiong, X.L., 2009, Rapid Na, Cu exchange between synthetic fluid inclusions and external aqueous solutions: Evidence from LA-ICP-MS analysis: Geofluids, v. 9, p. 321–329.

Liebscher, A., and Heinrich, C.A., 2007, Fluid-fluid interactions in the earth's lithosphere: Reviews in Mineralogy and Geochemistry, v. 65, p. 1–13.

Liebscher, A., Meixner, A., Romer, R.L., and Heinrich, W., 2005, Liquid-vapor fractionation of boron and boron isotopes: Experimental calibration at 400°C/23 MPa to 450°C/42 MPa: Geochimica et Cosmochimica Acta, v. 69, p. 5693–5704.

Lowell, J.D., and Guilbert, J.M., 1970, Lateral and vertical alteration-mineralization zoning in porphyry ore deposits: Economic Geology, v. 65, p. 373–408.

Lowernstern, J.B., 2001, Carbon dioxide in magmas and implications for hydrothermal systems: Mineralium Deposita, v. 36, p. 490–502.

Maksaev, V., Munizaga, F., McWilliams, M., Fanning, M., Mathur, R., Ruiz, J., and Zentilli, M., 2004, New chronology for El Teniente, Chilean Andes, from U-Pb, ^{40}Ar/^{39}Ar, Re-Os, and fission track dating: Implications for the evolution of a supergiant porphyry Cu-Mo deposit: Society of Economic Geologists Special Publication 11, p. 15–54.

Mancano, D.P., and Campbell, A.R., 1995, Microthermometry of enargite-hosted fluid inclusions from the Lepanto, Philippines, high-sulfidation Cu-Au deposit: Geochimica et Cosmochimica Acta, v. 59, p. 3909-3916.

Manning, C.E., 1994, The solubility of quartz in H_2O in the lower crust and upper mantle: Geochimica et Cosmochimica Acta, v. 58, p. 4831–4839.

Masterman, G.J., Cooke, D.R., Berry, R.F., Walshe, J.L., Lee, A.W., and Clark, A.H., 2005, Fluid chemistry, structural setting, and emplacement history of the Rosario Cu-Mo porphyry and Cu-Ag-Au epithermal veins, Collahuasi district, northern Chile: Economic Geology, v. 100, p. 835–862.

Mathur, R., Titley, S., Barra, F., Brantley, S., Wilson, M., Philips, A., Munizaga, F., Maksaev, V., Vervoort, J., and Hart, G., 2009, Exploration potential of Cu isotope fractionation in porphyry copper deposits: Journal of Geochemical Exploration, v. 102, p. 1–6.

Mathur, R., Dendas, M., Titley, S., and Phillips, A., 2010, Patterns in the copper isotope composition of minerals in porphyry copper deposits in southwestern United States: Economic Geology, v. 105, p. 1457–1467.

Mavrogenes, J.A., Berry, A.J., Newville, M., and Sutton, S.R., 2002, Copper speciation in vapor-phase fluid inclusions from the Mole Granite, Australia: American Mineralogist, v. 87, p. 1360–1364.

Meinert, L.D., Hedenquist, J.W., Satoh, H., and Matsuhisa, Y., 2003, Formation of anhydrous and hydrous skarn in Cu-Au ore deposits by magmatic fluids: Economic Geology, v. 98, p. 147–156.

Meinert, L.D., Dipple, G.M., and Nicolescu, S., 2005, World skarn deposits: Economic Geology 100th Anniversary Volume, p. 299–336.

Mesmer, R.E., Marshall, W.L., Palmer, D.A., Simonson, J.M., and Holmes, H.F., 1988, Thermodynamics of aqueous association and ionization reactions at high temperatures and pressures: Journal of Solution Chemistry, v. 17, p. 699–718.

Métrich, N., Berry, A.J., O'Neill, H. St. C., and Susini, J., 2009, The oxidation state of sulfur in synthetic and natural glasses determined by X-ray absorption spectroscopy: Geochimica et Cosmochimica Acta, v. 73, p. 2382–2399.

Meyer, C., and Hemley, J.J., 1967, Wall rock alteration, in Barnes, H.L., ed., Geochemistry of hydrothermal ore deposits: New York, Holt, Rinehart and Winston, p. 166–235.

Meyer, C., Shea, E.P., Goddard, C.C., Jr., and staff, 1968, Ore deposits at Butte, Montana, in Ridge, J.D., ed., Ore deposits of the United States, 1933–67, v. 2: New York, American Institute of Mining, Metallurgical, and Petroleum Engineers, p. 1373–1416.

Minubayeva, Z., and Seward, T.M., 2010, Molybdic acid ionization under hydrothermal conditions to 300°C: Geochimica et Cosmochimica Acta, v. 74, p. 4365–4374.

Molnár, F., Jung, P., Kupi, L., Pogány, A., Vágó, E., Viktorik, O., and Pécskay, Z., 2008, Epithermal zones of the porphyry-skarn-epithermal ore complex at Recsk: Publications of the University of Miskolc Series A, Mining, v. 73, p. 101–130.

Moritz, R., and Benkhelfa, F., 2009, Fluids in high-sulfidation epithermal ore deposits: constraints from infrared microthermometry of enargite-hosted fluid inclusions, *in* Williams, P., et al., eds., Smart science for exploration and mining: Proceedings of 10th Biennial SGA meeting, Townsville, Australia, August 2009, p. 533–535.

Müller, B., Frischknecht, R., Seward, T. M., Heinrich, C. A., and Gallegos, W. C., 2001, A fluid inclusion reconnaissance study of the Huanuni tin deposit (Bolivia), using LA-ICP-MS micro-analysis: Mineralium Deposita, v. 36, p. 680–688.

Murakami, H., Seo, J.H., and Heinrich, C.A., 2010, The relation between Cu/Au ratio and formation depth of porphyry-style Cu-Au±Mo deposits: Mineralium Deposita, v. 45, p. 11–21.

Nagaseki, H., and Hayashi, K.I., 2008, Experimental study of the behavior of copper and zinc in a boiling hydrothermal system: Geology, v. 36, p. 27–30.

Nash, T.J., 1976, Fluid inclusion petrology data from porphyry copper deposits and applications to exploration: U.S. Geological Survey Professional Paper 907-D, 16 p.

Newton, R.C., and Manning, C.E., 2000, Quartz solubility in H_2O-NaCl and H_2O-CO_2 solutions at deep crust-mantle pressures and temperatures: 2–15 kbar and 500-900°C: Geochimica et Cosmochimica Acta, v. 64, p. 2993–3005.

——2009, Hydration state and activity of aqueous silica in H_2O-CO_2 fluids at high pressure and temperature: American Mineralogist, v. 94, p. 1287–1290.

Oelkers, E.H., Benezeth, P., and Pokrovski, G.S., 2009, Thermodynamic databases for water-rock interaction: Reviews in Mineralogy and Geochemistry, v. 70, p. 1–46.

Ossandón, G., Fréraut, R., Gustafson, L.B., Lindsay, D.D., and Zentilli, M., 2001, Geology of the Chuquicamata mine: A progress report: Economic Geology, v. 96, p. 249–270.

Palmer, D.A., Simonson, J.M., and Jensen, J.P., 2004, Partitioning of electrolytes to steam and their solubilities in steam, *in* Palmer, D.A., Fernàndez-Prini, R., and Harvey, A.H., eds., Aqueous systems at elevated temperatures and pressures: New York, Elsevier, p. 409–439.

Pettke, T., 2008, Analytical protocols for element concentration and isotope ratio measurements in fluid inclusions by LA-(MC)-ICP-MS: Mineralogical Association of Canada Short Course Series, v. 40, p. 189–218.

Pettke, T., Halter, W.E., Driesner, T., von Quadt, A., and Heinrich, C.A., 2001, The porphyry to epithermal link: Preliminary fluid chemical results from the Apuseni Mountains, Romania, and Famatina, Argentina: 11th Annual V.M. Goldschmidt Conference, Lunar and Planetary Institute, Houston, Abstract 3537, LPI Contribution no. 1088 (CD-ROM).

Pettke, T., Oberli, F., and Heinrich, C.A., 2010, The magma and metal source of giant porphyry-type ore deposits, based on lead isotope microanalysis of individual fluid inclusions: Earth and Planetary Science Letters, v. 296, p. 267–277.

Pettke, T., Oberli, F., Audétat, A., Wiechert, U., and Heinrich, C.A., 2011, Quantification of transient signals in multiple collector inductively coupled plasma mass spectrometry: accurate lead isotope ratio determination by laser ablation of individual fluid inclusions: Journal of Analytical Atomic Spectrometry, v. 26, p. 475–492.

Pettke, T., Oberli, F., Audétat, A., Guillong, M., Simon, A.C., Hanley, J.J., and Klemm, L.M., 2012, Recent developments in element concentration and isotope ratio analysis of individual fluid inclusions by laser ablation single and multiple collector ICP-MS: Ore Geology Reviews, v. 44, p. 10–38.

Philips, G.N., and Evans, K.A., 2004, Role of CO_2 in the formation of gold deposits: Nature, v. 429, p. 860–863.

Plyasunov, A.V., and Shock, E.L., 2001, Correlation strategy for determining the parameters of the revised Helgeson-Kirkham-Flowers model for aqueous nonelectrolytes: Geochimica et Cosmochimica Acta, v. 65, p. 3879–3900.

Pokrovski, G.S., 2010, Enhanced vapor-phase transport of tin in hydrothermal systems or experimental artifacts?: Journal of Volcanology and Geothermal Research, v. 194, p. 63–66.

Pokrovski, G.S., and Dubessy, J., 2012, In situ Raman spectroscopy reveals new sulfur forms in high-temperature geological fluids [abs.]: GeoRaman X, Nancy, France, Journal of Conference Abstracts, p. 77–78.

Pokrovski, G.S., and Dubrovinsky, L.S., 2011, The S_3^- ion is stable in geological fluids at elevated temperatures and pressures: Science, v. 331, p. 1052–1054.

Pokrovski, G.S., Gout, R., Zotov, A., Schott, J., and Harrichoury, J.C., 1996, Thermodynamic properties and stoichiometry of the arsenic(III) hydroxide complexes at hydrothermal conditions: Geochimica et Cosmochimica Acta, v. 60, p. 737–749.

Pokrovski, G.S., Zakirov, I.V., Roux, J., Testemale, D., Hazemann, JL., Bychkov, A.Y., and Golikova, G.V., 2002a, Experimental study of arsenic speciation in vapor phase to 500°C: Implications for As transport and fractionation in low-density crustal fluids and volcanic gases: Geochimica et Cosmochimica Acta, v. 66, p. 3453–3480.

Pokrovski, G.S., Kara, S., and Roux, J., 2002b, Stability and solubility of arsenopyrite, FeAsS, in crustal fluids: Geochimica et Cosmochimica Acta, v. 66, p. 2361–2378.

Pokrovski, G.S., Roux, J., and Harrichoury, J.-C., 2005a, Fluid density control on vapor-liquid partitioning of metals in hydrothermal systems: Geology, v. 33, p. 657–660.

Pokrovski, G.S., Roux, J., Hazemann, J.-L., and Testemale, D., 2005b, An X-ray absorption spectroscopy study of argutite solubility and germanium aqueous speciation in hydrothermal fluids to 500°C and 400 bar: Chemical Geology, v. 217, p. 127–145.

Pokrovski, G.S., Borisova, A.Yu., Roux, J., Hazemann, J.-L., Petdang, A., Tella, M., and Testemale, D., 2006, Antimony speciation in saline hydrothermal fluids: A combined X-ray absorption fine structure and solubility study: Geochimica et Cosmochimica Acta, v. 70, p. 4196–4214.

Pokrovski, G.S., Borisova, A.Yu., and Harrichoury, J.-C., 2008a, The effect of sulfur on vapor-liquid fractionation of metals in hydrothermal systems: Earth and Planetary Science Letters, v. 266, p. 345–362.

Pokrovski, G.S., Roux, J., Hazemann, J.-L., Borisova, A.Yu., Gonchar, A.A., and Lemeshko, M.P., 2008b, In situ X-ray absorption spectroscopy measurement of vapor-brine fractionation of antimony at hydrothermal conditions: Mineralogical Magazine, v. 72, p. 667–681.

Pokrovski, G.S., Tagirov, B.R., Schott, J., Hazemann, J.-L., and Proux, O., 2009a, A new view on gold speciation in sulfur-bearing hydrothermal fluids from in situ X-ray absorption spectroscopy and quantum-chemical modeling: Geochimica et Cosmochimica Acta, v. 73, p. 5406–5427.

Pokrovski, G.S., Tagirov, B.R., Schott, J., Bazarkina, E.F., Hazemann, J.-L., and Proux, O., 2009b, An in situ X-ray absorption spectroscopy study of gold-chloride complexing in hydrothermal fluids: Chemical Geology, v. 259, p. 17–29.

Pokrovski, G.S., Dubrovinsky, L.S., and Dubessy, J., 2011, A new view on sulfur speciation in geological fluids at elevated temperatures and pressures [abs.]: Goldschmidt Conference Abstracts, Mineralogical Magazine, p. 1654.

Pokrovski, G.S., Roux, J., Ferlat, G., Jonchiere, R., Seitsonen, A., Vuilleumier, R., and Hazemann, J.-L., 2013, Silver in saline hydrothermal fluids from in situ X-ray absorption spectroscopy and first-principles molecular dynamics: Geochimica et Cosmochimica Acta, doi: http://dx.doi.org/10.1016/j.gca.2012.12.02.

Pollard, P J., Taylor, R.G., and Peters, L., 2005, Ages of intrusion, alteration, and mineralization at the Grasberg Cu-Au deposit, Papua, Indonesia: Economic Geology, v. 100, p. 1005–1020.

Porter, J.P., Schroeder, K., and Austin, G., 2012, Geology of the Bingham Canyon porphyry Cu-Mo-Au deposit, Utah: Society of Economic Geologists Special Publication 16, p. 127–146.

Proffett, J.M., 2003, Geology of the Bajo de la Alumbrera porphyry copper-gold deposit, Argentina: Economic Geology, v. 98, p. 1535–1574.

——2009, High Cu grades in porphyry Cu deposits and their relationship to emplacement depth of magmatic sources: Geology, v. 37, p. 675–678.

Pudack, C., Halter, W.E., Heinrich, C.A., and Pettke, T., 2009, Evolution of magmatic vapor to gold-rich epithermal liquid: The porphyry to epithermal transition at Nevados de Famatina, northwest Argentina: Economic Geology, v. 104, p. 449–477.

Rankin, A.H., Ramsey, M.H., Coles, B., Vanlangevelde, F., and Thomas, C.R., 1992, The composition of hypersaline, iron-rich granitic fluids based on laser-ICP and synchrotron-XRF microprobe analysis of individual fluid inclusions in topaz, Mole Granite, eastern Australia: Geochimica et Cosmochimica Acta, v. 56, p. 67–79.

Redmond, P.B., and Einaudi, M., 2010, The Bingham Canyon porphyry Cu-Mo-Au deposit. I. Sequence of intrusions, vein formation, and sulfide deposition: Economic Geology, v. 105, p. 43–68.

Redmond, P.B., Einaudi, M.T., Inan, E.E., Landtwing, M.R., and Heinrich, C.A., 2004, Copper deposition by fluid cooling in intrusion-centered systems: New insights from the Bingham porphyry ore deposit, Utah: Geology, v. 32, p. 217–220.

Reed, M., 1997, Hydrothermal alteration and its relationship to ore fluid composition, *in* Barnes, H.L., ed., Geochemistry of hydrothermal ore deposits, 3rd ed.: New York, John Wiley & Sons, p. 303–365.

Rempel, K.U., Williams-Jones, E.E., and Migdisov, A.A., 2009, The partitioning of molybdenum (VI) between aqueous liquid and vapour at temperatures up to 370°C: Geochimica et Cosmochimica Acta, v. 73, p. 3381–3392.

Richards, J.P., 2003, Tectonomagmatic precursors for porphyry Cu-(Mo-Au) deposit formation: Economic Geology, v. 98, p. 1515–1533.

——2011, Magmatic to hydrothermal metal fluxes in convergent and collided margins: Ore Geology Reviews, v. 40, p. 1–26.

Roedder, E., 1967, Fluid inclusions as samples of ore fluids, *in* Barnes, H.L., ed., Geochemistry of hydrothermal ore deposits: New York, Holt, Rinehart and Winston, p. 515–574.

——1971, Fluid inclusion studies on the porphyry-type ore deposits at Bingham, Utah, Butte, Montana, and Climax, Colorado: Economic Geology, v. 66, p. 98–120.

——1984, Fluid inclusions: Reviews in Mineralogy, v. 12, 646 p.

Roedder, E., and Bodnar, R.J., 1980, Geologic pressure determinations from fluid inclusion studies: Annual Review of Earth and Planetary Sciences, v. 8, p. 263–301.

——1997, Fluid inclusion studies of hydrothermal ore deposits, *in* Barnes, H.L., ed., Geochemistry of hydrothermal ore deposits, 3rd ed., New York, John Wiley & Sons, p. 657–697.

Rose, A.W., 1970, Zonal relations of wall-rock alteration and sulfide distribution at porphyry copper deposits: Economic Geology, v. 65, p. 920–936.

Rudnick, R.L., and Gao, S., 2003, Composition of the continental crust: Treatise on Geochemistry, v. 3, p. 1–64.

Ruggieri, G., Lattanzi, P., Luxoro, S. S., Dessi, R., Benvenuti, M., and Tanelli, G., 1997, Geology, mineralogy, and fluid inclusion data of the Furtei high-sulfidation gold deposit, Sardinia, Italy: Economic Geology, v. 92, p. 1–19.

Rusk, B., and Reed, M., 2002, Scanning electron microprobe-cathodoluminescence analysis of quartz reveals complex growth histories in veins from the Butte porphyry copper deposit, Montana: Geology, v. 30, p. 727–730.

Rusk, B., Reed, M.H., Dilles, J.H., and Klemm, L., 2004, Compositions of magmatic-hydrothermal fluids determined by LA-ICPMS of fluid inclusions from the porphyry copper-molybdenum deposit at Butte, Montana: Chemical Geology, v. 210, p. 173–199.

Rusk, B.G., Miller, B.J., and Reed, M.H., 2008a, Fluid inclusion evidence for the formation of Main Stage polymetallic base-metal veins, Butte, Montana, USA: Arizona Geological Society Digest 22, p. 573–581.

Rusk, B.G., Reed, M.H., and Dilles, J.H., 2008b, Fluid inclusion evidence for magmatic-hydrothermal fluid evolution in the porphyry copper-molybdenum deposit at Butte, Montana: Economic Geology, v. 103, p. 307–334.

Rusk, B., Emsbo, P., Hunt, A., Hofstra, A., Landis, G., and Rye, R., 2008c, Fluid inclusion insights into the origins of fluids and metals in porphyry copper deposits: Pacrim Congress 2008, Gold Coast, Queensland, 2008, Extended Abstracts, p. 289–294.

Rusk, B., Emsbo, P., Hammersli, J., Hofstra, A., Hunt, A., Landis, G., and Rye, R., 2011, Origin and composition of fluids that form giant porphyry Cu (Mo-Au) deposits, *in* Barra, F., Reich, M., Campos, E., and Tornos, F., eds., Let's talk ore deposits: Proceedings 11th SGA Biennial Meeting, 26–29 September 2011, Antofagasta, Chile, p. 414–416.

Ryan, C.G., Cousens, D.R., Heinrich, C.A., Griffin, W.L., Sie, S.H., and Mernagh, T.P., 1991, Quantitative PIXE microanalysis of fluid inclusions based on a layered yield model: Nuclear Instruments and Methods in Physics Research, B, v. 54, p. 229–297.

Rye, R. O., 1993, The evolution of magmatic fluids in the epithermal environment—the stable isotope perspective: Economic Geology, v. 88, p. 733–753.

Ryzhenko, B.N., 1981, Equilibria in hydrothermal solutions: Moscow, Nauka (in Russian).

Saunders, J.A., 1990, Colloidal transport of gold and silica in epithermal precious metal systems: Evidence from the Sleeper deposit, Humboldt County, Nevada: Geology, v. 18, p. 757–760.

Saunders, J.A., and Schoenly, P.A., 1995, Boiling, colloid nucleation and aggregation, and the genesis of bonanza Au-Ag ores of the Sleeper deposit, Nevada: Mineralium Deposita, v. 30, p. 199–210.

Saunier, G., Pokrovski, G.S., and Poitrasson, F., 2011, First experimental determination of iron isotope fractionation between hematite and aqueous solution at hydrothermal conditions: Geochimica et Cosmochimica Acta, v. 75, p. 6629–6654.

Sawkins, F.J, and Scherkenbach, A.A., 1981, High copper content of fluid inclusions in quartz from northern Sonora: Implications for ore-genesis theory: Geology, v. 9, p. 37–48.

Seedorff, E., and Einaudi, M.T., 2004, Henderson porphyry molybdenum system, Colorado: II. Decoupling of introduction and deposition of metals during geochemical evolution of hydrothermal fluids: Economic Geology, v. 99, p. 39–72.

Seedorff, E., Dilles, J.H., Proffett, J.M., Jr., Einaudi, M.T., Zurcher, L., Stavast, W.J.A., Johnson, D.A., and Barton, M.D., 2005, Porphyry deposits: Characteristics and origin of hypogene features: Economic Geology 100th Anniversary Volume, p. 251–298.

Seedorff, E., Barton, M.D., Stavast, W.J.A., and Maher, D.J., 2008, Root zones of porphyry systems: Extending the porphyry model to depth: Economic Geology, v. 103, p. 939–956.

Seo, J.H., Guillong, M., and Heinrich, C.A., 2009, The role of sulfur in the formation of magmatic-hydrothermal copper-gold deposits: Earth and Planetary Science Letters, v. 282, p. 323–328.

Seo, J.H., Guillong, M., Aerts, M., Zajacz, Z., and Heinrich, C.A., 2011, Microanalysis of S, Cl, and Br in fluid inclusions by LA-ICP-MS: Chemical Geology, v. 284, p. 35–44.

Seo, J.H., Guillong, M., and Heinrich, C.A., 2012, Separation of molybdenum and copper in porphyry deposits: The roles of sulfur, redox, and pH in ore mineral deposition at Bingham Canyon: Economic Geology, v. 107, p. 333–356.

Seward, T.M., and Barnes, H.L., 1997, Metal transport by hydrothermal ore fluids, in Barnes, H.L., ed., Geochemistry of hydrothermal ore deposits, 3rd ed.: New York, John Wiley and Sons, p. 435–486.

Sheppard, S.M.F., Nielsen, R.L., and Taylor, H.P., Jr., 1971, Hydrogen and oxygen isotope ratios in minerals from porphyry copper deposits: Economic Geology, v. 66, p. 515–542.

Sherman, D.M., 2010, Metal complexation and ion association in hydrothermal fluids: insights from quantum chemistry and molecular dynamics: Geofluids, v. 10, p. 41–57.

Shinohara, H., and Hedenquist, J.W., 1997, Constraints on magma degassing beneath the Far Southeast porphyry Cu-Au deposit, Philippines: Journal of Petrology, v. 38, p. 1741–1752.

Shmulovich, K., Heinrich, W., Möller, P., and Dulski, P., 2002. Experimental determination of REE fractionation between liquid and vapour in the systems NaCl-H2O and CaCl2-H_2O up to 450°C: Contributions to Mineralogy and Petrology, v. 44, p. 257–273.

Shock, E.L., Sassani, D.C., Willis, M., and Sverjensky, D.A., 1997, Inorganic species in geologic fluids: Correlations among standard molal thermodynamic properties of aqueous ions and hydroxide complexes: Geochimica et Cosmochimica Acta, v. 61, p. 907–950.

Shvarov, Y.S., 2008, HCh: New potentialities for the thermodynamic simulation of geochemical systems offered by windows: Geochemisty International, v. 46, p. 834–839.

Sillitoe, R.H., 1979, Some thoughts on gold-rich porphyry copper deposits: Mineralium Deposita, v. 14, p. 161–174.

——1994, Erosion and collapse of volcanoes: Causes of telescoping in intrusion-centered ore deposits: Geology, v. 22, p. 945–948.

——2010, Porphyry copper systems: Economic Geology, v. 105, p. 3–41.

Sillitoe, R.H., and Hedenquist, J.W., 2003, Linkages between volcanotectonic settings, ore-fluid compositions, and epithermal precious metal deposits: Society of Economic Geologists Special Publication 10, p. 315–343.

Sillitoe, R.H., and Mortensen, J.K., 2010, Longevity of porphyry copper formation at Quellaveco, Peru: Economic Geology, v. 105, p. 1157–1162.

Simmons, S.F., and Browne, P.R.L., 1997, Saline fluid inclusions in sphalerite from the Broadlands-Ohaaki geothermal system: A coincidental trapping of fluids boiled toward dryness: Economic Geology, v. 92, p. 485–489.

Simmons, S.F., Gemmell, J.B., and Sawkins, F.J., 1988, The Santo Niño silver-lead-zinc vein, Fresnillo, Mexico: Part II. Physical and chemical nature of oreforming solutions: Economic Geology, v. 83, p. 1619–1641.

Simmons, S.F., White, N.C., and John, D.A., 2005, Geological characteristics of epithermal precious and base metal deposits: Economic Geology 100th Anniversary Volume, p. 485–522.

Simon, A.C., Pettke, T., Candela, P.A., Piccoli, P.M., and Heinrich, C.A., 2004, Magnetite solubility and iron transport in magmatic-hydrothermal environments: Geochimica et Cosmochimica Acta, v. 68, p. 4905–4914.

Simon, A.C., Frank, M.R., Pettke, T., Candela, P.A., Piccoli, P.M., and Heinrich C.A., 2005, Gold partitioning in melt-vapor-brine systems: Geochimica et Cosmochimica Acta, v. 69, p. 3321–3335.

Simon, A.C., Pettke, T., Candela, P.A., Piccoli, P.M., and Heinrich, C.A., 2006, Copper partitioning in a melt-vapor-brine-magnetite-pyrrhotite assemblage: Geochimica et Cosmochimica Acta, v. 70, p. 5583–5600.

Simon, A.C., Pettke, T., Candela, P.A., and Piccoli, P.M., 2008, The partitioning behavior of silver in a vapor–brine–rhyolite melt assemblage: Geochimica et Cosmochimica Acta, v. 72, p. 1638–1659.

Sourirajan, S., and Kennedy, G.C., 1962, System H_2O-NaCl at elevated temperatures and pressures: American Journal of Science, v. 260, p. 115–141.

Spooner, E.T.C., 1981, Fluid inclusion studies of hydrothermal ore deposits: Mineralogical Association of Canada Short Course Handbook, v. 6, p. 209–240.

Stefánsson, A., and Seward, T.M., 2003, Experimental determination of the stability and stoichiometry of sulphide complexes of silver(I) in hydrothermal solutions to 400°C: Geochimica et Cosmochimica Acta, v. 67, p. 1395–1413.

——2004, Gold(I) complexing in aqueous sulphide solutions to 500°C at 500 bar: Geochimica et Cosmochimica Acta, v. 68, p. 4121–4143.

Sterner, S.M., Hall, D.L., and Bodnar, R.J., 1988, Synthetic fluid inclusions. IV. Solubility relations in the system NaCl-KCl-H_2O under vapor-saturated conditions: Geochimica et Cosmochimica Acta, v. 52, p. 989–1005.

Styrikovich, M.A., Khaibullin, I.K., and Tshvirashvili, D.G., 1955, A study of salt solubility in high-pressure water steam: Doklady Akademii Nauk of the Union of Soviet Socialist Republics (USSR), v. 100, p. 1123–1126.

Styrikovich, M.A., Tshvirashvili, D.G., and Hebieridze, D.P., 1960, A study of the solubility of boric acid in saturated water vapor: Doklady Akademii Nauk of the Union of Soviet Socialist Republics (USSR), v. 134, p. 615–617 (in Russian).

Sverjensky, D.A., Shock, E.L., and Helgeson, H.C., 1997, Prediction of the thermodynamic properties of aqueous metal complexes to 1000°C and 5 kb: Geochimica et Cosmochimica Acta, v. 61, p. 1359–1412.

Tagirov, B.R., and Seward, T.M., 2010, Hydrosulfide/sulfide complexes of zinc to 250°C and the thermodynamic properties of sphalerite: Chemical Geology, v. 269, p. 301–311.

Tagirov, B.R., Salvi, S., Schott, J., and Baranova, N.N., 2005, Experimental study of gold-hydrosulphide complexing in aqueous solutions at 350–500°C, 500 and 1000 bars using mineral buffers: Geochimica et Cosmochimica Acta, v. 69, p. 2119–2132.

Takenouchi, S., and Kennedy, G.C., 1965, Solubility of carbon dioxide in NaCl solutions at high temperatures and pressures: American Journal of Science, v. 263, p. 445–454.

Tanger, J.C., and Helgeson, H.C., 1988, Calculation of the thermodynamic and transport properties of aqueous species at high pressures and temperatures: Revised equations of state for the standard partial molal properties of ions and electrolytes: American Journal of Science, v. 288, p. 19–98.

Testemale, D., Brugger, J., Liu, W., Etschmann, B., and Hazemann, J-L., 2009, In-situ X-ray absorption study of iron(II) speciation in brines up to supercritical conditions: Chemical Geology, v. 264, p. 295–310.

Testemale, D., Pokrovski, G. S., and Hazemann, J.-L., 2011, Speciation of As^{-III} and As^{-V} in hydrothermal fluids by in situ X-ray absorption spectroscopy: European Journal of Mineralogy, v. 23, p. 379–390.

Titley, S.R., 1982, The style and progress of mineralization and alteration in porphyry copper systems: American Southwest, *in* Titley, S.R., ed., Advances in geology of the porphyry copper deposits, southwestern North America: Tucson, University of Arizona Press, p. 93–116.

——1993, Characteristics of porphyry copper occurrence in the American Southwest: Geological Association of Canada Special Paper 40, p. 433–464.

Tosdal, R.M., and Richards, J.P., 2001, Magmatic and structural controls on the development of porphyry Cu ± Mo ± Au deposits: Reviews in Economic Geology, v. 14, p. 157–181.

Ulrich, T., and Mavrogenes, J., 2008, An experimental study of the solubility of molybdenum in H_2O and KCl-H_2O solutions from 500°C to 800°C and 150 to 300 MPa: Geochimica et Cosmochimica Acta, v. 72, p. 2316–2330.

Ulrich, T., Günther, D., and Heinrich, C.A., 1999, Gold concentrations of magmatic brines and the metal budget of porphyry copper deposits: Nature, v. 399, p. 676–679.

——2001, Evolution of a porphyry Cu-Au deposit, based on LA-ICP-MS analysis of fluid inclusions, Bajo de la Alumbrera, Argentina: Economic Geology, v. 96, p. 1743–1774 (reprinted with corrections in 2002, v. 97, p. 1888–1920).

Valencia, V.A., Ruiz, J., Barra, F., Gehrels, G., Ducea, M., Titley, S.R., and Ochoa-Landin, L., 2005, U-Pb zircon and Re-Os molybdenite geochronology from La Caridad porphyry copper deposit: insights for the duration of magmatism and mineralization in the Nacozari district, Sonora, Mexico: Mineralium Deposita, v. 40, p. 175–191.

Vallance, J., Fontboté, L., Chiaradia, M., Markowski, A., Schmidt, S., and Vennemann, T., 2009, Magmatic-dominated fluid evolution in the Jurassic Nambija gold skarn deposits (southeastern Ecuador): Mineralium Deposita, v. 44, p. 389–413.

Vanko, D.A., Bonnin-Mosbah, M., Philippot, P., Roedder, E., and Sutton, S.R., 2001, Fluid inclusions in quartz from oceanic hydrothermal specimens and the Bingham, Utah porphyry-Cu deposit: a study with PIXE and SXRF: Chemical Geology, v. 173, p. 227–238.

Vennemann, T.W., Muntean, J.L., Kesler, S.E., Oneil, J.R., Valley, J.W., and Russell, N., 1993, Stable isotope evidence for magmatic fluids in the Pueblo Viejo epithermal acid-sulfate Au-Ag deposit, Dominican Republic: Economic Geology, v. 88, p. 55–71.

von Quadt, A., Peytcheva, I., Kamenov, B., Fanger, L., Heinrich, C.A., and Frank, M., 2002, The Elatsite porphyry copper deposit in the Panagyurishte ore district, Srednogorie zone, Bulgaria: U-Pb zircon geochronology and isotope-geochemical investigations of magmatism and ore genesis: Geological Society, London, Special Publication 204, p. 119–135.

von Quadt, A., Erni, M., Martinek, K., Moll, M., Peytcheva, I., and Heinrich, C.A., 2011, Zircon crystallization and the lifetimes of ore-forming magmatic-hydrothermal systems: Geology, v. 39, p. 731–734.

Vry, V.H., Wilkinson, J.J., Seguel, J., and Millan, J., 2010, Multistage intrusion, brecciation, and veining at El Teniente: Evolution of a nested porphyry system: Economic Geology, v. 105, p. 119–153.

Wallier, S., Rey, R., Kouzmanov, K., Pettke, T., Heinrich, C.A., Leary, S., O'-Connor, G., Tamas, C.G., Vennemann, T., and Ullrich, T., 2006, Magmatic fluids in the breccia-hosted epithermal Au-Ag deposit of Rosia Montana, Romania: Economic Geology, v. 101, p. 923–954.

Walther, J.V., and Helgeson, H.C., 1977, Calculation of thermodynamic properties of aqueous silica and solubility of quartz and its polymorphs at high-pressures and temperatures: American Journal of Science, v. 277, p. 1315–1351.

Walther, J.J., and Orville, P.M., 1983, The extraction-quench technique for determination of the thermodynamic properties of solute complexes: Application to quartz solubility in fluid mixtures: American Mineralogist, v. 68, p. 731–741.

Wang, Y.S., Sasaki, M., Sasada, M., and Chen, C.H., 1999, Fluid inclusion studies of the Chinkuashih high-sulfidation gold-copper deposits in Taiwan: Chemical Geology, v. 154, p. 155–167.

Watanabe, Y., and Hedenquist, J.W., 2001, Mineralogic and stable isotope zonation at the surface over the El Salvador porphyry copper deposit, Chile: Economic Geology, v. 96, p. 1775–1797.

Weisbrod, A., 1981, Fluid inclusions in shallow intrusive: Mineralogical Association of Canada Short Course Handbook, v. 6, p. 241–271.

Wilkinson, J.J., 2001, Fluid inclusions in hydrothermal ore deposits: Lithos, v. 55, p. 229–272.

Wilkinson, J.J., Rankin, A.H., Mulshaw, S.C., Nolan, J., and Ramsey, M.H., 1994, Laser ablation-ICP-AES for the determination of metals in fluid inclusions—an application to the study of magmatic ore fluids: Geochimica et Cosmochimica Acta, v. 58, p. 1133–1146.

Wilkinson, J.J., Wilkinson, C.C., Vry, V.H., Rusk, B.G., Séguel, J., Zentilli, M., and Jeffries, T.E., 2008, Ore fluid chemistry in super-giant porphyry copper deposits: Pacrim Congress 2008, Gold Coast, Queensland, November 24–26 2008, Extended Abstracts, p. 295–299.

Williams-Jones, A.E., and Heinrich, C.A., 2005, Vapor transport of metals and the formation of magmatic-hydrothermal ore deposits: Economic Geology, v. 100, p. 1287–1312.

Williams-Jones, A.E., Samson, I.M., Ault, K.M., Gagnon, J.E., and Fryer, B.J., 2010, The genesis of distal zinc skarns: Evidence from the Mochito deposit, Honduras: Economic Geology, v. 105, p. 1411–1440.

Wolfe, R.C., and Cooke, D.R., 2011, Geology of the Didipio region and genesis of the Dinkidi alkalic porphyry Cu-Au deposit and related pegmatites, northern Luzon, Philippines: Economic Geology, v. 106, p. 1279–1315.

Wood, S.A., and Samson, I.M., 1998, Solubility of ore minerals and complexation of ore metals in hydrothermal solutions: Reviews in Economic Geology, v. 10, p. 33–80.

Wopenka, B., and Pasteris, J.D., 1986, Limitations to quantitative analysis of fluid inclusions in geological samples by laser Raman microprobe spectroscopy: Applied Spectroscopy, v. 40, p. 144–151.

Zajacz, Z., Halter, W.E., Pettke, T., and Guillong, M., 2008, Determination of fluid/melt partition coefficients by LA-ICPMS analysis of co-existing fluid and silicate melt inclusions: controls on element partitioning: Geochimica et Cosmochimica Acta, v. 72, p. 2169–2197.

Zajacz, Z., Hanley, J.J., Heinrich, C.A., Halter, W.E., and Guillong, M., 2009, Diffusive reequilibration of quartz-hosted silicate melt and fluid inclusions: are all metal concentrations unmodified?: Geochimica et Cosmochimica Acta, v. 73, p. 3013–3027.

Zhang, L., Audétat, A., and Dolejs, D., 2012, Solubility of molybdenite (MoS_2) in aqueous fluids at 600–800°C, 200 MPa: A synthetic fluid inclusions study: Geochimica et Cosmochimica Acta, v. 77, p. 175–185.

Zotov, A.V., Kudrin, A.V., Levin, K.A., Shikina, N.D., and Var'yash, L.N., 1995, Experimental studies of the solubility and complexing of selected ore elements (Au, Ag, Cu, Mo, As, Sb, Hg) in aqueous solutions, in Shmulovich, K.I, Yardley, B.W.D., and Gonchar, G.G., eds., Fluids in the crust. Equilibrium and transport properties: London, Chapman & Hall, p. 95–138.

Zotov, A.V., Shikina, N.D., and Akinfiev, N.N., 2003, Thermodynamic properties of the Sb(III) hydroxide complex $Sb(OH)_3(aq)$ at hydrothermal conditions: Geochimica et Cosmochimica Acta, v. 67, p. 1821–1836.